0002 AD - Final Technical Report

CONTROL OF FORMATION FLYING SATELLITES

For the Period May 13, 1999 - May 12, 2000

by

Dr. Peter M. Bainum, Principal Investigator
Avaine Strong, Research Asst. and Zhaozhi Tan, Sr. Research Assoc.
Howard University
Department of Mechanical Engineering
Washington, D.C. 20059

E-mail pbainum@fac.howard.edu

Any opinions, findings and conclusions or recommendations expressed
in this material are those of the author(s) and should not be interpreted
as representing the official policies, either expressly or implied, of the
Defense Advanced Research Projects Agency or the U.S. Government.

20000601 043

DISTRIBUTION STATEMENT AUTHORIZATION RECORD

Title: _Control of Formation Flying Satellites_

Authorizing Official: _Dr. Ephrahim Garcia_

Agency: _DARPA_   Ph. No. _(703) 696-2229_

☐ Internet Document: URL: _____
    (DTIC-OCA Use Only)

Distribution Statement: (Authorized by the source above.)

☒ **A:** Approved for public release, distribution unlimited.

☐ **B:** U. S. Government agencies only. (Fill in reason and date applied). Other requests shall be referred to (Insert controlling office).

☐ **C:** U. S. Government agencies and their contractors. (Fill in reason and date applied). Other requests shall be referred to (Insert controlling office).

☐ **D:** DoD and DoD contractors only. (Fill in reason and date applied). Other requests shall be referred to (Insert controlling office).

☐ **E:** DoD components only. (Fill in reason and date applied). Other requests shall be referred to (Insert controlling office).

☐ **F:** Further dissemination only as directed by (Insert controlling DoD office and date), or higher authority.

☐ **X:** U. S. Government agencies and private individuals or enterprises eligible to obtain export-controlled technical data in accordance with DoD Directive 5230.25.

NOTES: _____

_____

_____

_____

J. Keith
DTIC Point of Contact

15 JUN 2000
Date

REPORT DOCUMENTATION PAGE

Public reporting burden for the collection of information is estimated to average 1 hour per response, including the time for reviewing instructions, searching existing data sources, gathering and maintaining the data needed, and completing and reviewing the collection of information. Send comments regarding this burden estimate or any other aspect of this collection of information, including suggestions for reducing this burden, to Washington Headquarters Services, Directorate for Information Operations and Reports, 1215 Jefferson Davis Highway, Suite 1204, Arlington, VA 22202-4302, and to the Office of Management and Budget, Paperwork Reduction Project (0704-0188), Washington, DC 20503.

1. AGENCY USE ONLY *(Leave blank)*	2. REPORT DATE May 26, 2000	3. REPORT TYPE AND DATES COVERED Final May 13, 1999 – May 12, 2000

4. TITLE AND SUBTITLE Final Technical Report Control of Formation Flying Satellites	5. FUNDING NUMBERS C#MDA 972-99-C-0020

6. AUTHOR(S)

Peter M. Bainum , Avaine Strong, Zhaozhi Tan

7. PERFORMING ORGANIZATION NAME(S) AND ADDRESS(ES) Howard University Dept. of Mechanical Engineering Washington, D.C. 20059	8. PERFORMING ORGANIZATION REPORT NUMBER 0002 AD

9. SPONSORING/MONITORING AGENCY NAME(S) AND ADDRESS(ES) Defense Advanced Research Projects Agency Defense Sciences Office 3701 N. Fairfax Drive Arlington, VA 22203-1314	10. SPONSORING/MONITORING AGENCY REPORT NUMBER

11. SUPPLEMENTARY NOTES

12a. DISTRIBUTION/AVAILABILITY STATEMENT DARPA/DSO – Dr. Ephrahim Garcia DARPA/ASBD Library Defense Technical Information Center: DTIC-BCS	12b. DISTRIBUTION CODE

13. ABSTRACT *(Maximum 200 words)*   This report summarizes the work completed during the reporting period cited above. A technique for maintaining nominal separation distance between adjacent satellites in an elliptically orbiting constellaton is developed and parametric trade-off studies performed. This technique is based on an initial impulsive-type correction of the daughter spacecraft at the first perigee in order to shift the direction of the line of apsides by a small angle. The technique works well in Keplerian orbits. In the presence of perturbations the results are critically dependent on the amplitude of the shift angle. Without subsequent corrections near collision situations can exist over the long term. Additional feedback type of correctional control is recommended to prevent unwanted secular drifts. Two types of feedback control strategies are considered here: an application of the linear quadratic regulator (LQR) theory based on errors in position, and also based on a Lyapunov function using osculating orbital elements. A preliminary deployment strategy is introduced based on near Hohmann-type of transfer orbits, and shows deployment can be achieved in one orbit.

14. SUBJECT TERMS Final technical report; orbital station keeping; formation flying; perturbations; deployment; LQR theory; Lyapunov function	15. NUMBER OF PAGES 126
	16. PRICE CODE

17. SECURITY CLASSIFICATION OF THIS REPORT unclassified	18. SECURITY CLASSIFICATION OF THIS PAGE unclassified	19. SECURITY CLASSIFICATION OF ABSTRACT unclassified	20. LIMITATION OF ABSTRACT

Table of Contents

I. INTRODUCTION AND METHODOLOGY

The notion of orbital formation flying has been known for some time; recent budget reductions have prompted renewed interest in this technology. The National Aeronautics and Space Administration (NASA) Cross Enterprise Technology Development Program (CETDP) is developing critical space technologies that enable innovative and less costly missions[1][1]. Thus efforts within the Distributed Spacecraft thrust area (TA) represent technological developments which will support NASA's ability to accomplish its task by surpassing traditional approaches to utilizing space and the limitation inherent to them, by enhancing the ability of new and emerging technologies, and sciences, and further accomplishing the challenges of looking closer at the world and understanding the processes which define in composition and evolution, looking deeper into the universe to explore neighboring planets, galaxies and to seek an understanding of their origin. The trend is to develop technology that will allow a distributed network of autonomous spacecraft to act collaboratively as a single collective unit. An advantage of flying multiple, small, low-cost spacecraft in formation is that this provides correlated instrument measurements formerly possible only by flying many instruments on a single large platform [2]. Distribution of components on a number of satellites allows the advantage that a single component failure results in the replacement of a small, cheap spacecraft and not an abort of the mission. Areas of formation flying application in remote sensing include stereographic viewing, interferometry, conducted by DeCou [3], and synthetic aperture synthesization for

---

[1] Numbers in brackets designate References at end of this report.

1

radar and other applications conducted by Kong, Miller and Sedwick [4-5]. DeCou discussed the basic orbital configuration for interferometry missions and the thrust requirements for station keeping of a two-satellite formation, while Kong, et al., discussed synthesization of aperture, using orbital dynamics which included environmental perturbations such as non-spherical Earth effects, atmospheric drag, solar radiation pressure and magnetic field interaction. NASA has suggested at least three formations of small spacecraft in low earth orbit (LEO) for scientific data collection. Among these are:

(1)   An "Auroral Cluster" system of up to four spacecraft in formation where the main objective would be to measure for the first time the curl of the Earth's magnetic field vector. It is anticipated that this mission would involve separation distances from a few meters and up to 200 km over a year's interval. For the present study, 500 km will be considered the nominal separation distance.

(2)   A second mission would involve two spacecraft in the same orbit, one following the other, as closely as 5 km, then moving away to distances of ¼ to ½ orbit. Instrumentation on-board would correlate distance measurements in the atmosphere over a wide range of separation ranges.

(3)   A third mission dedicated to space based interferometry would deploy three spacecraft flying precise "zero-drag" trajectories with positional accuracy of the order of cm, with the objective of measuring gravity waves under zero-drag conditions. For this mission the interferometry base line set up by the formation would be of a few km. with the main disturbances attributed to the effects of solar radiation pressure.

(4)   In addition to the three proposed Low Earth Orbit (LEO) missions, another

interesting concept, currently in the planning phase by NASA Goddard Space Flight Center (GSFC) is:

A solar stereo mission involving two spacecraft in heliocentric orbit, one behind the Earth and the second in front of the Earth with a separation distance of 1 astronomical unit (a.u.) The objective would be to measure the solar corona mass ejection from different vantage points within a prescribed base-line accuracy.

(5) In addition to these proposed scientific uses for orbital formation flying, clusters of spacecraft would be the core of the IRIDIUM, Alcatel, Globalstar, Ellipso and other proposed orbital communication systems of the future. Depending on the application the number of spacecraft could vary from a handful up to 50 or 100s, with separation distances from the order of km to thousands of km with a wide range of orbital altitudes.

A search of technical publications, technical memoranda, and other reports pertaining to this subject has been conducted. The majority of the literature surveyed on Constellation Station Keeping, comes from reports of completed research or major phases of research presented in NASA programs which includes extensive data or theoretical analyses. Furthermore, these reports include compilations of significant scientific and technical data and information deemed to be of continuing value. Other reports are mentioned and referenced throughout this document.

An early study by Walker presents a systematic approach to the analysis of coverage of the Earth by means of circular orbit systems [6]. The study ensured that every point on the Earth's surface can always see at least one satellite (or two satellites for double coverage) above some minimum elevation angle. It is shown that five or six (properly phased) geosynchronous altitude satellites can provide (continuous worldwide) single coverage, and seven or nine satellites double coverage; and a generalized approach to such coverage assessments is presented. Walker also recognized that low Earth orbit (LEO) systems had unique properties and advantages, and he proposed and analyzed a 48 satellite system concept which became the basis of the Loral Globalstar system [7].

A recent paper presents the Goddard Space Flight Center (GSFC) closed-loop control

method to fly in either constellations or formations through the use of an autonomous closed loop three-axis navigation control and innovative orbit maintenance support [8]. An operational control method for maintenance of constellation formation flying is developed in this paper. Examples were taken from the Earth Observing-1 (EO-1) spacecraft that is part of NASA's New Millennium Program (NMP) and from the proposed Earth System Science Program Office (ESSPO) constellations. Results can be used to determine the appropriateness of constellations and formation flying for a particular case as well as the operational impacts. After constellation and formation analysis was completed, implementation of a maneuver maintenance strategy became the driver.

Brochet et al present a new method to solve the linear station keeping optimization problem [9]. Several optimization models were proposed for the problem of resetting drifting satellites to ensure desired coverage to include those satellites that may fail during the life of the constellation. Each model consists in minimizing the total fuel consumption due to maneuvers. As in all station keeping models, the objective is to minimize the total fuel consumption associated with satellite maneuvers. The minimization takes into account the trajectory of each satellite and constraints on their relative positions. An additional constraint is introduced to limit the number of satellites that can be simultaneously controlled. All satellites cannot thrust simultaneously. This is a Mixed Integer Non-Linear Programming (MINLP) optimization problem, containing Boolean and real variables. Boolean variables determine which satellite can be maneuvered at each step, and the real variables correspond to the thrust value of the maneuvers. One has to solve the optimization station keeping problem or find these values for each cycle. This problem is split on the basis of the generalized Bender's decomposition method (projection on the Boolean variable space) [10]. (1) The first model is linear and differential (relative satellite positions). The subproblem (calculation of the impulsive thrusts) is solved by a dual approach that finds the solution in a finite number of steps. (2) The second model is nonlinear and non-differential. It represents the real problem without simplifications. The resolution of the subproblem is done using a direct search approach (Hook and Jeeves algorithm [11]) to determine real variables in the subproblem. The objective is to minimize the total fuel consumption of each satellite subject

4

to (a) a coverage constraint (distance between two satellites $|\Delta d|$ must not exceed a threshold Φ), and (b) three remaining operational constraints.

In conclusion[9] for the two models: Linear and differential optimization problem and Nonlinear and non-differential station keeping problem, the method presented is very efficient since it can provide the global minimum (optimal maneuvers needed to ensure a good coverage) just by resolving a system of linear equations and can be applied to every station keeping problem. The second model can solve more complicated cases (nonlinear mixed variables problem). It is more precise than the linear one. It allows for various constraints on position (i.e., relative or absolute positions of satellites), and various definitions of the fuel consumption. This model can also be used as a first approach to calculate optimal maneuvers needed to replace a failed satellite. However, the global problem, including the choice of the spare satellite, needs to be stated.

The flying of spacecraft in constellations and formations will permit the accurate determination of three - dimensional and time - varying phenomena and will make it possible to distinguish between spatial and temporal variations. However, constellations and formation flying impose additional complications on orbit selection and orbit maintenance, especially when each spacecraft has its own orbit or science requirements. Every object in orbit follows approximately the second Keplerian law [12]. Therefore, there is a natural tendency of separations. To maintain constant separation distance between pairs of spacecraft is not an easy problem if the orbits are elliptical. Hughes and Hall [13] investigated an optimization scheme to determine the best configuration for a four spacecraft formation in a circular orbit. Ulybyshev [14] used the linear-quadratic regulator technique for feedback control to maintain station keeping of a circular orbiting constellation. Carpenter [15] suggested a distributed satellite formation, modeled as an arbitrary number of fully connected nodes in a network, for an equatorial circular Keplerian orbit, could be controlled using a decentralized controller framework. Cao, Modi, et. al., explored the possibility of using separately and a combination of Feedback Linearization Technique (FLT) and Linear-Quadratic Regulator (LQG) to study the control theory of an elastic space platform-based flexible manipulator with four links, two free to slew while the other two were permitted to

5

deploy [16]. Chao, Pollard, and Janson [17] described a method for determining cluster orbital elements and the relative geometry and dynamics of satellites under a two-body force field with the secular Earth's oblateness J_2 influences(Because the term J_2 will be referred to often in this document, the reader is referred to the derivation, in Battin[18]. They also examined the disruption of the formation due to natural perturbations and the feasibility of a formation-keeping strategy. Smith, Proulx, et al. [19], investigated the use of genetic algorithms to generate optimal station keeping strategies, by constraining the orbit of an Ellipso™ Borealis satellite and developed the minimum fuel optimal burn strategy by minimizing the fuel required to maintain the orbit for a given period of time. Sabol, Burns and McLaughlin[20] used the Draper Semianalytic Satellite Theory (DSST) to study several satellite formation flying designs and their evolution through time. The DSST equations of relative motion are used in a manner similar to the BG14 propagator[21]. The DSST equations are derived for Keplerian two body dynamics (like the Hill's equations, or the better known Clohessy Wiltshire (CW) [22] equations, which are a special form of Hill's equations). BG14 is a high precision orbit propagator simulation written by McDonnell Douglas. The BG14 propagator takes into account the solar pressure, oblateness of the Earth(up to 40x40) and air density variation with the Jacchia 70 (J70) model. The DSST Semianalytic Theory can also be modified to include effects of oblateness, drag, etc. To be more exact, all the references cited , up to this point, relate to these Hill's equations or the Clohessy-Wiltshire (CW) set of equations, these have been used primarily to analyze modern guidance and rendezvous problems. These include nonlinear error analysis, station keeping, targeting, surveillance and satellite clustering. These equations have severe limitations and drawback. The CW equations are of a linear nature with constant coefficients, and describe the coasting terminal motion of the ferry vehicle relative to the target, when the target is in a circular orbit. The main limitation of CW equations is that the relative gravitational influence is expanded to only first order terms in the ratio of separation distance to orbital radius (ρ/r) ending up with a fast growing error term as the probe moves away from the station or target.

It may be convenient to use the not so well-known Tschauner and Hempel equations

[23]. These equations are sets of linear equations which resemble the CW equations in their derivation and describe the motion of a spacecraft near a satellite in an arbitrary elliptic orbit relative to a rotating orthogonal coordinate frame fixed in the satellite. Tschauner and Hempel found complete solutions for elliptical orbits in terms of the eccentric anomaly. Tschauner followed this article with two others [24,25]. It was a considerable task to verify the results, not solely due to the fact that the articles are written in German. Carter and Humi [26,27] applied these equations to more general Keplerian orbits and later Carter and Brient[28,29,30] investigated impulsive or thrust maneuvers using these equations. A complete search revealed only an outline of the derivation of the Tschauner and Hempel equations; therefore, a complete derivation is based on Van der Ha and Mugellesi [31].

It will soon become apparent, that a multiple set of disciplines is needed to treat the problem considered in this report. These include:

- Physics - Orbital Mechanics
- Engineering - Linear and Nonlinear Dynamic Programming and Control Theory
- Mathematics - Differential Equations and Mathematical Modeling

This research consists of a station keeping stage and a deployment stage. The totality is summed up in five chapters. In actuality, the order of events is a deployment stage followed by station keeping. However, for purposes of this research, it will be assumed that the desired configuration has been reached; therefore, station keeping will be analyzed first, and deployment will be addressed in the later part of this document. The organization of this report is as follows. Following the Introduction and Methodology (Chapter One), is Chapter Two. Chapter Two deals with the Selection of the Strawman Configurations and Comparison with the ESA Auroral Cluster Configuration and the Proposed NASA Multiscale System. Chapter Three, Station Keeping Maneuvers, consists of two parts. The first part involves, a detailed study of station keeping of spacecraft using the BG14 propagator, where instantaneous impulses were conducted at perigee and apogee to cause the in-plane shift of the line of apsides. Secondly, the study of station keeping in a co-planar non-Keplerian orbit is conducted based on the Tschauner-Hempel equations of motion. Chapter

7

4 deals with the deployment and Station Keeping of spacecraft based on a Lyapunov function control strategy. Although deployment is an important part of formation flying, this subject apparently, until now, has received little attention. A preliminary study by Badesha, et al. [32] involves the deployment of six micro-satellites, one at a time, from a bus. At the initialization state, the satellites fly in an along-track trajectory separated by nominal spacing. The study entailed the development of a two-body (bus and satellite) relative motion propagator based on the Clohessy-Wilshire equations with drag, from which the relative motion of the micro-satellites is deduced. Their investigation did not result in an optimum deployment strategy. Badesha is hopeful that information gained will be useful for future studies involving minimizing global fuel and cost. Other references pertaining to deployment/Station Keeping can be found in Chapter 4 of this document.

As a background, control theory deals with the dynamic response of a system to commands or disturbances. The translation of physical design objectives into a dynamical system gives rise to the control problem. The key elements involved are:

- A dynamical system which is to be "controlled"
- A desired output or objective of the system
- A set of allowable (or admissible) "controls" (i.e., inputs)
- A performance functional, (or cost function) which measures the effectiveness of a given "control action"

The notion of performance functional, performance index or cost function is no stranger to physics. As a brief review and motivation on this topic, recall the statement from Hamilton's principle for conservative systems in classical physics, "of all possible paths along which a dynamical system may move from one point to another within a specified time interval (consistent with any constraints), the actual path followed is that which minimizes the time integral of the difference between the kinetic and potential energies." Therefore, the cost function or performance index is defined as the action

$$J = \int_0^T L(q,u)dt \qquad (1.1)$$

where $\quad q \equiv$ generalized coordinate vector $\hspace{2cm}$ (1.2)

$u = \dot{q} \equiv$ generalized velocities $\hspace{2.5cm}$ (1.3)

$U(q) \equiv$ potential energy $\hspace{3.3cm}$ (1.4)

$T(q,u) \equiv$ kinetic energy $\hspace{3.3cm}$ (1.5)

$L(q,u) \equiv T(q,u) - U(q)$, the Lagrangian of the system $\hspace{0.3cm}$ (1.6)

Similarly, the general system dynamics are given by the physics of the problem and can

be represented as, $\hspace{2cm} x = f(x,u) \hspace{3cm}$ (1.7)

with

$$x \in R^n \hspace{1.5cm} \text{and} \hspace{1.5cm} u \in R^m , \hspace{2cm} (1.8)$$

(superscript on f means it can in general be time-varying)

while the performance index (PI)

$$J = \frac{1}{2} x^T S x + \frac{1}{2} \int_{t_0}^{t} (x^T Q x + u^T R u) \hspace{2cm} (1.9)$$

J is defined over the interval of interest [i,N], where S is an n x n symmetric , positive definite, constant matrix, Q is an n x n symmetric, positive definite, time-varying matrix and R is an m x m symmetric time-varying positive definite matrix. R is to be fixed at the outset by the designer and the positive definite requirement is to assure each element of u is bounded. Although the above equations are shown for continuous-linear quadratic regulator systems they can easily be set up for a discrete- linear quadratic regulator[14]. Distinctions are noted when dealing with non-linear systems; as is the case when it is necessary to construct a scheme that makes the system follow (or track) a desired trajectory over some time interval.

Control signals in physical systems are usually obtained from equipment which can provide only a limited amount of force or energy. This necessitates placing restrictions or

constraints upon the set of controls which satisfy the constraints (set of admissible controls). For most physical systems, the desired objective can be attained by many admissible inputs, each of which results in a different response. Therefore, the best one needs to be selected. This requires the use of a performance criterion (functional).

Linear programming is concerned with the science of decision and its application. The concept of optimization is now well rooted as a principle underlying the analysis of many complex decision or allocation problems. It offers a certain degree of philosophical elegance that is hard to dispute, and it often offers an indispensable degree of operational simplicity. Using this optimization philosophy, complex decision problems involving the selection of values for a number of interrelated variables will be approached by focusing attention on a single objective designed to quantify performance and measure the quality of the decision. The one objective is maximized (or minimized) subject to the constraints that may limit the selection of decision variable values [33,34,35]. Stated mathematically, problems such as these belong to the calculus of variations or the Brachistochrone problem.

Optimal Control Theory (a means of determining or finding for a given process the control that is best in some sense) was developed as a result of attempting to solve the dynamics of classical systems which were no longer linear time - invariant; that is, those systems whose components could no longer be adequately described by ordinary linear differential equations with constant coefficients. It provides the means of combining linear programming with control theory. It is a branch of applied mathematics and also of control engineering. Methods for designing optimal control systems require sophisticated mathematical tools. Linear Quadratic Regulator (LQR) theory [36] will play major roles in the development of algorithms used in this research. Kluever and Tanck [37] investigated a feedback control law for autonomous station keeping maneuvers based on the discrete version of the linear Clohessy-Wiltshire equations of motion and the discrete time asymptotic LQR. Tan, Bainum and Strong [38] investigated a nonlinear feedback control law, based on a Lyapunov function, for maintaining separation distances between several spacecraft in a coplanar elliptical orbit, by applying this function to the osculating orbital elements of the daughter spacecraft. Typically, to solve a LQR problem, one begins by defining a

performance index to be optimized or the Hamiltonian function, such as

$$H = \frac{1}{2}(x^T Q x + u^T R u) + \lambda^T (A x + B u) \qquad (1.10)$$

where the state and costate equations are

$$x = \frac{\partial H}{\partial \lambda} = A + B u$$

$$\lambda = \frac{\partial H}{\partial x} = Q x + A^T \lambda \qquad (1.11)$$

and the stationarity condition, provided u is unconstrained is

$$0 = \frac{\partial H}{\partial u} = R u + B^T \lambda \qquad (1.12)$$

accordingly $\qquad u = -R^{-1}B^T \lambda \qquad (1.13)$

so the optimal control sequence is determined if the costate sequence can be found. The constraint or system equation is a recursion for the state x that develops forward in time, while the costate equation is a recursion for λ that develops backward in time. The (fictitious) Lagrange multiplier is thus a variable that is determined by its own dynamical equation, and it will be seen that the optimal controller is not causal.

Deployment of spacecraft is based on maneuvers from a "mother satellite." In this research two approaches are suggested:

(1)   Based on near Hohmann type transfer orbits where the impulses of the thrusters is used to augment the energy required from the transient orbit to the final orbit and the four spacecraft are deployed sequentially from the initial circular orbit with a small time delay selected to correspond to the desired shift in the angle between the

semimajor axes of the orbits of the adjacent satellites. For the first spacecraft a single impulse Hohmann transfer is required. For the remaining three a very small second impulse would also be required at the second perigee position in the final elliptical orbit. This method, described in Chapter 4, is based on the utilization of the least maneuver energy.

(2)   Based on a solution to the nonlinear (track a desired trajectory over time) two point boundary value problem (TPBVP) following Pontryagin's Principle[39,40]. The TPBVP is evident by the state equation and the adjoint costate system, since the boundary conditions required for solution are the initial state x_0 and the final costate λ_N. These problems are in general extremely difficult to solve. Implementation may involve numerical techniques for solving TPBVP such as the quasilinearization or shooting techniques.

The solution to two-point boundary value problems has been attempted in a variety of methods, among them: Interpolation methods, variational methods, method of collocation, Picard's method, discrete methods, finite different methods, quasilinearization, and shooting methods. The 'shooting method' and quasilinearization will be relied on to solve these equations, mainly because of the familiarity in these two areas[41,42]. Quasilinearization will be satisfied with the aid of recent advances in MATLAB. A summary of the two techniques is listed below :

1. Quasilinearization. This method is applicable only to two-point boundary value problems for systems of nonlinear ordinary differential equations. The original nonlinear problem is replaced by a sequence of more easily solved linear problems whose solutions converge under appropriate conditions to the solution of the original problem.

2. Shooting methods. This method takes its name from the situation in the two-point boundary value problem for a single second order differential equation with initial and final values of the solution prescribed. The initial slope is varied to give rise to a set of profiles which suggest the trajectory of a projectile "shot" from the initial point. That initial slope is sought which results in the trajectory "hitting" the target, the final value.

These methods may not be so well-known, mainly due to perhaps the mis-perception

that they lack a certain amount of elegance. The reader can be assured that these methods contain all the mathematic rigor in development worthy of its place in pure and applied mathematics [43,44,45,46].

In this report only the first approach to the deployment problem will be treated. The two point boundary value problem approach(TPBVP), currently in progress, will be treated in the second year final report.

## II. SELECTION OF BASELINE (STRAWMAN) CONFIGURATION

A study was conducted of proposed NASA and ESA constellation configurations which would measure and study upper atmospheric phenomena. The Auroral Cluster (Multi scale) System, the Distance Measurement System, the Orbiting Interferometer System, as suggested by NASA for LEO mission together with the Solar Stereo System in heliocentric orbit were all considered as possible baseline or "strawman" configurations [47]. In addition information was also obtained from the ESA web page on the proposed ESA Cluster mission with the objective of determining physical processes involved in the interaction between the solar wind and the magnetosphere by visiting key regions such as the polar cusps and the magnetotail. Up to four Cluster spacecraft would map in three dimensions the plasma structure contained in these regions. Simultaneous multi-point measurements would also allow differential plasma quantities to be derived for the first time. Cluster's main goal is to study the small scale plasma structures in space and time in key plasma regions: solar wind and bow shock; magnetopause; polar cusp; magnetotail; and the auroral zone. The preliminary design of each cluster spacecraft would be based on spin stabilization at a nominal rate of 15 rpm, with the in-orbit configuration characterized by two 5 m long experiment radial booms, four 50m long experiment wire booms, and two axial telecommunications antenna booms, with the spacecraft diameter of 2.9 m, height of 1.3 m, dry mass of 550 kg, propellant mass of 650 kg, and payload mass of 72 kg [48].

After reviewing the candidate configurations for satellite constellations, the Auroral Multiscale Mission (AMM) was chosen as a baseline or "strawman" model for this research. The reason for this selection is that the AMM has the objective of upper atmosphere science, and its configuration is relatively uncomplicated. A brief description and sketch of this system is given in Fig.2.1 and Table 2.1. It is assumed that this relatively simple system would not have autonomous navigation capability. Initially for this study the "strawman" configuration would be based on four spacecraft in the same plane, principally along the orbit track. The perigee altitude is selected to be 600 km, the apogee altitude is selected to be 8000 km. And the nominal separation distance between two adjacent satellites is taken to be 500

km.

Figure 2.1

<u>Auroral Multiscale</u>
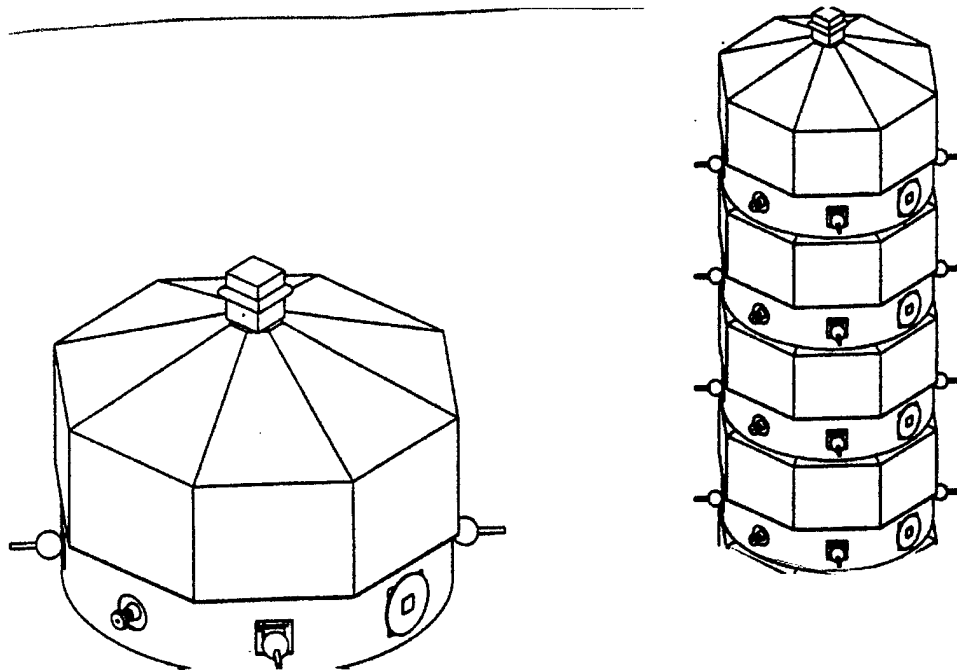
Single AMM Spacecraft/Stowed Configuration   **Launch Configuration**

Table 2.1

Strawman Configuration

Mission	Multi-point 3-dimensional data collection of auroral phenomena
Orbit	600×8000 km, 83° inclination*
Launch Vehicle	Taurus (2110 vehicle), Insertion Mass of 465.5 kg, argp=203.1°
Spacecraft Size	40 inch diameter (across flats)
Spacecraft Mass	90 kg each
Science Payload	Ion/Electron spectrometer, UV Auroral Imager, Magnetometer, Electric Fields (3-axis)
Position Knowledge	GPS, Knowledge to 100 meters (3 sigma)
Attitude Knowledge	0.01° Star Tracker (referenced to magnetometer), star-tracker implementation. Spinning sun-sensor / magnetometer provides coarse attitude.
Power	Solar array capability: 40 watts orbit average power. Energy Storage: Dual IPACS Flywheel momentum bias system used for both power and attitude control

*83 degrees is the proposed inclination angle for the AMM. To simplify the problem and calculations for initial positions/velocities components, it is easier to assume $i = 0$, which has been done in this report.

III.. STATION KEEPING MANEUVERS

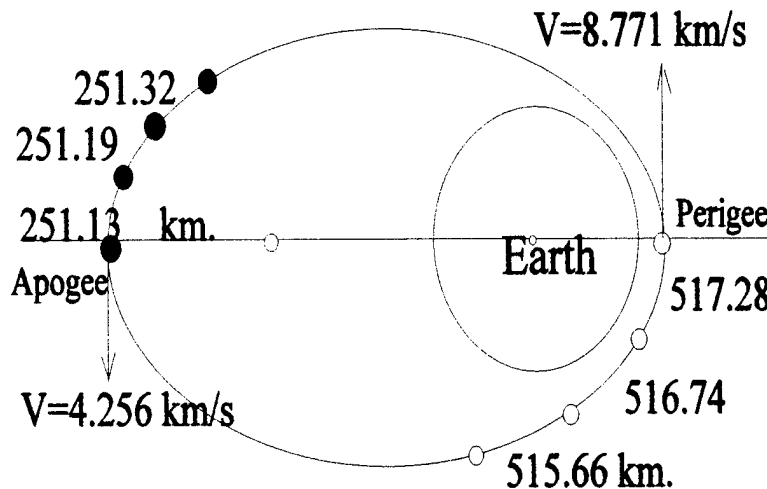### 3.1 In Plane Station Keeping Based on Shift of Line of Apsides

Fig. 3.1.1 Variable Velocities & Phase Distances

Following and expanding on the article by Tan, Bainum, and Strong [49], where it was noted that without any perturbation or any control in a nominal Keplerian orbit, given the velocity at perigee and separation distance, then one would achieve near apogee the separations shown in Fig.3.1.1. From Fig.3.1.1 it is seen that the separation distances at perigee are more than twice the separation distances at apogee. This is a direct consequence of Kepler's law of equal areas being swept out in equal time by the radius from the Earth to the particular spacecraft. To maintain constant separation distance in such an orbit, one scenario would be based on the necessity to correct the orbit continuously; the tremendous amount of energy required makes this strategy unfeasible.

A novel idea for implementation of the separation distances for the AMM mission was proposed in Ref [49] and is further explained in this section. If there are two satellites in a constellation, the first satellite is appointed as a reference satellite, or mother satellite. The semi-major axis of the orbit of the second satellite should be shifted by a very small angle (something like 1°) with respect to the orbit of the mother satellite in order to achieve

17

the approximately constant separation distance (Fig.3.1.2). The propulsive maneuvers required for such a separation can be calculated based on Lagrange's equations for impulsive thrust [50], and is presented in the Section 3.5. If there are two satellites flying in the orbits shown as Fig.3.1.2, both co-planar and, in 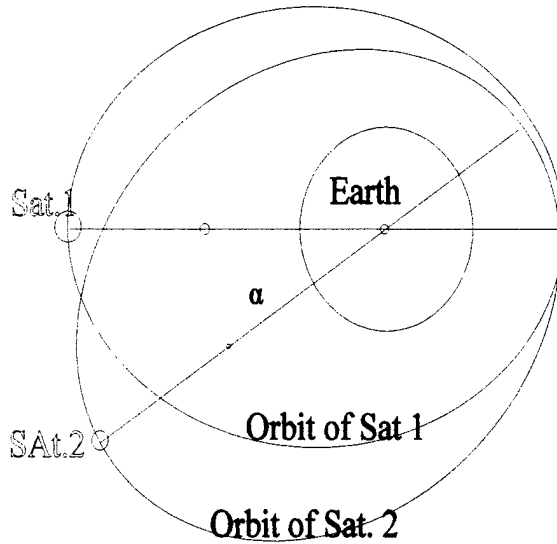the counter clockwise direction, at exactly the same time that they arrive at their perigees and apogees, respectively, the distance between the two satellites is defined as the geometric distance, roughly the distance caused by the shift of the semi-major axis of the orbit; if the satellites are flying in exactly the same orbit (shown in Fig.3.1.1), the distance between the adjacent satellites is defined as the phase distance, i.e . the distance accounted for the time in which the second satellite will reach the mother satellite's current position. From Fig.3.1.2, it is seen that the geometric distance at the perigees is smaller than the one at the apogees. The strategy here is that if the phase distance is compensated by the geometric distance, then the resulting separation distance between the adjacent satellites is maintained to be essentially constant. The details of the calculation are presented as follows:

Fig. 3.1.2 Angle Between Orbits of Two SAT

From Fig.3.1.2, if the angle between the two semi-major axes is α, the distances between satellites 1 and 2 at perigee and apogee (the geometric distances) are

$$2(R + \text{perigee altitude})\text{Sin}(\alpha/2) \quad \text{and} \quad 2(R + \text{apogee altitude})\text{Sin}(\alpha/2)$$

respectively, where R is the radius of the Earth. Let the phase distances at perigee and apogee be Pp and Pa, respectively (Fig 3.1.1), We try to make the resulting distance at apogee the

18

same as the one at perigee, e.g. 500 km. i.e.

$$2(R+perigee\ altitude)\sin(\frac{\alpha}{2})+Pp = 500 \qquad (3..1.1)$$

$$2(R+apogee\ altitude)\sin(\frac{\alpha}{2})+Pa = 500 \qquad (3..1.2)$$

From Fig.3.1.1, it is noticed that

$$\frac{Pp}{Pa} = \frac{517.28}{251.13} \qquad (3.1.3)$$

The solution of equations (3.1.1)-(3.1.3) is $\alpha = 1.34118979436401$ degree. Pp=336.626 km, Pa=163.426 km. That means, satellite 2 arrives at its own perigee (or apogee) 38.396 seconds later than satellite 1 does. Note the ratio defined as Pp/Pa has a value of 2.05980688507. The term ratio will be used extensively in the parametric studies, section 3.4 (Table 3.4.1 (a) and (b)).

3.2 Verification With Orbital Dynamics Simulation Software

It is the intent of this preliminary treatment to illustrate the advantage of the in-plane station keeping based on the (initial) shift of the line of apsides between a mother and daughter spacecraft An example of the constellation in an orbit described above, with separation distance of 500 km., is now given. The simulation is performed by MATLAB for a little more than half an orbit and BG14 [21] for longer time response. BG14 requires precision orbital calculations, based on orbital mechanics, to be used in part as its Initialization Phase. Simulation results are identical, as shown in Table 3.2.1 and Figure 3.2.1(a), respectively.

19

Table 3.2.1.

Time History of Distance between Adjacent Satellites

T sec	D km	T sec	D km	T sec	D km	T sec	D km	T sec	D km	T sec	D km
*	500.0	1152	482.9	2323	477.7	3494	488.0	4646	497.6	5760	499.8
96	499.9	1248	481.4	2419	478.2	3590	489.0	4742	498.1	5856	499.5
192	499.3	1344	480.2	2515	478.9	3686	489.9	4838	498.5	5952	499.3
288	498.4	1440	479.1	2630	479.7	3782	490.9	4934	498.9	6048	498.9
384	497.1	1550	478.1	2726	480.5	3878	491.8	5030	499.3	6144	498.5
480	495.6	1651	477.5	2822	481.4	3974	492.6	5126	499.5	6240	498.1
576	493.8	1747	477.0	2918	482.2	4070	493.5	5222	499.8	6336	497.6
672	491.9	1843	476.8	3014	483.2	4166	494.3	5318	499.9	6432	497.0
768	490.0	1939	476.7	3110	484.1	4262	495.0	5414	500.0	6528	496.4
864	488.1	2035	476.7	3206	485.1	4358	495.7	**	500.0	6624	495.7
960	486.2	2130	476.9	3302	486.1	4454	496.4	5568	500.0	6720	495.0
1056	484.5	2227	477.2	3398	487.0	4550	497.0	5664	499.9	6816	494.3

T is the time from the perigee, D is the distance between adjacent satellites, * is the perigee, T=0;
** is the apogee, T=5490.7 sec. from perigee.

Without perturbations, such as the atmosphere drag, flatness of the Earth, the effect of the magnetic fields of the Earth, the perturbations from the Moon, the Sun and the planets, and so on, the resulting separation distance will be kept essentially constant forever; Fig 3.2.1(b), over a 30 day duration, gives credence to this notion. The energy expended is only to be used to compensate for these relatively small perturbations. According to this design, significant control energy can be saved while maintaining relatively constant separation distances between adjacent satellites in an elliptical orbit. In addition, the control logic and its implementation for constant separation distance within a constellation are much easier than for the case of time varying separation distance. If the separation is varying, that is, the separation distance is different at each point of the orbit, the measurement of the error of the

20

separation distance requires the information of the satellite location in the orbit. If the separation distance is constant, the measurement requires only a distance sensor.

To study the effect of perturbations due to a non-spherical Earth and the atmospheric drag the BG 14 program was utilized with the same initial conditions used in Table 3.2.1. The effects of the Moon and the Sun are also included but are thought to cause much smaller perturbations. Figures 3.2.1(a) through 3.2.2(f) show the results from this numerical procedure. There is virtually no indistinguishable difference in separation distance between the case with first order oblateness and drag as compared with the case of first order oblateness without drag. This is attributed to the relatively high perigee altitude of 600 km used in this example. This result is different than that shown in the paper [49], due mainly to precision of significant figures. Fig 3.2.2(a) ,which includes gravity degree 4, drag, and solar radiation is the same as Fig 3.2.2(b) but over a shorter time. Fig 3.2.2(c) includes the perturbations of gravity degree 4, drag, and solar radiation, and shows the response of Figs 3.2.2(a) and 3.2.2(b) over a longer period of time with the one radial thrust-impulse at the first perigee; a secular perturbation, where the amplitude of oscillation increases with time, however the mean value decreases. Fig 3.2.2(d) includes the perturbations of gravity degree 4, and solar radiation. Fig 3.2.2(e) includes the perturbations of gravity degree 4, and drag. Fig 3.2.2(f) is included to show the effect of no initial shifting of the lines of apsides in a perturbed orbit. In the same article by Badesha [32], formation flying for circular orbits was also addressed. It is not the intent to compare 'apples with oranges,' but it can be seen from these examples, better results and seemingly better control are achieved than that of Badesha. In Badesha's paper, the spacing between two spacecraft oscillate between 10 and 70 m with the orbital period. The amplitude of the oscillation decreases with time but starts to increase after 9 days. After approximately 21 days, the satellites have a potential to collide. It can be concluded for both the cases shown in Table 3.2.1 and Fig.3.2.1, that subsequent station keeping requirements would be far less than those associated with the original system shown in Fig.3.1.1. As compared with the Keplerian results of Table 3.2.1 or Figs 3.2.1(a) and 3.2.1(b), using the same initial orientation between the lines of apsides of the mother and daughter satellites, it is seen that the separation distance at each subsequent apogee is less

21
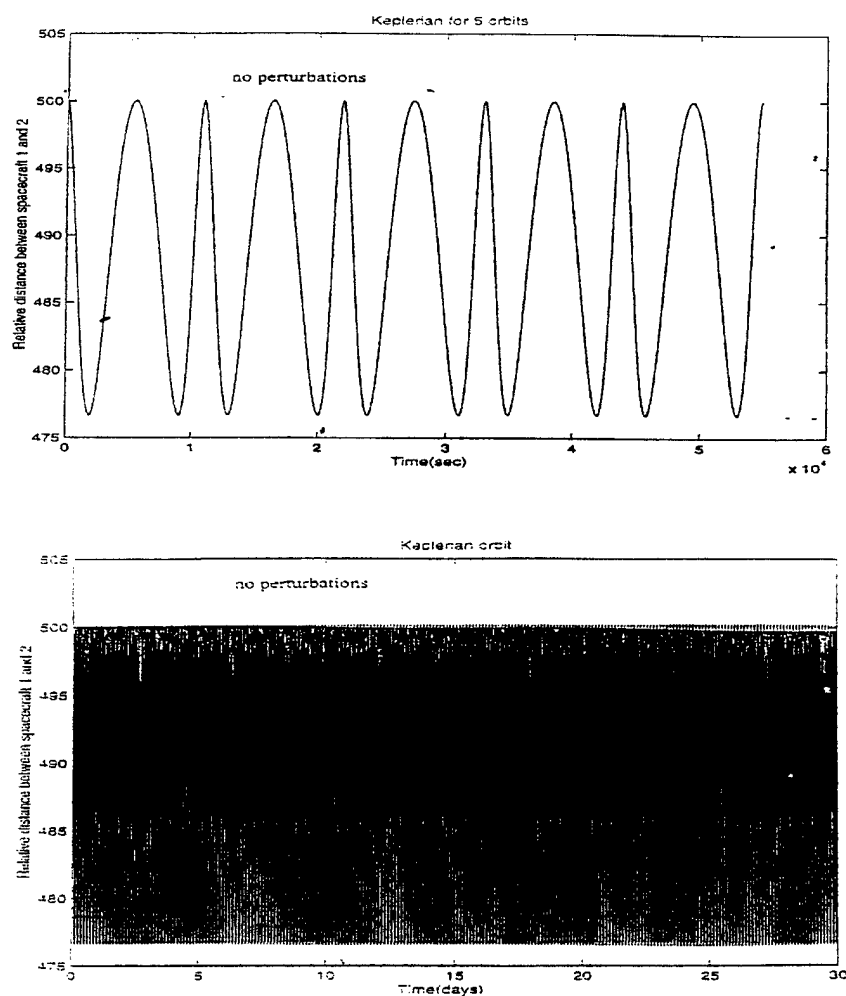
than the required 500 km.

Fig. 3.2.1(a & b). 30 Day Time History of Separation Distance between Mother and Daughter Satellite Keplerian Orbit
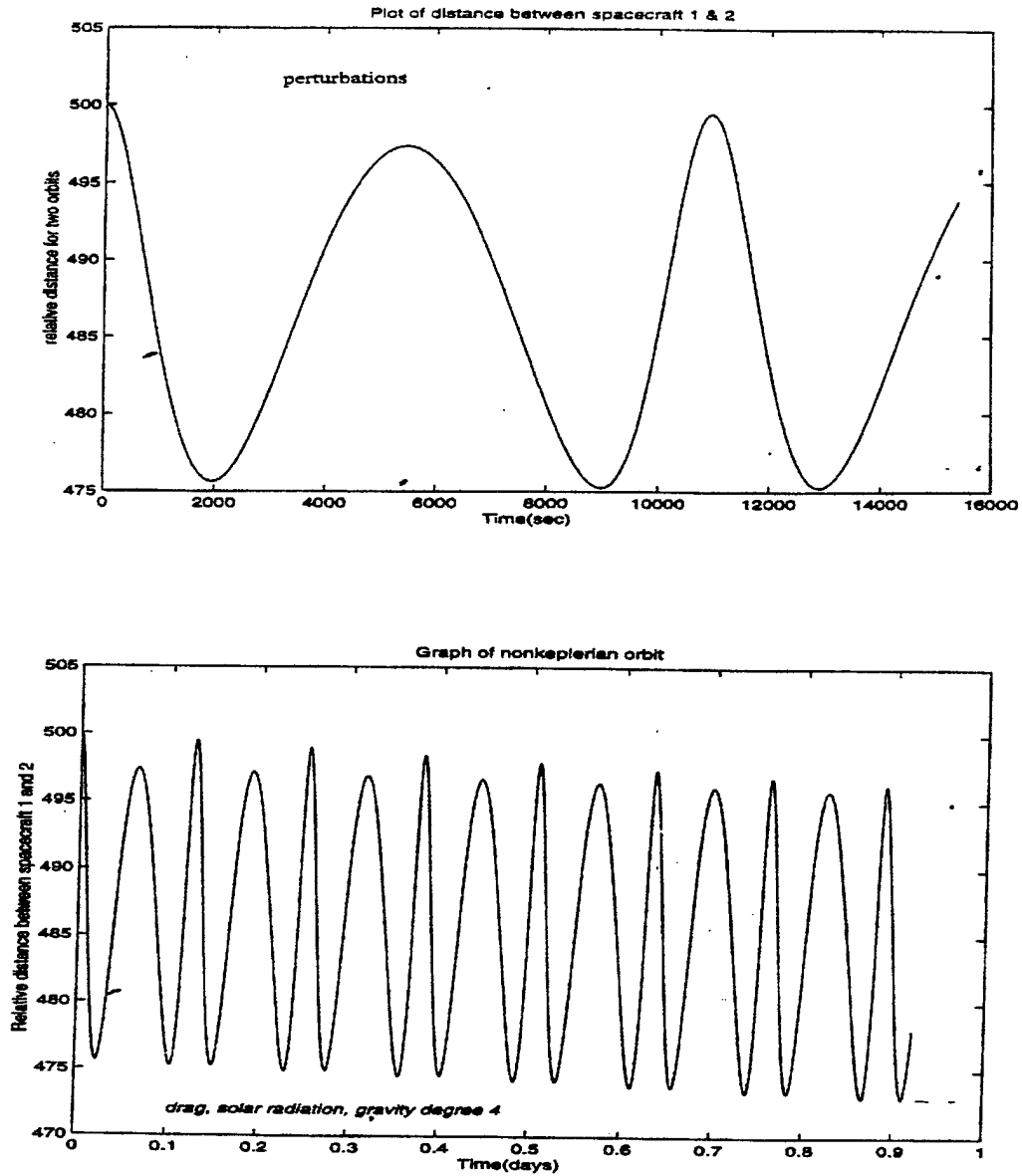
22

Fig. 3.2.2(a & b). The Distance between Adjacent Satellites
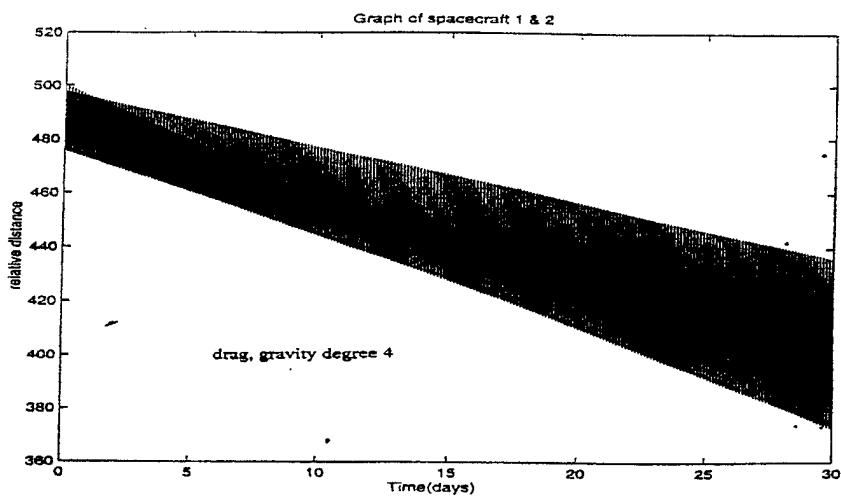with Various Perturbations Simulated by BG14

23
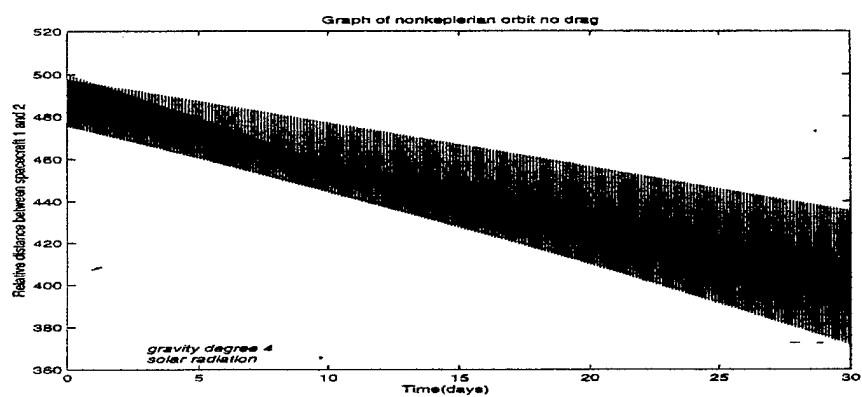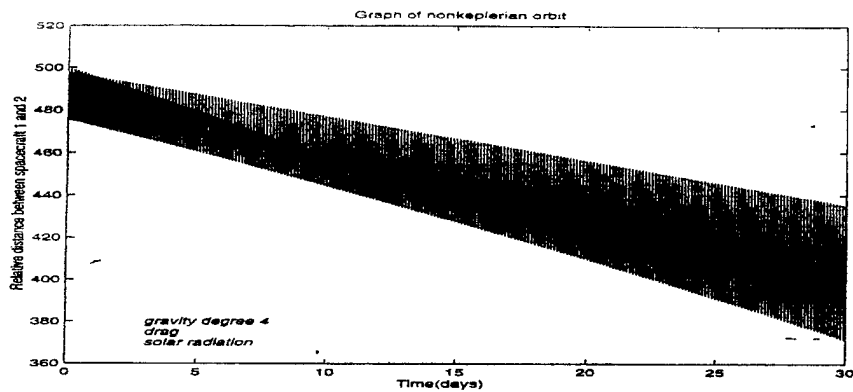
Fig. 3.2.2(c,d & e). 30 Day Time History of Separation Distance between Mother and Daughter Satellite Various Perturbations

24

Plot o *f* spacecraft, *NO* initial shift

(y-axis: Relative distance km; x-axis: Time(days))

drag, solar radiation, gravity degree 4
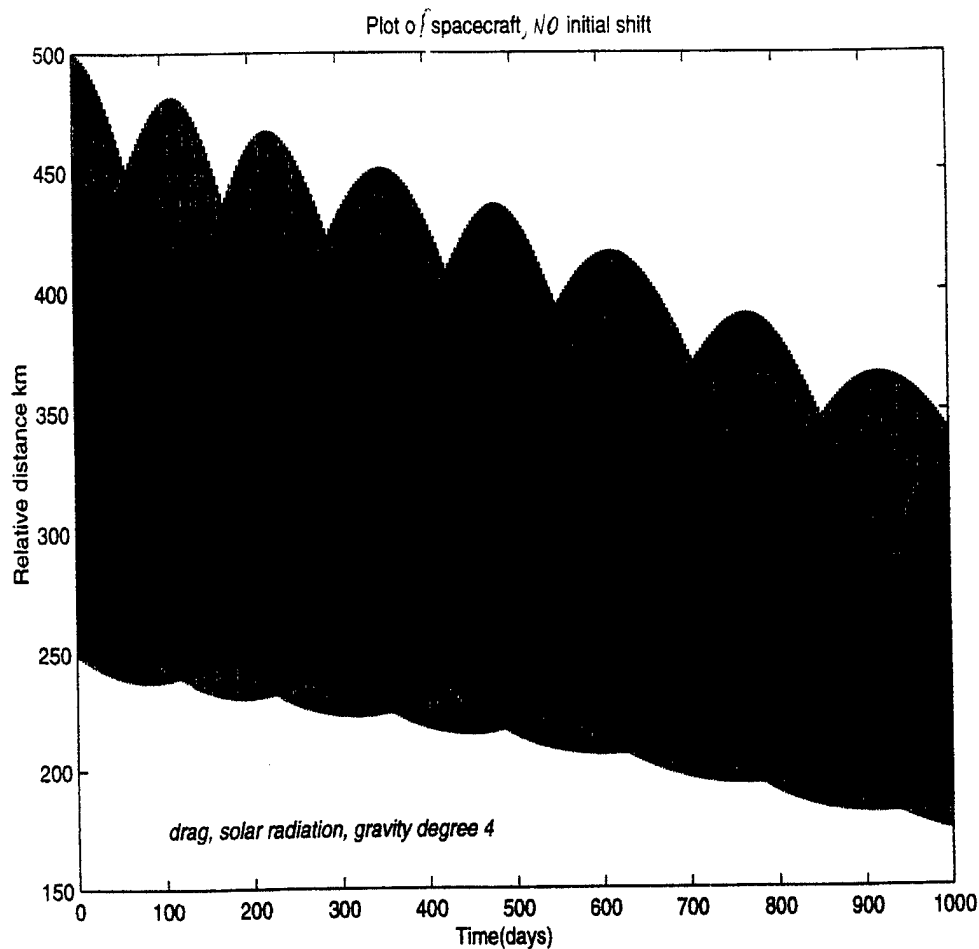
Fig. 3.2.2(f). 30 Day Time History of Separation Distance between Mother and Daughter Satellite Non-Keplerian Orbit

Figures 3.2.2(c) through 3.2.2(e) show that the Earth's oblateness (J_2) is perhaps the dominating factor causing the secular perturbation. In a perturbed orbit, and allowing no shifting of the lines of apsides and the spacecraft are allowed to be separated as in Fig. 3.1.1, the secular perturbation still exists(see Fig. 3.2.2f), but the amplitude of the oscillations is much greater than in Figs. 3.2.2(c) through (e). Another interesting observation that can be

25

especially recognized from Figures3. 2.1(a), 3.2.2(a) and 3.2.2(b), is Kepler's second law in effect (i.e., equal areas in equal time). From these plots, perigee being the first amplitude, reveals a smaller area under the curve than the area under the next amplitude (apogee). As the secular drift continues, a natural question would be, "what happens after 30 days", or "will the satellites ever collide if not further corrected, and if so,when?" These concerns are addressed in Section 3.6.3.

A series of programs (software) were used to aid in the execution of BG14 and to generate plots. One program was used to provide inputs, based on the desired configuration, as part of the initialization phase for BG14. From the BG14 input file an output file is produced. The short routine, which follows, written in MATLAB, is used to make many of the plots contained in this document:

```
[trial_dat, trial_desc] = readbg14(' filename ');
plot(trial_dat(:,1), trial_dat(:,2));
xlabel(trial_desc(1,:));
ylabel(trial_desc(2,:)); or alternate ylabel(' appropriate comments' );
title(' desired caption' );
text( enter coordinates, ' \ it { desired comments }');
legend( 'a+b', 'a = sin(x)', 'b = cos(x)');          legend may not be necessary
```

It should be noticed that this program requires the function routine (readbg14) in order to read the output file produced by BG14's input file.

3.3 Further Improvement {consider thrust at apogee and perigee}

In order to compensate for those initial effects, as depicted in section 3.2, additional impulses may be desired. From the article by Schaub, et.al.[51], correcting a particular orbital element (a, e, i, Ω, ω, M) causes subsequent errors in other orbit elements. Two corrections schemes will be investigated for removal of the secular perturbation. A feedback control system and a scheme made popular by Battin will be investigated for possible control sometime after the impulsive maneuver. The correction scheme is now introduced following the derivation of Battin, Chap 11, Sect. 6 [52], where Encke's method is used to

26

calculate a ΔV, in an attempt to further improve station keeping after initially shifting the line of apsides. Encke's method involves the planetary equations of motion. Orbital elements are derived from these equations of motion. Thus, correcting a single orbit element has an effect on the equations of motion, in general. With the aid of a transition matrix, a ΔV was calculated which in turn was used to calculate the impulse needed to make the desired maneuver (due to the nature of BG14). The result, as will be seen, of this scheme produced no added benefit as compared with the single orbit correction scheme as initially used. To proceed, Neustadt[53], and also Stern and Potter[54] noted that, at most, n impulses are needed if the state space is n-dimensional. Thus at most 4 impulses are needed for this problem. Therefore, a second impulse was assumed at apogee. To develop the required mathematics and transition matrix, suppose that at some time, t, the spacecraft is found to deviate from the reference path by an amount $\partial r(t)$ in position and $\partial v(t)$ in velocity. One must determine what the velocity deviation should be for that particular position deviation so that the vehicle will arrive at the target point at the predetermined or reference time (t_a, i.e., time at apogee in the Keplerian orbit).

$$\begin{pmatrix} \partial r(t) \\ \partial v(t) \end{pmatrix} = \Phi(t, t_1) \begin{pmatrix} 0 \\ \partial v(t_a) \end{pmatrix}$$

It remains to determine the partitioned transition matrix where it is noted that at any time t later than t_1:

27

$$R^*(t_1) = -R^T(t)$$

where

$$\Phi(t,t_1) = \begin{pmatrix} \tilde{R}^*(t) & R^*(t) \\ \tilde{V}^*(t) & V^*(t) \end{pmatrix} = \begin{pmatrix} \partial r / \partial r_1 & \partial r / \partial v_1 \\ \partial v / \partial r_1 & \partial v / \partial v_1 \end{pmatrix}_{ref}$$

and

$$\begin{pmatrix} \partial r_1 \\ \partial v_1 \end{pmatrix} = \Phi(t_1,t) \begin{pmatrix} \partial r \\ \partial v \end{pmatrix}$$

$$\Phi(t_1,t) = \begin{pmatrix} \partial r_1 / \partial r & \partial r_1 / \partial v \\ \partial v_1 / \partial r & \partial v_1 / \partial v \end{pmatrix}_{ref}$$

so that $\Phi(t,t_1)\Phi(t_1,t) = \tilde{I}$ $\tilde{R}(t_1) = \tilde{I}$ $\tilde{V}(t_1) = 0$

$$R(t_1) = 0 \qquad \text{and} \qquad V(t_1) = \tilde{I}$$

R and V matrices represent deviations in position and velocity from the reference path. Also $r_{ref}(t)$ and $v_{ref}(t)$ are the position and velocity vectors at time t for a vehicle in a reference orbit. Then $\partial r(t) = R^* \partial v(t_a)$ & $\partial v(t) = V^*(t)\partial v(t_a)$ eliminating $\partial v(t_a)$ one obtains the velocity vector V (whose gradient with respect to r is C*) and is that velocity required at r to reach the target point. If a velocity correction $\Delta V(t)$ is to be made at this time, it can be expressed as

$$\Delta V(t) = \partial v(t^+) - \partial v(t^-) = C^*(t)\partial r(t^+) - \partial v(t^-)$$

where the superscripts - and + are used to distinguish the velocity just prior to a correction from the velocity immediately following the correction. For these calculations to remain valid, it is necessary to restrict the magnitude of the deviations from the corresponding nominal values. Alternately, one could target any intermediate point r_T such as the point on the planet's sphere of influence through which the reference orbit passes at the reference time t_T. Then, if r and v are the position and velocity of the vehicle at the time the correction is to be made, these vectors can be extrapolated to the time t_T, using an orbital integration technique, such as Encke's method, in order to determine the point r'_T where the spacecraft would be found at the reference time if no corrective action were taken. By calculating the conic arc connecting the position vectors r and r'_T with a transfer time of $t_T - t$ (i.e., solving Lambert's problem, Battin[52] Chapter 7) the conic velocity v_{c1} (Non-Keplerian orbit) at r is determined. A second conic arc connecting the spacecraft position vector r and the desired target point t_T produces the conic velocity vector v_{c2} (Keplerian orbit). The difference between the conic velocity and the vehicle's actual velocity is a good measure of the effect of the disturbing perturbations. If this velocity is corrected for the effect of perturbations, the velocity necessary to reach the desired target from position r is obtained. Therefore an excellent approximation to the required velocity correction is just the difference between the two conic velocities; specifically,

$$\Delta V = v_{c2} - v_{c1}$$

In other words, the ΔV needed for a pursuer spacecraft (non-Keplerian orbit) and target spacecraft (Keplerian orbit) can be approximated, by noting the small differences in velocity of the two spacecraft with respect to small differences in their respective orbits.

This computation may be repeated iteratively to achieve the desired degree of convergence. One would repeat the algorithm(Fig. 3.3.1) performing step 2 through 6 as often as necessary. At present this is very time consuming and laborious. Obviously there is a need for automation, whereby, the process can function or execute iteratively.
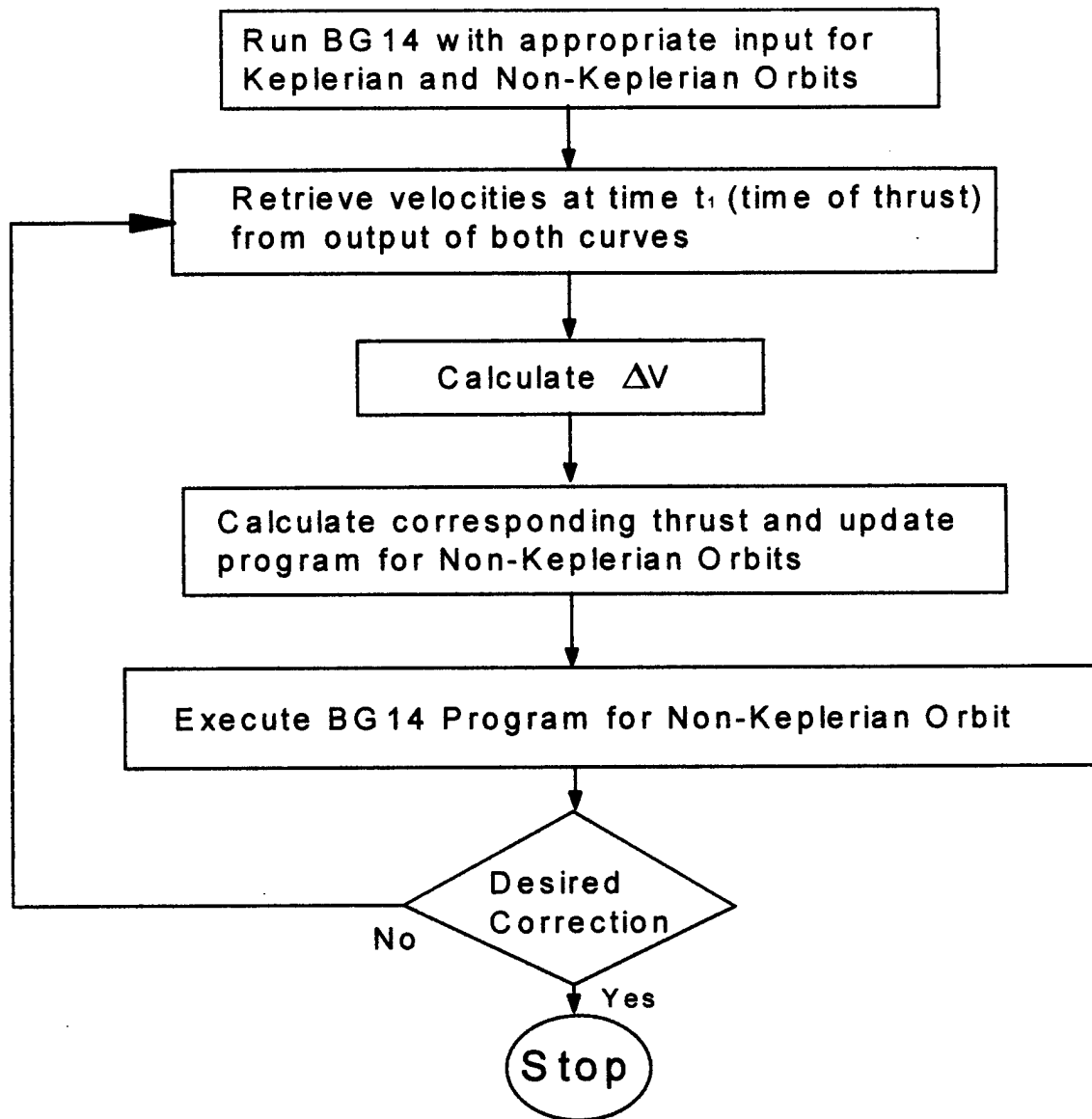
Figure 3.3.1 Computation Algorithm

Employing the above algorithm with the following velocities and calculated values as in Table 3.3.1.

Table 3.3.1

	Keplerian Orbit	**Non-Keplerian Orbit**	**ΔV(km/s)**	**Δ $\hat{V}_i$ (km/s)***
$\dot{x}(1)$	.11455918796536	.14669367598619	-.032134488021	-.960574973467
$\dot{y}(1)$	-4.25483469618012	-4.2641354338482	.00930073767	.278020792948
$\dot{z}(1)$	.00000154838281	.00001488945842	$-1.334107561 \times 10^{-5}$	-.01178
$\dot{x}(2)$	-.05991132583111	-.02700319251021	$-3.21100658009 \times 10^{-2}$	-.950518573882
$\dot{y}(2)$	-4.25609922462398	-4.26659407793047	.0104948533	.310667472738
$\dot{z}(2)$	.00000166706955	.00001526738801	$-1.360031845 \times 10^{-5}$	-.000402595104525

(Apogee occurs at $6.35416666667 \times 10^{-2}$ days, values in table occurred at t just prior to apogee i.e. $6.3194444444 \times 10^{-2}$ days) Both spacecraft maneuvered based on an inertial system.   Note: * $\Delta \hat{V} \equiv \Delta \overline{V} / |\Delta \overline{V}|$

32

The burn times are calculated from the information in Section 3.5. In that section, a force impulse of 3.49397660879 NS was found. That is, an input of 1 Newton for 3.49397660879 seconds. This corresponds to $\Delta V = .0388219623199$ m/sec. In the case at hand, spacecraft no.1 has a $\Delta V_{c1} = .0334533887605$ m/sec and spacecraft no.2, $\Delta V_{c2} = .0337816289794$ m/sec. Therefore $\Delta V = .0003282402189$ m/sec, using ratio and proportion, it is determined that force impulses of 3.01080498844 Nt-Sec and 3.04034660815 Nt-Sec are needed, respectively. The magnitude and direction for velocity components are input via 'direction' into the BG14 input file. These directions are to be entered as input, in unit vector form. It is worth noting that there are different interpretations in terminology as it relates to the direction component, in the astronautical community. Instead of the normal right hand system one may be accustomed to, BG14 uses the right hand system as depicted in Figure 3.3.2. 'X' is radial, 'Y' is along track, and 'Z' is in the opposite direction (anti or nadir direction). In other systems, one may find radial as 'R' and the term 'altitude' used interchangeably, 'B' represents the tangential or along track component and 'N' represents the component normal to an orbit plane. For the case at hand, the 'Y' direction is along track, 'X' is radial, and 'Z' component input will be opposite to that as calculated in the table. The inputs are entered in the direction line of code, as unit vectors. Their order being: along track (Y component),
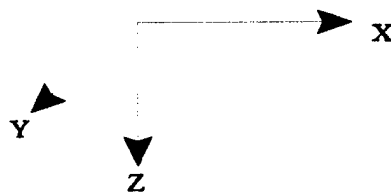crosstrack(Z component), and
radial (X component).

Figure 3.3.2

Both spacecraft maneuvered

Relative distance between spacecraft

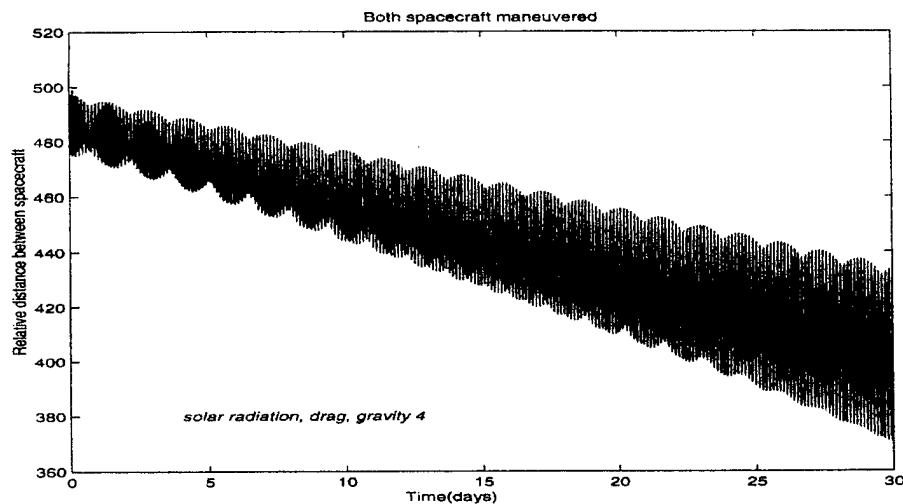*solar radiation, drag, gravity 4*

Time(days)

Figure 3.3.3 30 Day Time History of Separation Distance between Mother and Daughter Satellite Non-Keplerian Orbit

Utilizing the above method, Figure 3.3.3, shows the results with both spacecraft subject to impulsive maneuvers at the first apogee. There is no significant difference in the secular drift time history as compared with the results shown in Figs. 3.2.2(c) - (e) based on only the first impulse taken at the first perigee. A second study, considered the effect of a second impulsive maneuver of the daughter spacecraft alone, at the first apogee, after an initial maneuver at the first perigee. Then the Mother Spacecraft and its orbit will be considered as the reference or fixed orbit. Now with a revised algorithm, Table 3.3.2 becomes appropriate. Figure 3.3.4 shows the time response simulated by BG14 over a 30 day period. In this case a $\Delta V = .124057$ m/sec corresponding to an impulse of 11.1651 NS and is assumed to occur in the radial direction at the first apogee. This represents about three times the impulse assumed for the first radial maneuver at the first perigee. By comparing Figure 3.3.4 and Figures 3.2.2(c, d & e), it can be seen that the response of Figure 3.3.4 has

34

almost the same characteristics except for a small amplitude ("flattening out") of the maximum and minimum peak amplitudes. There is also no significant difference between the results of Fig. 3.3.3 and Fig. 3.3.4.

Table 3.3.2

Mother's Orbit		Daughter's Orbit	ΔV(km/s)	$\Delta \hat{V}_i$ (km/s)
$\dot{x}(1)$	.16993707421676	.29387179316892	-.123934718952	-.999012809158
$\dot{y}(1)$	-4.2633650433302	-4.25785404506646	-.00551099826	-.0444230470649
$\dot{z}(1)$	.00001498390224	.00001563415649	$-1.5025425 \times 10^{-7}$	-5.24156854877 X 10^{-6}

(Apogee for Mother is 5490.7 sec and 5529.096 sec for Daughter)

$\Delta V = .124057187071$ m/sec or an impulse of 11.1651468364 N S.
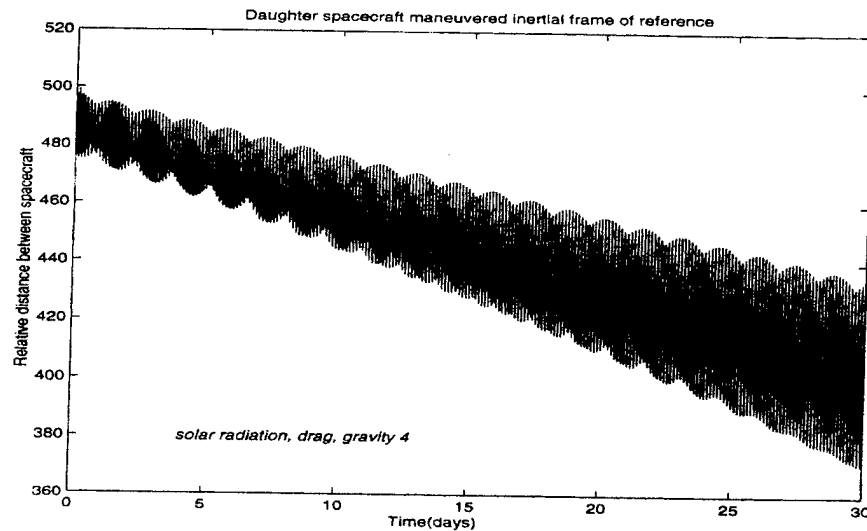
Figure 3.3.4 30 Day Time History of Separation Distance between Mother and Daughter Satellite Non-Keplerian Orbit

As a final point, all the above maneuvers were performed based on an inertial reference frame. The study now continues with a displacement in the relative motion in a rotating LVLH (local vertical, local horizontal), Table 3.3.3, coordinate system where Spacecraft no.1 is fixed. An explanation of an LVLH coordinate system, follows that of Bond and Allman [55].

Table 3.3.3

Chaser / Daughter's Orbit	ΔV(km/s)	$\Delta \hat{V}_i$ (km/s)
Δx	-497.30555231311	-.0910816030378	-.999846745675
Δy	-.00109369196631	-.0000002003098	-.00030046483
Δz	8.70752230559343	.0015947843	1.75067174844 X 10^{-2}

36

LVLH Coordinate System. (Time 5459.9999997 seconds)

ΔV = .0910955638269 m/sec or an impulse of 8.19860074442 NS. A plot of this maneuver (not included in document) supports the fact that the physics is the same, regardless of the reference system. Thus, the results are no different than those of Figures 3.3.3 and 3.3.4. However, now a ΔV = 0.0911 m/s corresponding to an impulse of 8.1986 NS was assumed to occur in the radial direction at the first apogee.

Assuming that the Battin's scheme is successful, the secular drift will again become a concern if spacecraft are allowed to travel for some additional time without a subsequent correction. In the final analysis, it is clear that a different type of subsequent maneuver is needed other than continuing to shift lines of apsides. A feedback control will be studied later in Section 3.6 of this document.

3.4 Parametric Trade - Off Studies

Tables 3.4.1(a) and (b) show a summary of the MATLAB input in preparation for using the BG14 software in order to conduct a parametric study over a range of nominal separation distances and phase difference ratios (or alternatively line of apsides orientation shift angles). The phase distance ratio is defined as the nominal ratio of separation distance at perigee to the separation distance at apogee in the nominal uncorrected Keplerian orbit. In this section, different than that of Section 3.1 and 3.2, distances between spacecraft and their phase distance ratio were arbitrarily chosen as input. In turn, corresponding shift angles and other initial conditions were calculated. That is, a priori, the ratio (2.05980966034) was calculated based on the separation between 'mother and daughter' at apogee. In Table 3.4.1, the initial conditions in cartesian coordinates for position and velocity components have been calculated and are used as inputs to the BG14 orbital propagator software. Note, in keeping with the BG14 coordinate System, the X component of velocity is given in an opposite direction than that calculated by the program used here.

A preliminarily study using six different scenarios or ordered pairs (separation, shift angle in degrees) were chosen as follows: (600, 1.628), (520, 1.402), (520, 1.386), (520, 1.2609),(500, 1.2124) and (100, .27147). For each case simulated, there are two different effects :

(1) The situation where a 4 x 4 non-spherical Earth's gravitational field, aerodynamic drag and solar radiation effects are included .

(2) The situation where only the non-spherical Earth's gravitational field is included- referred to as "no perturbations"

It is seen that there is negligible difference in the response, for the perturbed and non-perturbed cases. For a nominal separation distance of 600 km and an initial line of apsides shift angle of 2.1^{0}, both an increasing and decreasing secular shift in the mother - daughter separation distance is such that a near collision situation occurs approximately every 16 - 17 days. In addition, the maximum subsequent separation distance exceeds 20,000 km, indicating that the two spacecraft are located on opposite sides of the orbit.

For combinations of separation distances and line of apsides shift angles of

38

(520, 2.2), (520, 2.04), (520, 1.8) and (500, 1.8), show similar tendencies to those as the 600 km separation, but alternating between near collisions and maximum separation distance on opposite sides of the orbit. The extreme sensitivity between separation distance history and the initial line of apsides shift angle is particularly apparent by comparison of (520, 2.2), (520, 2.04); representing a difference of 0.16 deg in shift angle. Although both scenarios are clearly unacceptable, the frequency between the near collision events and the maximum separation distance epochs is noticeably different.

The parametric selection of 100 km represents a drastic change in nominal separation distance and 0.27147 deg in line of apsides shift angle. After an initial secular decrease in separation distance followed by near collision, there is a secular increase in the separation distance to almost a maximum of 4500 km at the end of the 30 days. Simulation shows that the 100 km separation case has an initial downward trend, which begins at about day 200, and perhaps a zero relative separation after about 800 days.

Although the results of this parametric study, up to this point, are far from conclusive, the results are quite dramatic. In order to avoid near collision possibility (followed by a maximum separation extending to opposite sides of the orbit...chaos), the success of the initial maneuver is critically dependent on the amplitude of the initial line of apsides shift angle which results from an initial radial impulsive thrusting maneuver.

Table 3.4.1 (a)

Trade-off Studies Using BG-14 Software

Separation	Ratio	Shift Angle degrees	$x1$ km	$y1$ km	$x2$ km	$y2$ km
600	2.1	1.6289008847	6964.102386146758	599.835765352191	6978.14	0.0
520	2.2	1.4022541	6978.321029613882	566.8205583353445	6978.14	0.0
520	2.1	1.4117022666	6967.595400672765	519.8930767241359	6978.14	0.0
520	2.04	1.3862096862	6967.516326413141	519.8914670338451	6978.14	0.0
520	1.8	1.2609713096	6967.133025595134	519.8834931600558	6978.14	0.0
500	2.2	1.3944447015	6968.501857349625	499.9070973826904	6978.14	0.0
500	2.1	1.3574034351	6968.390758465615	499.9049432461227	6978.14	0.0
500	2.04	1.3328914763	6968.317652302147	499.9035120363998	6978.14	0.0
500	1.8	1.2124705669	6967.963280272655	499.8964237732126	6978.14	0.0
490	2.2	1.3665544718	6968.883448342178	489.912559507882	6978.14	0.0
490	2.1	1.3302541343	6968.776750739195	489.91053187127320	6978.14	0.0
490	2.04	1.3062324803	6968.706540682686	489.909185415297	6978.14	0.0
490	1.8	1.1882202775	6968.366206991123	489.9025138004483	6978.14	0.0
250	2.2	.69720944502	6975.730072346111	249.9883826038613	6978.14	0.0
250	2.1	.67868981321	6975.702306271525	249.9881142267019	6978.14	0.0
250	2.04	.66643446716	6975.68403525283	249.987937556445	6978.14	0.0
250	1.8	.60622679964	6975.595467936702	249.9870491241593	6978.14	0.0
100	2.2	.27888233266	6977.754394017853	99.99925353798552	6978.14	0.0
100	2.1	.27147459208	6977.749951986059	99.99922059295476	6978.14	0.0
100	2.04	.26657252458	6977.747028638967	99.99923485956863	6978.14	0.0
100	1.8	.2424897697	6977.732858668894	99.99921363543054	6978.14	0.0

$z1 = z2 = 0$

Table 3.4.1 (b)

Trade-off Studies Using BG-14 Software

Separation	Ratio	Shift Angle degrees	$\dot{x}1$ km/s	$\dot{y}1$ km/s	$\dot{x}2$ km/s	$\dot{y}2$ km/s
600	2.1	1.628901	.751663795138	8.72682812807	0.0	8.75913966311
520	2.2	1.4022541	.20954545507477	8.76555905578956	0.0	8.76806334707253
520	2.1	1.4117022666	.65196146981314	8.73757305465386	0.0	8.76186262409621
520	2.04	1.3862096862	.65197229681564	8.73764604822093	0.0	8.76193622093917
520	1.8	1.2609713096	.65202457063491	8.73799991601468	0.0	8.7622929974399
500	2.2	1.3944447015	.62698519749379	8.73991894922326	0.0	8.76237945291506
500	2.1	1.3574034351	.62699985494731	8.74002158570968	0.0	8.76248287512021
500	2.04	1.3328914763	.62700948319525	8.74008912662367	0.0	8.76255093185438
500	1.8	1.2124705669	.62705597084535	8.74041655778747	0.0	8.76288085016669
490	2.2	1.3665544718	.61450020639866	8.74111151932122	0.0	8.76268458275625
490	2.1	1.3302541343	.6145140039868	8.74121012999996	0.0	8.76278391824823
490	2.04	1.3062324803	.61452306827408	8.74127502151602	0.0	8.76284928566164
490	1.8	1.1882202775	.61456682905557	8.74158960791318	0.0	8.76316616643501
250	2.2	.69720944502	.31402199545938	8.76253789991239	0.0	8.76816287833623
250	2.1	.67868981321	.31402383464524	8.76256374962109	0.0	8.76818877733018
250	2.04	.66643446716	.31440250448148	8.7625807596817	0.0	8.7682058198194
250	1.8	.60622679964	.31403087096743	8.762663217904	0.0	8.76828843380099
100	2.2	.27888233266	.12566819543109	8.76888348495991	0.0	8.76978392368624
100	2.1	.27147459208	.12566829343061	8.76888762984303	0.0	8.76978806954898
100	2.04	.26657252458	.12566840308474	8.76889035650879	0.0	8.76979079750519
100	1.8	.2424897697	.12566882106324	8.76890357598226	0.0	8.76980402161085

$$\dot{z}1 = \dot{z}2 = 0, \qquad \dot{x} < 0$$

For completeness, further studies of the nominal 500 km separation distance were studied concentrating on the small range of shift angles near 1.3414581297943 degrees.

41

The objective was twofold: (1) To determine if other optimal ratios exists, and (2) to determine the level of sensitivity. Table 3.4.2(a,b) contains summary of the data used surrounding the 500 km analysis.

Table 3.4.2(a)

Trade-off Studies for 500 km Separation

Ratio	Shift Angle degrees	$x1$ km	$y1$ km	$x2$ km	$y2$ km
2.2	1.3944447015	6968.501857349625	499.9070973826904	6978.14	0.0
2.1	1.3574034351	6968.390758465615	499.9049432461227	6978.14	0.0
2.04	1.3328914763	6968.317652302147	499.9035120363998	6978.14	0.0
2.05980688507 *	1.3414581297943	6962.3129552193	499.7697508871	6978.14	0.0 *
2.05981	1.34119108298	6968.342368768165	499.9039972175107	6978.14	0.0
2.06	1.34126967	6968.342603013903	499.9040014341221	6978.14	0.0
1.8	1.2124705669	6967.963280272655	499.8964237732126	6978.14	0.0

* Optimal accepted value

Table 3.4.2(b)

Trade-off Studies for 500 km Separation

Ratio	Shift Angle degrees	$\dot{x}1$ km/s	$\dot{y}1$ km/s	$\dot{x}2$ km/s	$\dot{y}2$ km/s
2.2	1.3944447015	.62698519749379	8.73991894922326	0.0	8.76237945291506
2.1	1.3574034351	.62699985494731	8.74002158570968	0.0	8.76248287512021
2.04	1.3328914763	.62700948319525	8.74008912662367	0.0	8.76255093185438
2.05980688507 *	1.3414581297943	.51916724165269	8.7527292910018	0.0	8.770063506 *
2.05981	1.34119108298	.6270062295741	8.74006629141183	0.0	8.76252792236339
2.06	1.34126967	.62700619826428	8.74006607505535	0.0	8.76252770432113
1.8	1.2124705669	.62705597084535	8.74041655778747	0.0	8.76288085016669

* Optimal accepted value, $\dot{x} < 0$

Plots from the scenario using a ratio of 2.05981, which equates to a change in ratio

by .00000311493 from the nominal value, revealed similar results to those already mentioned. That is, an alternation between near collisions and maximum separation distance on opposite sides of the orbits. The change in ratio equates to $1.2886159899913922 \times 10^{-6}$ degrees, hardly a realizable angle for practical purposes. To add, the stated change in ratio causes the following changes in positions and velocities:

Increase in x_1 by $\Delta x_1 = .02941354886500 km$

Increase in y_1 by $\Delta y_1 = .13424633041070 km$

Decrease in v_{x1} by $\Delta v_{x1} = .10783898792141 km / \sec$

Increase in v_{y1} by $\Delta v_{y1} = .012662299958997 km / \sec$

Increase in v_{y2} by $\Delta v_{y2} = .00753558363661 km / \sec$

There is room for error. The above values were generated via a fourth degree polynomial. Thus human selection is needed to pick the desired root. Nevertheless, this supports the fact that very small changes in ratios create significant changes in the kinematics variables.

To verify or to access the possibility of other optimal values, then one could undertake the time laboring tasks of examining possible sequences, and thus determining the range of values for a calculated ratio. Any elementary statistic text on the subject of counting techniques will state:

In a sequence of n events in which the first one has k1 possibilities, the second event has k2, the third has k3, etc., the total possibilities of the sequence will be k1 • k2 • k3 ··· kn.

Therefore, examining the sequence of numbers 2.05980688507 and knowing that 2.05981 is out of the range for acceptable station keeping, then there exist at most

$10 • 10 • 10 • 10 • 10 • 10 • 10 = 10^7 - 1$ variations between the sequence of numbers. The minus 1 accounts for the one already known value. A sufficient proof would be for one to begin with the unacceptable value, while performing necessary variations and proceeding toward the accepted value, or vise versa.

It is now theorized that at most one optimal shift angle exists for each nominal separation. That is, there is one unique ratio (phase to geometry distances) per each given separation, apogee and perigee. To determine the optimal angle for a general separation, a systematic calculation as performed in Section 3.1 must be executed. Attempts to find this unique ratio were investigated using Kepler's law dealing with equal areas. This method also proved to be unsuccessful due to an additional approximation of letting an arc be equal to that of a straight line. To eliminate the additional approximation, the laws of momentum were used to find these angles and thus the relevant coordinates. A glance of the numbers in Table 3.4.3 will not reveal much discernment. However, a plot of the relative separation using BG14 showed the difference. The relative separation of spacecraft produced as a result of conservation of momentum is shown in Figures 3.4.1 and 3.4.2 for 100 and 400 kilometers separations, and is regarded as that based on the most accurate input coordinates.

Table 3.4.3

Coordinates of 400 Kilometers Separation

coordinates found by using Kepler's law of equal area	α=1.0731572546746 degrees		
x1 (km) 6978.137	y1 (km) 0.0	x1' (km/s) 0.0	y1' (km/s) 8.765248946906 3
x2 (km) 6983.33319994463	y2 (km) 399.9508485336767	x2' (km/s) -.50200516804901	x2' (km/s) 8.75086 1666858 54
coordinates found using conservation of momentum	α=1.0731418694681 degrees		
x1 (km) 6978.137	y1 (km) 0.0	x1' (km/s) 0.0	y1' (km/s) 8.77006 3506186 98
x2 (km) 6968.01020467271	y2 (km) 399.87178947311	x2' (km/s) -0.41542669857296	y2' (km/s) 8.75896 9265945 06

Using the data for the input coordinates and velocities from Table 3.4.3 and assuming that an initial impulsive maneuver to shift the line of apsides has just been completed at perigee, Figures 3.4.1 and 3.4.2 show 30 day time histories of separation distances between mother

46

and daughter satellites for nominal separation distances of 400km (Figs 3.4.1 a & b) and 100 km (Figs 3.4.2 a & b). For each separation distance the first plot (Figs 3.4.1a, 3.4.2a) shows separation distance in a nominal Keplerian orbit and verifies the concept of an initial impulsive shift in the line of apsides; the second plot (Figs 3.4.1b, 3.4.2b) shows the secular drift attributed to oblateness and atmospheric drag. In comparison with previous results for the nominal 500 km separation, it is observed in general that the smaller the nominal separation distance, the smaller is the amplitude of the oscillation in the amplitude of the separation distance for the ideal Keplerian orbits. In addition the amplitudes of the oscillations for the secular drifts caused mainly by oblateness, is increased for the larger nominal separation distances.
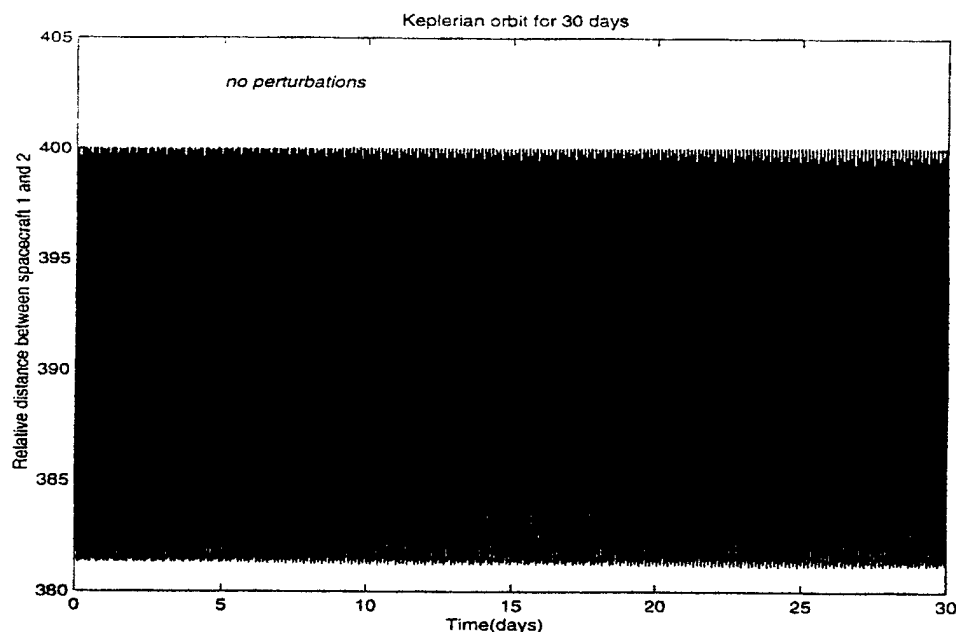

Figure 3.4.1(a) 30 Day Time History of Separation Distance between Mother and Daughter Satellite Keplerian Orbit
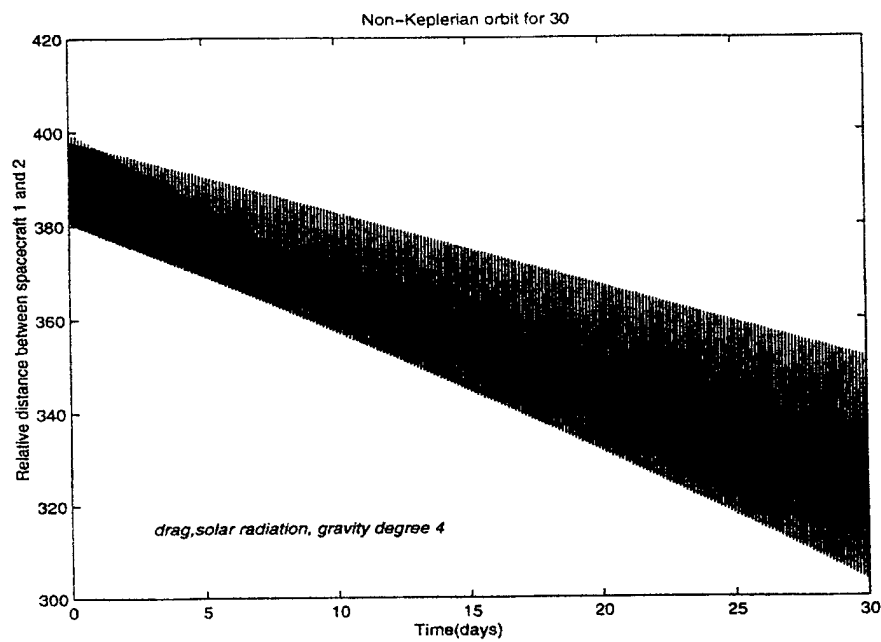
47

Figure 3.4.1(b) 30 Day Time History of Separation Distance between Mother and Daughter Satellite Non-Keplerian Orbit
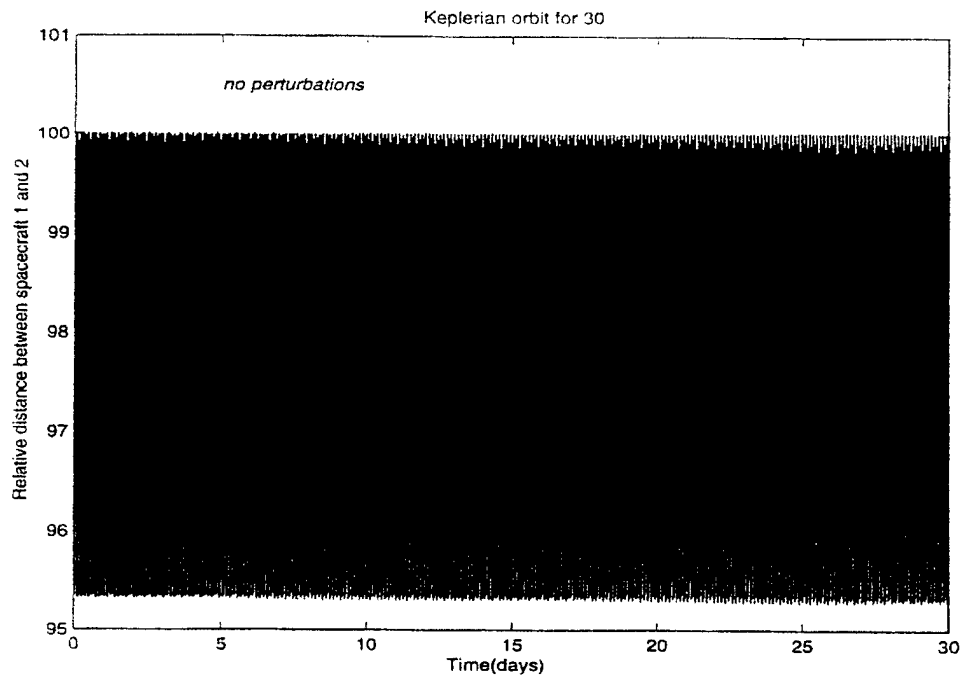
Figure 3.4.2(a) 30 Day Time History of Separation Distance between Mother and Daughter Satellite Keplerian Orbit
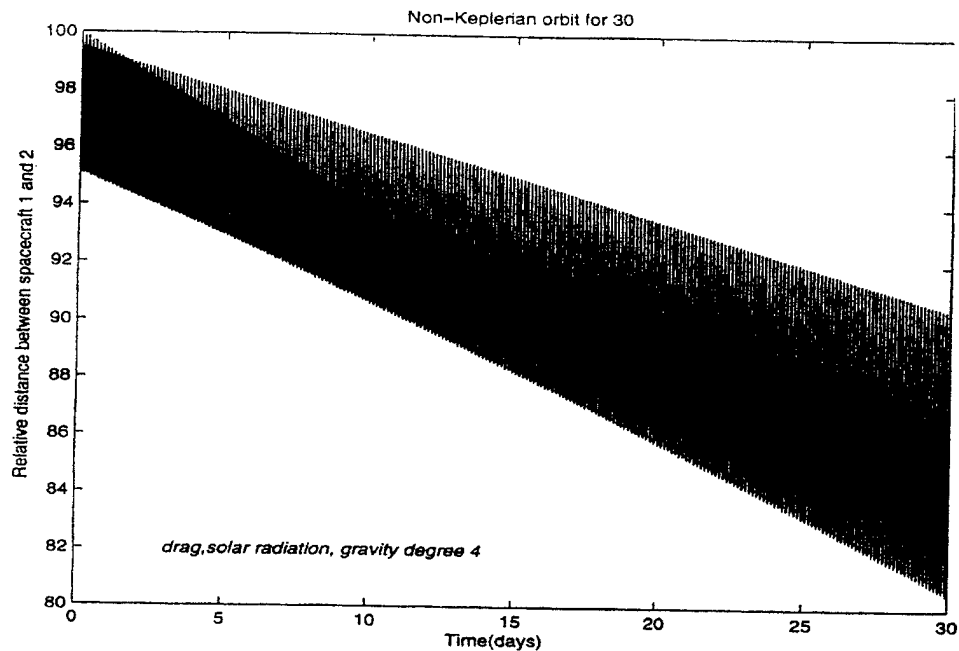
Figure 3.4.2(b) 30 Day Time History of Separation Distance between Mother and Daughter Satellite Non-Keplerian Orbit

To remove the secular perturbation, a feedback control system will be investigated for possible control sometime after the impulsive maneuver. Feedback control will be studied later in Section 3.6 of this document.

50

3.5 Implementation - Propulsive Requirements Based on Lagrange's Planetary Equations for Impulsive (thrust) Perturbations

In order to study the implementation of the in-plane station keeping strategy Lagrange's planetary equations for impulsive perturbations are evaluated. These equations are taken from Ref. [49] and are available in several texts devoted to celestial mechanics and are listed as follows:

$$\frac{d\Omega}{dt} = \frac{nar}{\mu\sqrt{1-e^2}} N \sin u \, \cosec i$$

$$\frac{di}{dt} = \frac{nar}{\mu\sqrt{1-e^2}} N \cos u$$

$$\frac{de}{dt} = \frac{na^2}{\mu}\sqrt{1-e^2}[R\sin\theta + B(\cos\theta + \cos E)]$$

$$\frac{d\tilde\omega}{dt} = \frac{na^2}{\mu e}\sqrt{1-e^2}[-R\cos\theta + B(1+\frac{r}{p})\sin\theta] + 2\sin^2(\frac{1}{2})i\frac{d\Omega}{dt}$$

$$or \quad \frac{d\omega}{dt} = \frac{na^2}{\mu e}\sqrt{1-e^2}[-R\cos\theta + B(1+\frac{r}{p})\sin\theta] - \cos i\frac{d\Omega}{dt}$$

$$\frac{da}{dt} = \frac{2na^2}{\mu}[R\frac{ae}{\sqrt{1-e^2}}\sin\theta + B\frac{a^2\sqrt{1-e^2}}{r}]$$

$$or \quad \frac{dn}{dt} = -\frac{3}{2}\frac{n}{a}\frac{da}{dt} \qquad . \qquad .$$

51

The left side represents the time-rate of change for the various orbital elements and parameters. The force impulse per unit mass is

$$\bar{F} = R\hat{r} + N\hat{h} + B\hat{h} \times \hat{r}$$

where R represents the radial (altitude) direction component;

N represents the component normal to the orbit plane;

B represents the tangential (along track) component;

$\hat{r}$ - unit vector along the outward radius;

$\hat{h}$ - unit vector in the direction of the orbital angular momentum vector;

$\hat{h} \times \hat{r}$ is a unit vector in the positive tangential direction (local horizontal).

The following symbols represent the customary orbital elements:

a: semi-major axis;

e: eccentricity;

Ω: longitude of the ascending node;

i: orbit plane inclination angle with respect to the equator;

ω: argument of perigee (perihelion).

In addition n represents the mean angular rate in the orbit and

$\tilde{\omega} = \Omega + \omega$ is the longitude of perigee; it is measured first in the ecliptic plane to the ascending node, and then in the plane of the orbit to the direction of perigee. E is the eccentric anomaly, θ is the true anomaly, $u = \theta + \omega$, and p is the semi-latus rectum

$p = h^2/\mu = a(1-e^2)$,   and μ = Earth's gravitational constant.

In Fig 3.5.1, a geometric interpretation is provided to describe those six commonly used elements of the orbit. The Sun is at O, Ox points toward the vernal equinox and Oz toward the north pole of the ecliptic. Letting the plane of the orbit cut the celestial sphere in the great circle HPA, then H is the point where the body in its orbit rises north of the ecliptic, called the ascending node. The point at which the body crosses the ecliptic, moving south, is the descending node. The angle xOH is the longitude of the ascending node; it is

Figure 3.5.1

written as Ω, measured eastward around the ecliptic. The angle between the plane of the orbit and the ecliptic (angle between $\hat{h}$ and $\hat{z}$) is called the inclination; it is written as i (often times right ascension and declination are used interchangeably with celestial equator and vernal equinox). The angle HOP is called the argument of perihelion; it is written as ω.

For geocentric orbits, the Earth is at point O and the ecliptic plane is replaced by the Earth's equatorial plane.

Back to the research at hand, one possible strategy that will result in a change of the orientation of the semi-major axis without changing the length of the semi-major axis nor the eccentricity is to provide force impulses only in the radial direction at the perigee and /or apogee positions, and maintaining B = N = 0. With this strategy the mean orbital angular rate n remains constant as well as the values of Ω and i.

Using the parameters for the strawman configuration: a = 10678.14 km.; e = 0.34650029347059; n = 5.69423×10^{-4} rad/sec. and μ = 398603.361 km^3 / sec^2 the value of the force impulse can be calculated from the expression for dω /dt. We recall that R dt = (R$_f$ /m) dt where R$_f$ is the actual thrust in N and m is the mass of each spacecraft in the constellation (m = 90 kg). If it is desired to cause a change in the argument of perigee of 1 degree (1/57.3 rad) then a force impulse of 3.49397660879 NS at perigee (or apogee) would be required. This appears to be well inside the performance limits for the proposed pulse plasma thrusters (PPT). Of course other thrusting strategies could be employed at different points along the orbit and utilizing other components of the thrust vector. The example presented here is to show capability and may not represent an "optimum" design strategy.

To convert impulse in terms of ΔV

53

$$F = dP/dt$$

or

$$\Delta tF = \Delta m v + m \Delta v$$

assuming mass is constant, then

$$\Delta v = Fdt/m = 0.0388219623199 \text{ m/sec.}$$

3.6 Analytical Solution to Station Keeping Under Continuous Thrust Via Tschauner - Hempel Equation of Motion

In this section, the relative motion of two spacecraft (m1 and m2) is discussed. Each spacecraft is orbiting a third (massive) body such as the Earth (m3). The general (linear) state equations are replaced by the Tschauner - Hempel equations. In the present form, the equation

$$\ddot{r} + \frac{\mu}{r^3}\vec{r} = \vec{F} \qquad \text{has a singularity at } r = 0. \qquad \vec{F}$$

represents the perturbation forces, μ is the reduced mass and r denotes the radial displacement.

This equation has the integral $\quad E = \frac{1}{2}m\dot{r}^2 - \frac{\mu}{x} = const.$,

or where $\vec{F} = 0$ therefore $\dot{r} \to \infty$ as $r \to 0$.

If the true anomaly of the target vehicle is used as the independent variable (as does Tschauner - Hempel) instead of time, then this should eliminate the requirements to numerically solve Kepler's equations at each time step as well as accomplishing the task of regularizing the two body problem. Other forms of regularization have been accomplished by using a "fictitious" time, the so-called Sundmann transformation[55]. Regularization is defined as the elimination of singularities from the differential equation. However, the process of eliminating a singularity from a differential equation of motion by the use of one or more integrals is referred to as embedding.

A general formulation for the relative motion allowing for arbitrary perturbing or thrust forces on each of the two spacecraft is presented. F Has the form $F = P - \dfrac{\partial V(r,t)}{\partial r}$

where the P components are perturbations not generally derivable from a potential, such as thrust and drag. V(r,t) is the perturbing potential that can depend explicitly on time if

required. Approximate perturbation solutions for the linearized relative motion equation with continuous radial or circumferential forces acting on the spacecraft will be established.

A pseudo method for station keeping will now be investigated. After a shift in the lines of apsides is made, the Tschauner-Hempel equations involving a continuous control function will be used to find a control law for the control of thrusting, using continuous linear quadratic regulator (LQR) theory. The derivation of the Tschauner-Hempel equations is outlined in Ref.[31]. In obtaining a general analytical solution, in an earlier study, Tschauner obtained a canonical transformation that simplifies the homogeneous part of the equation. The control influence matrix, **B,** ordinarily becomes quite complicated and thus no advantage gained. However, the **B** matrix in this case of study, is also simplified. Thus a delightful added benefit gained by the use of these equations, besides the fact they are already linearized, is that they exhibit a relative motion in the local vertical/local horizontal system.

3.6.1 Development of LQR

The most general development of station keeping strategy, using feedback, will now be developed. The adaptation is as outlined in Kirk [56] and Lewis [57], where the interest is not in regulating a state near zero but the state is to follow a nonzero reference. Therefore, the optimal control will consist of a feedback and a feedforward command. Given this robust development, restrictions can be imposed whereby adaptations can be made for almost any situation.

For a fixed final state - the desired system is to maintain a constant state $r(\theta_f) = R_N$ or separation for all θ, and more specifically, some $\theta = \theta_f$ (reachability is required)

$$x(\theta_f) = r(\theta_f) = R_N \qquad (3.6.1.1)$$

and given the system $\quad x'(\theta) = A(\theta) + B(\theta)u + d \qquad$ $x \in R^n$ and $u \in R^m$ $\quad$ (3.6.1.2)

d is a small disturbance; the most general form of quadratic performance index (PI)

$$J = \frac{1}{2}\left[x(\theta_f) - R_N\right]^T S\left[x(\theta_f) - R_N\right] +$$

$$\frac{1}{2}\int_{\vartheta_0}^{\vartheta_f}\left\{ \left[x(\theta) - r(\theta)\right]^T Q(\theta)\left[x(\theta) - r(\theta)\right] + u^T(\theta)R(\theta)u(\theta) \right\}d\theta$$

$$\equiv \frac{1}{2}\left\|x(\theta_f) - R_N\right\|^2 S + \frac{1}{2}\int_{\vartheta}^{\vartheta_f}\left\{ \left\|x(\theta) - r(\theta)\right\|^2 Q + \left\|u(\theta)\right\|^2 R \right\}d\theta \quad (3.6.1.3)$$

The performance measure indicates that the state $x(\theta)$ is to be maintained close to R_N and $r(\theta)$ without excessive expenditure of control effort. R is a function of θ only if it is desired to vary the weighting on the control effort. S and Q are real symmetric positive semi-definite matrices (i.e., ≥ 0), whereby, R is a real symmetric positive definite matrix (i.e., > 0). This guarantees the existence of R^{-1} for all $\theta \in [\theta_0, \theta_f]$. Once the PI weighting matrices Q and R have been selected, the determination of the optimal feedback gain K is a formal procedure relying on the solution of nonlinear coupled matrix equations. Therefore, the engineering judgment in modern LQR design appears in the selection of Q and R. There are some guidelines for this; all of which will be discussed later. The objective is to find the optimal control sequence $u_{radial}, u_{tangential}, u_{perpendicular}$ that maintains the desired separation, $x(\theta_f) = R_N$ while minimizing the performance function.

Now as in Chapter 1, but for a continuous system, the Hamiltonian can be represented as

$$H(x(\theta), u(\theta), p(\theta), \theta) = \frac{1}{2}\left\|x(\theta) - r(\theta)\right\|^2 Q + \frac{1}{2}\left\|u\right\|^2 R + p^T\left\{Ax + Bu\right\} \quad (3.6.1.4)$$

$$x' = \frac{\partial H}{\partial p} = Ax + Bu \tag{3.6.1.5}$$

$$p' = -\frac{\partial H}{\partial x} = -Qx - A^T p + Qr \tag{3.6.1.6}$$

Instead of using the stationary condition $\quad \dfrac{\partial H}{\partial u} = 0 = Ru + B^T p \tag{3.6.1.7}$

$$u = -R^{-1}B^T p \tag{3.6.1.8}$$

This is the minimum energy constrained input control expressed as a costate feedback. Substituting (3.6.1.8) into the state equation (3.6.1.5), yields the state and costate equations

$$\begin{bmatrix} x' \\ p' \end{bmatrix} = \begin{bmatrix} A(1,1) & \vdots & -BR^{-1}B^T(1,2) \\ -Q(2,1) & \vdots & -A^T(2,2) \end{bmatrix}\begin{bmatrix} x \\ p \end{bmatrix} + \begin{bmatrix} d \\ Qr \end{bmatrix} \tag{3.6.1.9}$$

The solution to these linear and θ varying differential equations where Qr is a forcing function is

$$\begin{bmatrix} x(\theta_f) \\ p(\theta_f) \end{bmatrix} = \varphi(\theta_f,\theta)\begin{bmatrix} x(\theta) \\ p(\theta) \end{bmatrix} + \int_{\vartheta}^{\vartheta_f} \varphi(\theta_f,\tau)\begin{bmatrix} d \\ Q(\tau)r(\tau) \end{bmatrix} d\tau \tag{3.6.1.10}$$

where φ is the transition matrix of the system (3.6.1.9). If φ is partitioned, and the integral

replaced by the 2n x 1 vector
$\begin{bmatrix} f_1(\theta) \\ \hline f_2(\theta) \end{bmatrix}$ (3.6.1.11)

then equation (3.6.1.10) can be written as

$$x(\theta_f) = \varphi_{11}(\theta_f, \theta)x(\theta) + \varphi_{12}(\theta_f, \theta)p(\theta) + f_1(\theta)$$
$$p(\theta_f) = \varphi_{21}(\theta_f, \theta)x(\theta) + \varphi_{22}(\theta_f, \theta)p(\theta) + f_2(\theta) \quad 3.6.1.12 \text{(a)} \& \text{(b)}$$

Now seeking to investigate the boundary conditions, Lewis [57] offers an excellent interpretation. It is assumed that $x(\theta_0)$ is known. Rewriting the cost function, equation (3.6.1.3) as

$$J = F(x(\theta_f, \theta_f)) + \int_{\theta_0}^{\theta_f} \left[L(x, u, \theta) + p^T(\theta)(f(x, u, \theta) - x') \right] d\theta$$

$$= F(x(\theta_f, \theta_f)) + \int_{\theta_0}^{\theta_f} \left[H(x, u, \theta) - p^T(\theta)x' \right] d\theta \qquad (3.6.1.13)$$

since $\qquad H(x, u, \theta) = L(x, u, \theta) + p^T(\theta)f(x, u, \theta) \qquad (3.6.1.14)$

Using Leibniz's rule, the increment in J as a function of increments in **x, p, u** and θ is

$$dJ = (F_x)^T dx \Big|_{\theta_f} + F_\vartheta d\vartheta \Big|_{\theta_f} + (H - p^T x')d\theta \Big|_{\vartheta_f} - (H - p^T x')d\theta \Big|_{\theta_0}$$
$$+ \int_{\theta_0}^{\theta_f} \left[H^T_x \partial x + H^T_u \partial u - p^T \partial x' + (H_p - x')^T dp \right] d\theta \qquad (3.6.1.15)$$

59

Subscripts denote a derivative with respect to that variable. To eliminate the variation of x', integrate by parts and find

$$-\int_{\theta_0}^{\theta_f} p^T \partial x' \, d\theta = -p^T \partial x \Big|_{\theta_f} + p^T \partial x \Big|_{\theta_0} + \int_{\theta_0}^{\theta_f} p^{T'} \partial x \, d\theta \qquad (3.6.1.16)$$

Substitute the fact from reference[56]

$$dx(\theta_f) = \partial x(\theta_f) + x'(\theta_f) d\theta_f \qquad (3.6.1.17)$$

into equation (3.6.1.16) then

$$\begin{aligned}
dJ = {} & (F_x - p)^T dx \Big|_{\theta_f} + (F_\theta + H - p^T x' + p^{T'} x')d\theta \Big|_{\theta_f} \\
& - (H - p^T x' + p^{T'} x')d\theta \Big|_{\theta_0} + p^T dx \Big|_{\theta_0} \\
& + \int_{\theta_0}^{\theta_f} \left\{ (H_x + p')^T \partial x + H^T_u \partial u + (H_p - x')^T \partial p \right\} d\theta
\end{aligned} \qquad (3.6.1.18)$$

Since R_N is fixed, then $dx \Big|_{\theta_f} = 0$. Therefore, the boundary conditions imply

$$p(\theta_f) = Sx(\theta_f) - Sr(\theta_f) \qquad (3.6.1.19)$$

Using equation (3.6.1.19) and substituting x(θ_f) from 3.6.1.12(a) into 3.6.1.12(b) then

$$\begin{aligned}
& S\left[\varphi_{11}(\theta_f, \theta)x(\theta) + \varphi_{12}(\theta_f, \theta)p(\theta) + f_1(\theta) \right] - Sr(\theta_f) \\
& = \varphi_{21}(\theta_f, \theta)x(\theta) + \varphi_{22}(\theta_f, \theta)p(\theta) + f_2(\theta)
\end{aligned} \qquad (3.6.1.20)$$

Solving for p(θ) yields

$$p(\theta) = \left[\varphi_{22}(\theta_f,\theta) - S\varphi_{12}(\theta_f,\theta)\right]^{-1}\left[S\varphi_{11}(\theta_f,\theta) - \varphi_{21}(\theta_f,\theta)\right]x(\theta)$$
$$+\left[\varphi_{22}(\theta_f,\theta) - S\varphi_{12}(\theta_f,\theta)\right]^{-1}\left[Sf_1(\theta) - SR_N - f_2(\theta)\right] \quad (3.6.1.21)$$

or $\qquad p(\theta) \equiv k(\theta)x(\theta) + m(\theta) \qquad$ (3.6.1.22) $\qquad$ Then

$$u(\theta) = -\left[R^{-1}(\theta)B^T(\theta)k(\theta)x(\theta) + R^{-1}(\theta)B^T(\theta)m(\theta)\right] \quad (3.6.1..23)$$

$$u(\theta) = -F(\theta)x(\theta) + v(\theta) \qquad (2^{nd}\text{ term in}3.6.1.\,23 < 0)$$

(3.6.1.24)

The first term (coefficient of x in equation 3.6.1.24), is the feedback gain and the second is the command signal or feedforward gain. $k(\theta)$ and $m(\theta)$ of equation (3.6.1.23) are the unique positive semi-definite solutions of the Riccati equations. Furthermore, $A(\theta)$, $B(\theta)$, $R(\theta)$\{R is not necessarily θ dependent\}, $Q(\theta)$ and S must be found or specified. By adjusting the elements' values, the weight and relative importance of the deviation of each of the states from their desired values is understood.

To avoid determining the transition matrix, differentiate (3.6.1.22)

$$p'(\theta) = k'(\theta)x(\theta) + k(\theta)x'(\theta) + m'(\theta) \qquad (3.6.1.25)$$

Substituting from (3.6.1.9) for $p'(\theta)$ and $x'(\theta)$ and using (3.6.1.22) to eliminate p(θ), then

$$\left[\; k' + Q + kA + A^T k - kBR^{-1}B^T k \;\right]x$$
$$+\left[m' + A^T m - kBR^{-1}B^T m - Qr + kd\right] = 0 \qquad (3.6.1.26)$$

61

(recalling matrices are θ dependent) also for every x(θ) and r(θ), then

$$-k' = kA + A^T k + Q - kBR^{-1}B^T k$$
$$-m' = \left[A^T - kBR^{-1}B^T \right] m - Qr + kd \qquad (3.6.1.27)$$

The set of equations in (3.6.1.27) are considered as differential Riccati equations . If the output is specified as a linear combination of states or $y(\theta) = Cx(\theta)$, then the second term on the right side of the second equation (3.6.1.27) becomes $C^T Qr$. Much can be said regarding whether these equations are well posed and stable. From *Computational Methods for Linear Control Systems* [58], a series of tests can be performed to check those conditions. Letting $N^T N = Q$ in the first equation of (3.6.1.26) or Q can be computed from N; and letting $V^T V = -Qr$, from the second equation, then if the pair (A,B) is controllable and the pairs (N, A) and (V, A) are observable, (i.e., $O \equiv \left[V \quad VA \quad VA^2 \cdots VA^{n-1} \right]$ has the full rank n and $O^T O$ is non-singular), the Riccati equations must have unique positive definite solutions. Thus, there exists a unique optimal control $u * (\theta)$ which minimizes equation (3.6.1.3) and may be expressed as a linear state feedback. It is understood that **A** must have constant coefficients in order to apply the LQR theory.

Boundary conditions imply the following:

$$p * (\theta_f) = Sx * (\theta_f) - Sr(\theta_f) \equiv k(\theta_f)x * (\theta_f) + m(\theta_f) \qquad (3.6.1.28)$$

$\forall \quad x * (\theta_f)$ and $\quad r(\theta_f)$ then $k(\theta_f) = S$ and $m(\theta_f) = -C^T Sr(\theta_f) \quad (3.6.1.29)$

$m(\theta)$ can be determined by integrating backward the closed-loop adjoint system, equation (3.6.1.29). Then $m(0)$ is known. During the actual control run, $m(0)$ is used in the forward equation, the second equation of (3.6.1.27). This method however, will not be used, but the

Riccati equation will be allowed to reach a steady-state solution. Therefore, the final boundary conditions will not be of consideration.

3.6.2 Solution of the LQR based on the Tschauner-Hempel Equations of Motion

Proceeding to place the Tschauner-Hempel equations into state space form, these equations can be represented as:

$$\xi'' - 2\eta' - \frac{3\mu r}{h^2}\xi = a_\xi$$
$$\eta'' + 2\xi' = a_\eta \qquad\qquad (3.6.2.1)$$
$$\zeta'' + \zeta = a_\zeta$$

where ξ, η, and ζ are non-dimensionalized coordinates centered at the target or reference spacecraft. ξ describes cross track (outward radial) motion, η - along track, and ζ out of the nominal orbit plane of the target spacecraft. Equation (3.6.2.1) can then be converted into state variable format, as:

$$\xi'' = 2\eta' + \frac{3\mu r}{h^2}\xi + a_\xi$$

$$\eta'' = -2\xi' + a_\eta$$

$$\zeta'' = -\zeta + a_\zeta$$

letting

$$\xi = x_1$$

$$\xi' = x_1' = x_2$$

$$\xi'' = x_2'$$

$$\eta = x_3$$

$$\eta' = x_3' = x_4$$

$$\eta'' = x_4$$

$$\zeta = x_5$$

$$\zeta' = x_5' = x_6 \qquad\qquad 3.6.2.2(a)$$

$$\zeta'' = x_6'$$

therefore

$$
\begin{matrix}\xi' \\ \xi'' \\ \eta' \\ \eta'' \\ \zeta' \\ \zeta''\end{matrix}
\begin{pmatrix} x_1' \\ x_2' \\ x_3' \\ x_4' \\ x_5' \\ x_6' \end{pmatrix}
=
\begin{pmatrix}
0 & 1 & 0 & 0 & 0 & 0 \\
\frac{3\mu}{h^2} & 0 & 0 & 2 & 0 & 0 \\
0 & 0 & 0 & 1 & 0 & 0 \\
0 & -2 & 0 & 0 & 0 & 0 \\
0 & 0 & 0 & 0 & 0 & 1 \\
0 & 0 & 0 & 0 & -1 & 0
\end{pmatrix}
\begin{pmatrix} x_1 \\ x_2 \\ x_3 \\ x_4 \\ x_5 \\ x_6 \end{pmatrix}
\begin{matrix}\xi \\ \xi' \\ \eta \\ \eta' \\ \zeta \\ \zeta'\end{matrix}
+
\begin{pmatrix}
0 & 0 & 0 \\
1 & 0 & 0 \\
0 & 0 & 0 \\
0 & 1 & 0 \\
0 & 0 & 0 \\
0 & 0 & 1
\end{pmatrix}
\begin{pmatrix} a_\xi \\ a_\eta \\ a_\zeta \end{pmatrix}
$$

Upon interchanging rows so the first three variables are position and the second three are velocity, then equation (3.6.30) in common state space representation, is:

$$
\begin{pmatrix} \xi' \\ \eta' \\ \zeta' \\ \xi'' \\ \eta'' \\ \zeta'' \end{pmatrix} = \begin{pmatrix} 0 & 0 & 0 & 1 & 0 & 0 \\ 0 & 0 & 0 & 0 & 1 & 0 \\ 0 & 0 & 0 & 0 & 0 & 1 \\ \dfrac{3\mu r}{h^2} & 0 & 0 & 0 & 2 & 0 \\ 0 & 0 & 0 & -2 & 0 & 0 \\ 0 & 0 & -1 & 0 & 0 & 0 \end{pmatrix} \begin{pmatrix} \xi \\ \eta \\ \zeta \\ \xi' \\ \eta' \\ \zeta' \end{pmatrix} + \begin{pmatrix} 0 & 0 & 0 \\ 0 & 0 & 0 \\ 0 & 0 & 0 \\ c1 & 0 & 0 \\ 0 & c2 & 0 \\ 0 & 0 & c3 \end{pmatrix} \begin{pmatrix} a_\xi \\ a_\eta \\ a_\zeta \end{pmatrix}
\qquad \text{3.6.2.2(b)}
$$

The nonlinear term in this matrix can be adjusted in a number of ways:

1. When it is assumed that r remains constant (i.e. equal to $r(\theta) = \dfrac{h^2}{\mu}$), true for a circle

and relatively short displacements, then the term becomes equal to 3.

2. If simulation is started at perigee or apogee then evaluate r at perigee or apogee respectively, and treat as constant for sufficiently short time thereafter.

3. If several orbits are needed to correct the disturbance, then use an average value for r with

$$
h = r \times v = \sqrt{\dfrac{b^2 \mu}{a}} .
$$

h is the angular momentum, a the semimajor axis and b

is the semiminor axis.

4. A final consideration, is to update 1 and 2 in a piecewise adapted manner along the orbit.

Although the T-H equations simplify the fundamental matrix, the right hand side (RHS) can become quite cumbersome, depending on the type/location of actuators. The terms on the RHS of (3.6.2.1) contain all the relative accelerations (i.e. drag, thrust and

Earth's oblateness). However, since the mass of each spacecraft is equal, and if the ballistic coefficients are the same, then the relative drag is approximately equal to zero. Therefore its contribution will not be considered as part of the acceleration term, but only the thrust and oblateness terms. If the variables $c1$, $c2$, and $c3$ are selected to include thrust and oblateness, the control will appear as $u_c = u - d$. The oblateness term will be included separately and the development will proceed as below.

The contribution of oblateness is as follows:

$$a = \frac{G}{r^2} \sum_{k=2}^{\infty} J_k \left(\frac{r_{eq}}{r} \right)^k \left[p'_{k+1}(\cos\varphi)\hat{i}_r - p'_k(\cos\varphi)\hat{i}_z \right] \qquad (3.6.2.3)$$

r_{eq} is the equatorial radius. In x, y, z coordinates(to be normalized in the ξ, η, ζ notation), where u = ω + θ, and from Battin [18,52], if only the second harmonic term is considered , then the acceleration terms are as follows:

$$\begin{pmatrix} a_x \\ a_y \\ a_z \end{pmatrix}_{J_2} = -\frac{3GJ_2 r^2_{eq}(1+e\cos\theta)^4}{a^4(1-e^2)^4} \begin{pmatrix} 1 - 3\sin^2(\omega + \theta)\sin^2 i \\ \sin(2\omega + 2\theta)\sin^2 i \\ \sin(\omega + \theta)\sin 2i \end{pmatrix}$$

$i = 0,$ \qquad (3.6.2.4)

$$\begin{pmatrix} a_x \\ a_y \\ a_z \end{pmatrix}_{J_2} = \begin{pmatrix} \dfrac{-3GJ_2 r_{eq}^2(1+e\cos\theta)}{a^4(1-e^2)^4} \\ 0 \\ 0 \end{pmatrix}$$

66

$$B = \begin{pmatrix} 0 & 0 & 0 \\ 0 & 0 & 0 \\ 0 & 0 & 0 \\ 1 & 0 & 0 \\ 0 & 1 & 0 \\ 0 & 0 & 1 \end{pmatrix} \quad \text{and} \quad d = \begin{pmatrix} 0 \\ 0 \\ 0 \\ aj \\ 0 \\ 0 \end{pmatrix} \qquad (3.6.2.5)$$

where
$$aj = \frac{-3J_2 r_{eq}^2 (1 + e\cos\theta)^4}{a^4 (1 - e^2)^4}$$

Now enough information is known to execute the program for LQR. This LQR program will be based on the linearize Tschauner Hempel equations of motion with respect to the LVLH coordinate frame. The origin of the LVLH is the mother spacecraft point on the reference ellipse. Again the ξ axis of the frame points radially outward along the local vertical direction, the η axis is along the direction of motion on the reference orbit, while the ζ axis is normal to the reference orbit plane. The initial state vector is $(\xi, \eta, \zeta, \xi', \eta', \zeta')$ and the initial perturbation variable as $x_0 = (\delta\xi, \delta\eta, \delta\zeta, \xi', \eta', \zeta')$ where $\delta\xi = \xi - \xi_{ref}$ $\delta\eta = \eta - \eta_{ref}$ and $\delta\zeta = \zeta - \zeta_{ref}$, etc. The Tschauner-Hempel equations will be linearized only once, in that, station keeping will be considered for spacecraft along track, thus the reference spacecraft, can be taken as the unperturbed position of any daughter's position.(If some other configuration is to be considered, such as a triangle, then these equations would need to be re-linearized around various places in the orbit, to accommodate an inherent two dimensional configuration). For example, a 501 km (mother - daughter) separation from a nominal 500 km, implies a one kilometer as input, as the variation of the daughter spacecraft from its unperturbed position along track.

The *aj* term in equation (3.6.2.5), and others when necessary, must be put into non-dimensional form; this will be accomplished in the coding, being mindful of theta dependance.

Once the state matrices are specified, then enough information is available to solve the differential Riccati equations. A couple of methods exists to solve equations (3.6.1.26 and 3.6.1.27). Since in general k and m are an n x n, symmetric matrices (n = 6), implies $n(n + 1)/2$ first- order differential equations must be solved. These equations can be integrated numerically, starting at $\theta = \theta_f$ and proceeding backward to $\theta = \theta_0$; $k(\theta)$ and $m(\theta)$ are stored, and the feedback gain matrix is determined from equation (3.6.1.23).

Now most Runge-Kutta integration routines run forward in time. To accomplish the backward integration, the RHS of (3.6.1.26) is multiplied by a (-1), and then integrated forward from $\theta = \theta_0$ (corresponding to t = 0). The resulting solution is reversed and shifted to $\theta = \theta_f$ (corresponding to t = T). The second part of the simulation is to find the optimal control law and update the system dynamics by integrating forward in time. Alternatively, to determine the k and m matrices, for an infinite time process, either perform a backward recursion integration until a steady state solution is obtained or simply solve the nonlinear algebraic Riccati equation (ARE), obtained by setting k' and m' equal to 0. The second part of the simulation still is to find the optimal control law and update the system dynamics by integrating forward in time. This method will be chosen to solve the Riccati equation, of which k and m are solutions. The program contains the following dimensions for the various matrices: $A \in R^{6 \times 6}$ $B \in R^{6 \times 3}$ $S \in R^{6 \times 6}$ $R \in R^{3 \times 3}$ $Q \in R^{6 \times 6}$; With $R_N \in R^{6 \times 1}$ and $x \in R^{6 \times 1}$ would imply a calculated value of control $u \in R^{3 \times 1}$, feedback and feedforward respectively, $k \in R^{3 \times 6}$ & $m \in R^{6 \times 1}$. If infinite time only is considered then the weighting matrix S = 0,(as in Eq. (3.6.1.3)), since only an engineering approximation is assumed. The MATLAB function [K S, e] = lqr(A, B, Q, R, N) will be

68

used to solve the ARE, for a particular Q and R; N is defaulted to zero. Further descriptions show that this function also calculates the optimal gain matrix K such that the state-feedback law

$$u = -Kx \qquad (3.6.2.6)$$

minimizes the quadratic cost function

$$J(u) = \int_0^\infty \left(x^T Qx + u^T Ru + 2x^T Nu\right)dt \qquad (3.6.2.7)$$

for the continuous time state space model $\dot{x} = Ax + Bu + d$ (3.6.2.8)

The oblateness is included as a disturbance term in (3.6.2.8). The state feedback gain K, **lqr** returns the solution S of the associated Riccati equation. As a note, be mindful of change of variables. For instance, in the MATLAB routine S is not the same as the weighting function S, and is the solution to the ARE.

$$A^T S + SA - (SB + N)R^{-1}(B^T S + N^T) + Q = 0 \qquad (3.6.2.9)$$

and the closed - loop eigenvalues $\qquad e = eig(A - B*K).$ (3.6.2.10)

Note that K is derived from S by $\qquad K = R^{-1}(B^T S + N^T)$ (3.6.2.11)

or $\qquad u = -R^{-1}(B^T S + N^T)x$ (3.6.2.12)

Again the problem data must satisfy the following limitations:

- (A, B) *stabilizable*
- $R > 0$ *and* $Q - NR^{-1}N^T \geq 0$ (3.6.2.13)
- $(Q - NR^{-1}N^T, A - BR^{-1}N^T)$

The last expression has no unobservable pole on the imaginary axis. Nevertheless, observability is not being considered here. That is, all states are assumed to be immediately available. Furthermore, for the purpose of this research, this problem is assumed to be in the

absence of noise. ARE, equations (3.6.1.27), will be solved using MATLAB notation and variables. The first of these is the same as equation (3.6.2.9) with N = 0. The second has the

solution $m = (A^T - SBR^{-1}B^T)^{-1}(C^T Qr - Sd)$ (3.6.2.14)

When the gain reaches a steady-state value and the closed-loop plant is stable then the optimal tracker is given by

$$-m' = (A - BK(\infty))^T m + C^T Qr + Sd$$

$$u = -K(\infty)x + R^{-1}B^T(A^T - SBR^{-1}B^T)^{-1}C^T Qr - R^{-1}B^T(A^T - SBR^{-1}B^T)^{-1}Sd \quad (3.6.2.15)$$

The second equation of equation (3.6.2.15), represents the control needed. The first term of this same equation, represents the feedback, second feedforward or tracking and the third allows for disturbance. The form of the control is similar to that which would result had the disturbance been included as part of the **B** matrix.

Letting the steady state track and disturbance be represented as,

$$track = R^{-1}B^T(A^T - SBR^{-1}B^T)^{-1}C^T Qr$$
$$and$$
$$disturb1 = R^{-1}B^T(A^T - SBR^{-1}B^T)^{-1}Sd$$

(3.6.2.16)

the state becomes

$$x' = Ax + Bu + d = Ax + B(-K(\infty)x + track - disturb1) + d$$

(3.6.2.17)

70

Upon substitution for **u**, this equation can be written as

$$x' = (A - BK)x + Btrack - Bdisturb1 + d \equiv Ax + f^{j} \qquad (3.6.2.18)$$

which has the solution of the form

$$x = \exp(A(\theta_f - \theta_0))x_0 + \exp(A\theta_f)\int_{\theta_0}^{\theta_f}\exp(A\theta)f^{j}d\theta \qquad (3.6.2.19)$$

where $A \equiv (A - BK)$

The auxiliary signal (the second part of equation (3.6.2.19)) can be integrated to be

$$f = \int_{\theta_0}^{\theta_f}(\exp A(\theta_f - \theta_0))f^{j}d\theta = (f^{j}/A)(1 - \exp A(\theta_f - \theta_0)) \qquad (3.6.2.20)$$

In the infinite-horizon limit, this signal is a constant and is represented by

$$f(\infty) = f^{j}/A = A^{-1}(Btrack - Bdisturb1 + d) \qquad (3.6.2.21)$$

The solutions to equations (3.6.2.15) and (3.6.2.19) are easily coded in the program *str_lqr*. This code allows one the option: (1).the use of feedforward (tracking) or (2) not to use feedforward (tracking).

Function lqr can be used alone or in conjuction with a general calculation of the optimal feedback for constant gain, first presented by Moerder and Calise [59] based on the Lyapunov equation. The Lyapunov equation is a variation of the Riccatti equation obtained by making a transformation of the fundamental matrix. The Lyapunov equation may be solved using the subroutine lyap.m in MATLAB (Control System Toolbox).The initialization of the program requires an initial stabilizing output feedback k0, (this k0 can be provided by lqr), the maximum number of iterations N, the magnification α of Δk, and the tolerance. The weighting Q and R are also inputs to the program. The number of iterations, the tolerance, and the magnification can determine the successful termination of the program. If α is "large" the matrix 'A - BKC' may not be Hurwitz. That is, it may not contain

71

negative real parts of the eigenvalues. In such cases, the algorithm will terminate with a warning. To alleviate the problem, decrease α. If the tolerance is very "small" then the program may terminate before achieving the desired tolerance. In that case, either increase N or the tolerance.

In the interest of time, that is for a timely completion of this phase of the research, **lqr** will be used in isolation of **lyap.m**. Thus any reference to this function will be 'commented out'. Refining of the optimal software can be explored in future research. The advantage of the combination software usage is that quicker satisfying weighting matrices may be determined.

As a final comment regarding the criterion functional, the system is desired to be optimal but must be very exact in the sense in which the system is optimal. Mathematical expressions must be found to measure how the system must be optimal in comparison with other system. The system response is usually of most interest. The exact form of S and Q is to be fixed by the designer at the outset. Thus a number is assigned to the response obtained by each control law u, and the optimum system is that whose control law gives the minimum cost function. The choice of Q is dictated by the relative importance of each state over some time interval or $[\theta_0 \leq \theta \leq \theta_f]$ in this case. Fast decay implies large control or large Q implies large u. The choice of S is dictated by the relative importance of each state at the final time or designation. The relative magnitudes of Q and R are in proportion to the relative values of the response and control energy. The larger Q is relative to R, the quicker the response and the higher the gain of the system.

The calculated thrust is a non-dimensional theta dependent quantity. Carter and Brient [29], stated that the Tschauner- Hempel vector $x(\theta)$ described by the Tschauner-Hempel equations can be obtained from the transformation $x(\theta) = r(\theta)X(\theta)$ (3.6.46)

where $X(\theta)$ is the actual relative position of the spacecraft in terms of θ. If the solution vector to these equations is used, then this would imply that

$$v(\theta) = r(\theta)X'(\theta) + r'(\theta)X(\theta)$$

$$\Rightarrow X'(\theta) = \frac{v(\theta) - r'(\theta)X(\theta)}{r(\theta)} \qquad (3.6.2.22)$$

$$v(t) = \frac{dX(\theta)d\theta}{dtd\theta} = X'(\theta)\dot{\theta}$$

Similarly, and using the fact that $\qquad \dot{\theta} = \frac{\mu^2}{h^3}r^2(\theta) \qquad (3.6.2.23)$,

it can be shown that

$$a(t) = \frac{\mu^4}{h^6}\left\{2r^2(\theta)r'(\theta)\left[v(\theta) - r'(\theta)X(\theta)\right]\right\}$$

$$\qquad (3.6.2.24)$$

$$+ \frac{\mu^4}{h^6}\left\{r^4(\theta)\left[a(\theta) - r''(\theta)X(\theta)\right] - 2r'(\theta)r^3(\theta)\left(v(\theta) - r'(\theta)X(\theta)\right)\right\}$$

using again the approximation $r(\theta) = \dfrac{h^2}{\mu}$, $\qquad\qquad (3.6.2.25)$

therefore

$$a(t) = \frac{\mu}{r}\left\{2r'(\theta)\left[v(\theta) - r'(\theta)X(\theta)\right]\right\}$$

$$\qquad (3.6.2.26)$$

$$+ \mu\left\{r(\theta)\left[a(\theta) - r''(\theta)X(\theta)\right] - 2r'(\theta)\left(v(\theta) - r'(\theta)X(\theta)\right)\right\}$$

From equation (3.6.2.22)

$$a(\theta) = 2r'X' + rX'' + r''X \approx 2r'X' + r''X \qquad (3.6.2.27)$$

then

$$a(t) = \frac{\mu}{r}\left\{2r'(\theta)\big[v(\theta) - r'(\theta)X(\theta)\big]\right\}$$
$$+ \mu\left\{r(\theta)\big[2r'(\theta)X'(\theta)\big] - 2r'(\theta)\big(v(\theta) - r'(\theta)X(\theta)\big)\right\} \qquad (3.6.2.28)$$

If equation (3.6.2.25) is not used, but instead $\qquad h = \sqrt{\dfrac{b^2\mu}{a}} \qquad (3.6.2.29)$

then

$$a(t) = \frac{\mu a^3}{b^6}\left\{2r^2 r'(v - r'X) + 2r^4 r'X' - r'r^3(v - r'X)\right\} \qquad (3.6.2.30)$$

Equation (3.6.2.28) or (3.6.2.30) are also programed using MATLAB and is included in the program str_lqr.

Assuming all states are immediately available and in the absence of noise, a parametric study will be investigated using various weighting functions. The task then is to select the combination of values for the state and control weighting matrices which will best answer questions for a given scenario, while maintaining other mathematical behaviors such

74

as positive definiteness and positive semi-definiteness(for purposes of stability). The three relevant questions the LQR should address are (1) How much control? (2) How much overshoot? and (3) How much time is needed for convergence? All of which equate to values needed to remove the error. Although the designed matrices were given an out-of-plane 'z' component as input, it was not until Figures 3.6.2.6 and 3.6.2.7 that a 'z' component error was inputted. Thus there are no 'z' responses for the earlier Figures since a z response at this point is irrelevant for a coplanar model. A discussion per Figure is delineated separately. The preliminary results shown here assume the initial LQR correction begins near perigee, at a true anomaly angle of 45^0. The periodic system matrix appearing in the Tschauner-Hempel equations is evaluated at that true anomaly angle. If the responses occur in a relatively short time, it is assumed that this value could be used throughout the maneuver. For longer time responses this matrix would have to be re-evaluated in a piece-wise adaptive manner. For all results presented here, the quadratic cost functional with the infinite time upper bound and $N = 0$ as in Eq. (3.6.2.7) has been selected as the quadratic cost function.
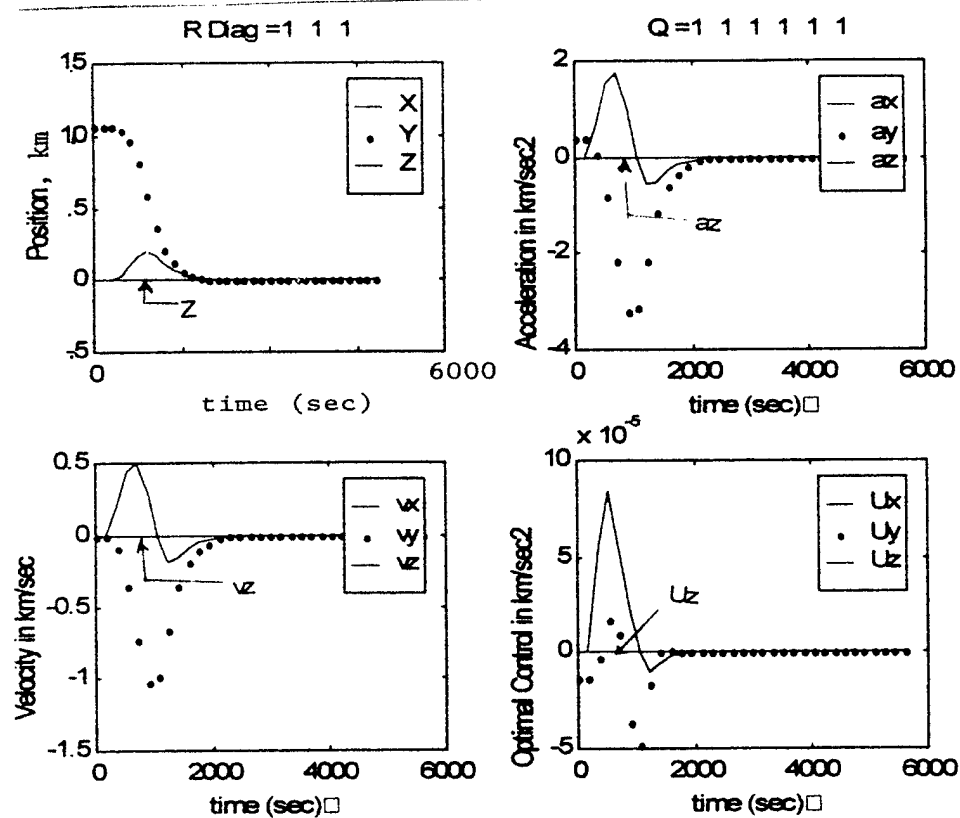
Figure 3.6.2.1

Figure 3.6.2.1 will be considered as the reference Figure for the others. The diagonal elements of the control **R** and state **Q** weighting matrices are given the value of ones. The off diagonal terms are assumed to be zero. The state here is defined as $(x \quad y \quad z \quad \dot{x} \quad \dot{y} \quad \dot{z})$ where x is in the radial cross-track direction in-plane, y is in the along track direction, and z represents out-of-plane displacement. The center of this moving

coordinate system is taken at the nominal position of any daughter satellite in the orbit. Thus

a displacement of 1 km along track actually represents a displacement of $d_{mother\text{-}daughter} + 1$ km

along track, where $d_{mother\text{-}daughter}$ is the desired mother-daughter separation distance for this

application.
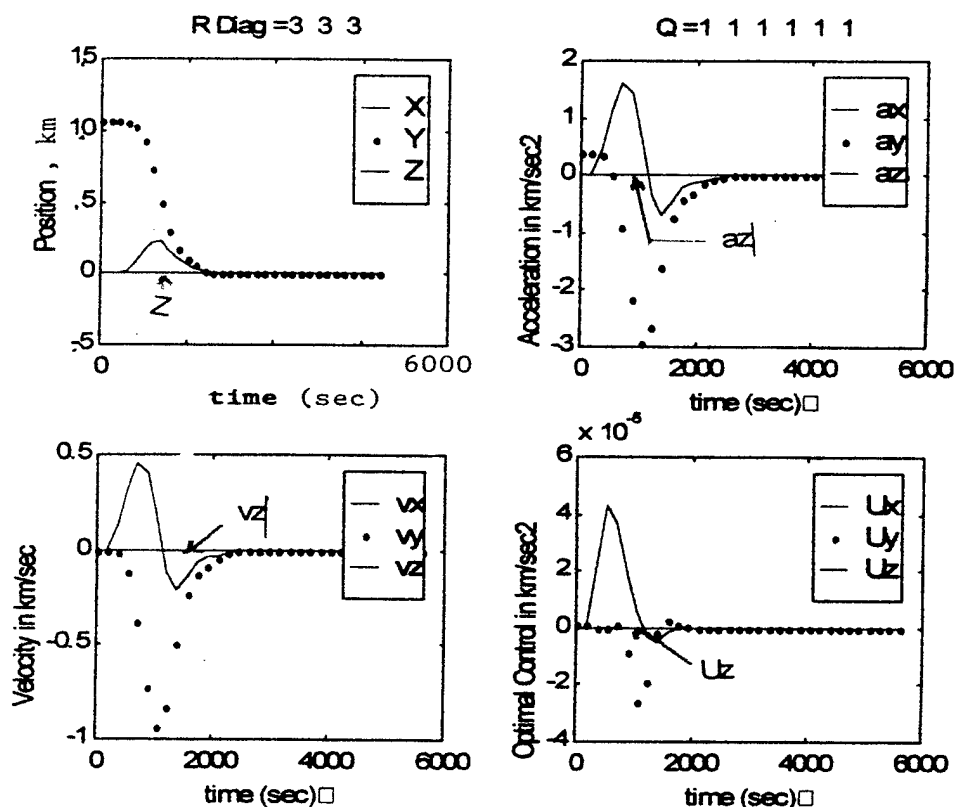
Figure 3.6.2.2

The diagonal elements of **R** are increased to 3. As such, the control effort decreases as

compared with Figure 3.6.2.1. Also some of the responses (velocity and acceleration) appear

to be slightly more sluggish or slow to respond.
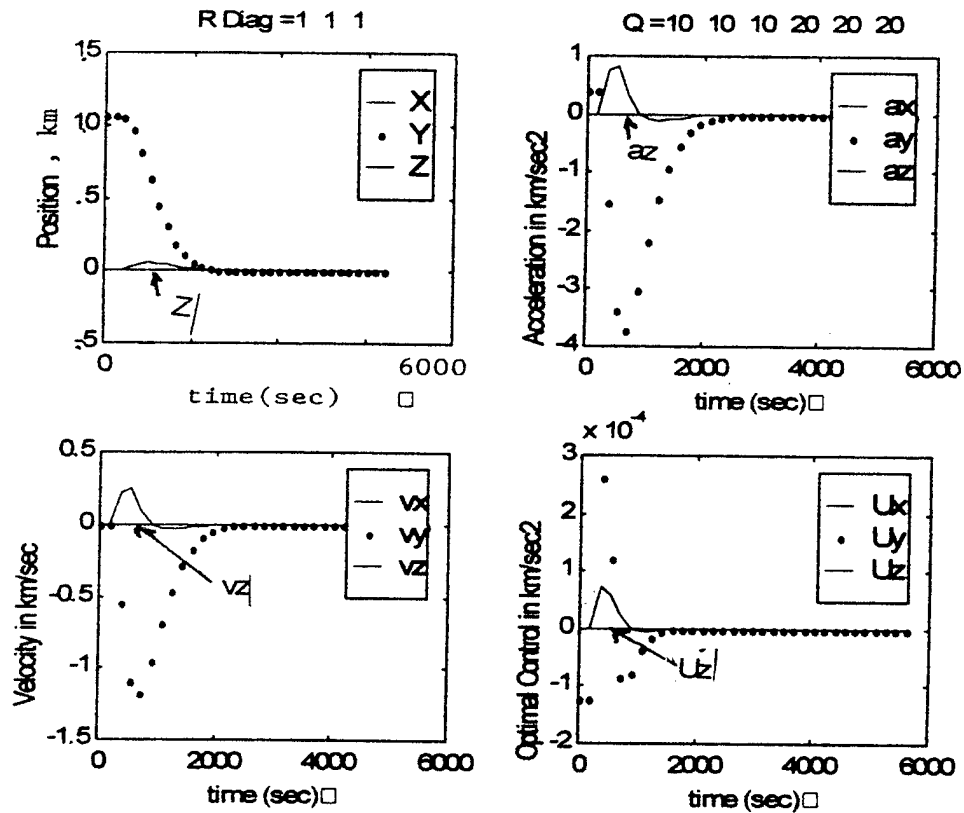
Figure 3.6.2.3

The penalty on all state components is increased. Some of the overshoots are noticeably

reduced as compared with Figure 3.6.2.1 responses. The responses of the x component of

acceleration and position are much faster. The peak control effort components are an order

of magnitude larger than in Figure 3.6.2.1.
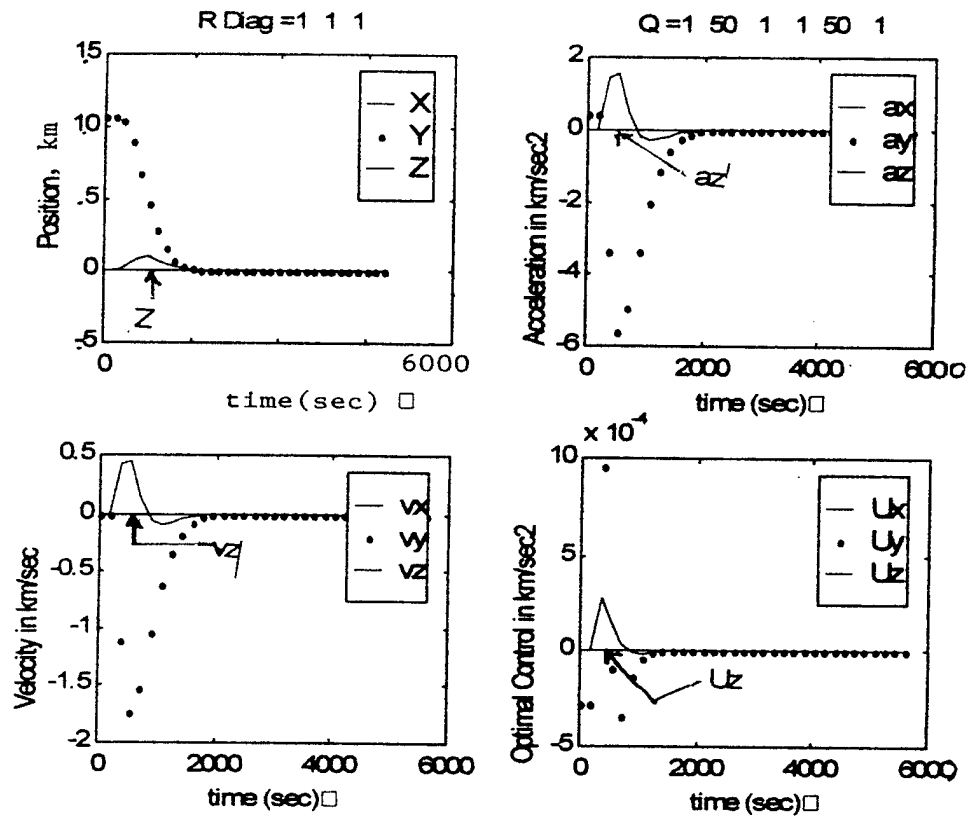
Figure 3.6.2.4

Now penalties on the y component of the state matrix and also on the $\dot{y}$ component of the

state matrix are increased 50 fold. The end result is almost an order of magnitude increase

in control effort, and a slight improvement in reducing some of the transient overshoots as

compared with the results in Figure 3.6.2.1.
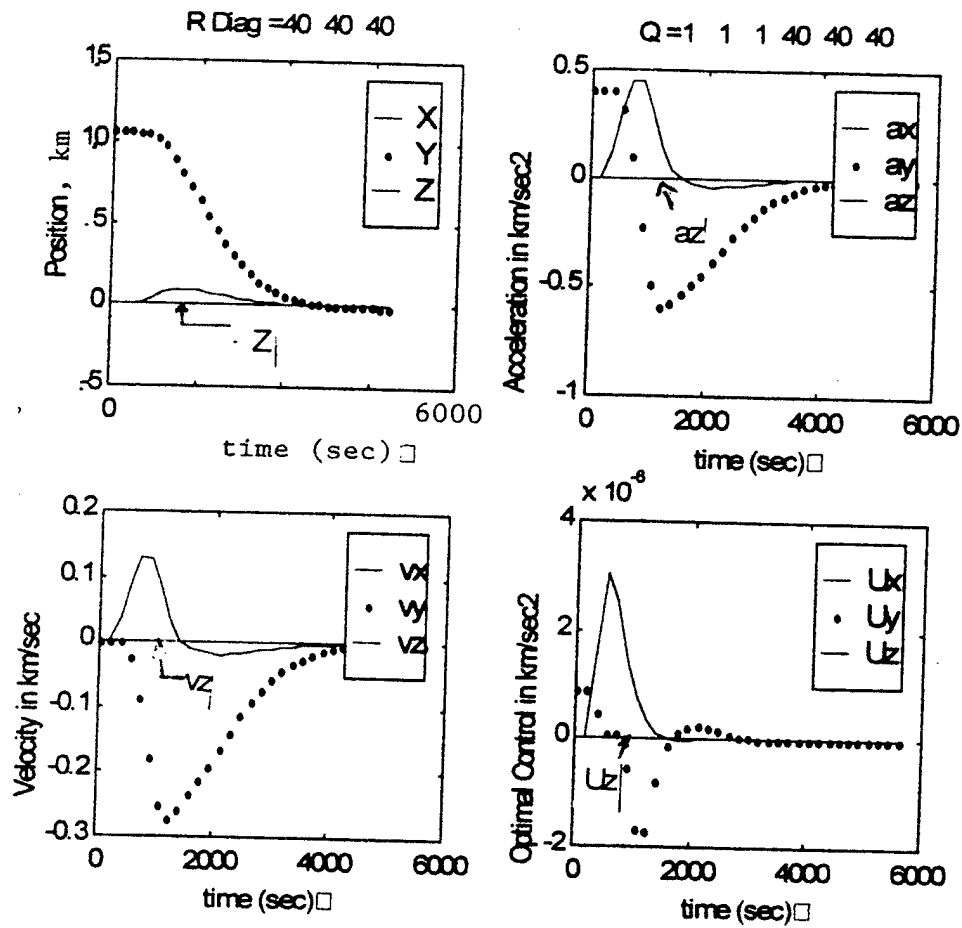
Figure 3.6.2.5

In this example, the split weighting strategy is employed. **R** is penalized more than before, requiring in some cases almost 4000 sec (twice the time of Figure 3.6.2.1) to reach steady state; this results in an order of magnitude reduction in control effort **u.**. Transient responses are noticeably more sluggish.
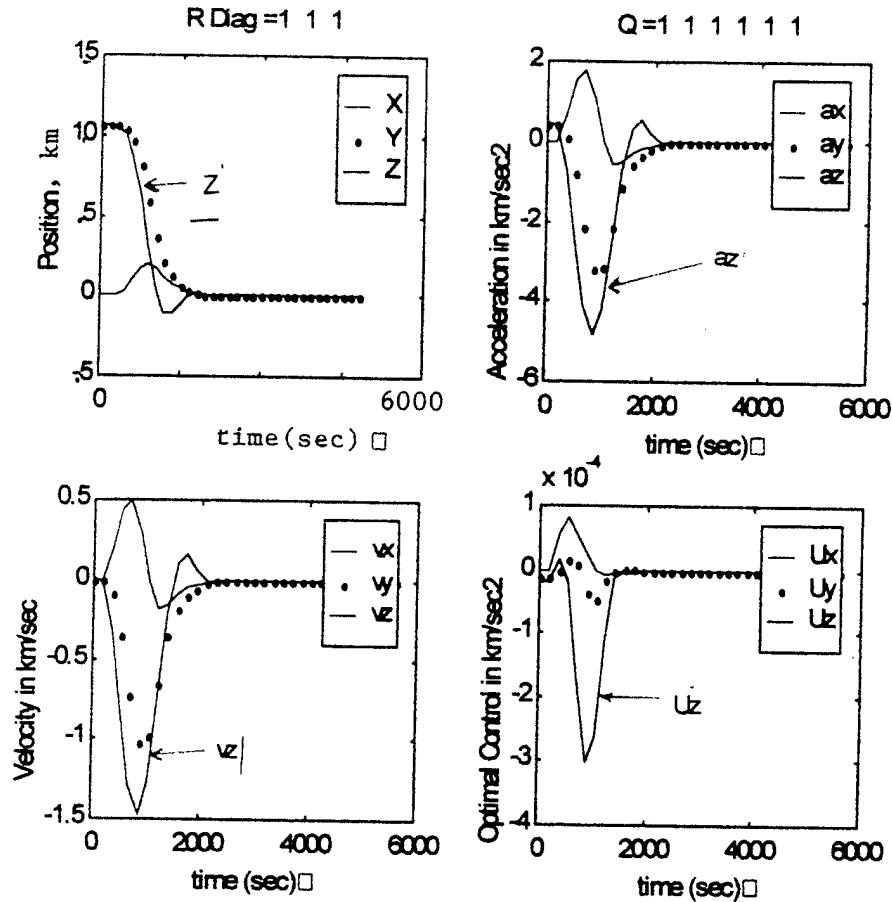
Figure 3.6.2.6

Although the previous results emphasized coplanar type maneuvers, here an out-of-plane error in position of 1 km is now given at the 45 ^{0} true anomaly point, in addition to the 1 km error along track. The weighting functions are the same as those of Figure 3.6.2.1. This Figure depicts consistence as it relates to input error. Furthermore, damped simple harmonic motion (SHM) is demonstrated as predicted by the out-of-plane Tschauner-Hempel equation.

Diagonal R = 1 1 1Q Diagonal = 1 1 1 1 1 1
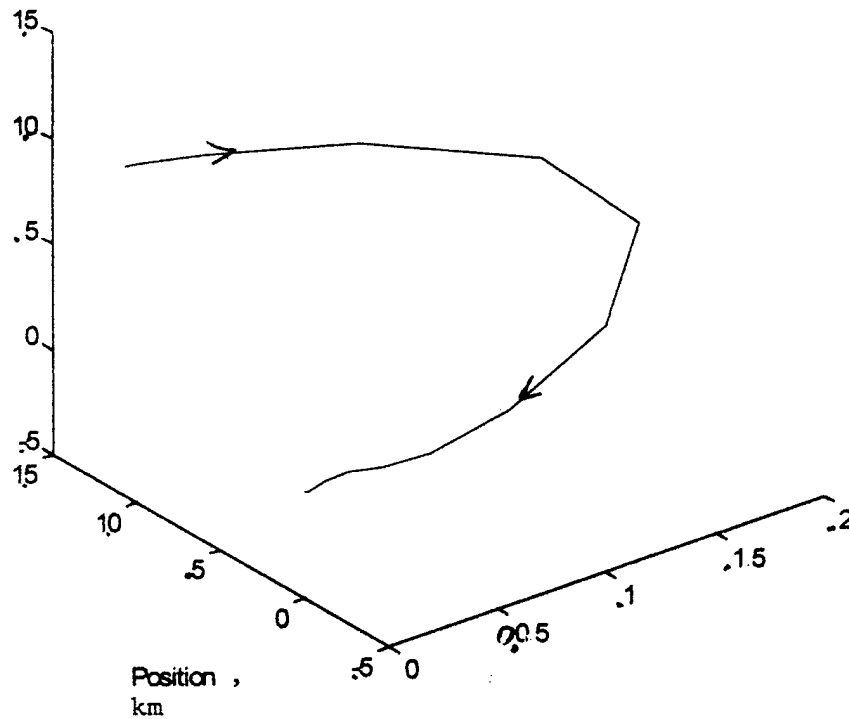
Figure 3.6.2.7

Figure 3.6.2.7 is a three dimensional depiction of Figure 3.6.2.6. The weighting elements

selected here by no means infer that these are the optimal choices or combination of choices,

only to demonstrate capability and workability.

Preliminary results assume the initial LQR correction begins near perigee, at a true

anomaly angle of 45 ^{0}. The preliminary results here validate the controllability and stability

82

of the LQR control strategy and verify convergence in a relatively short time interval in response to an initial displacement. The response time is much shorter than that of Tan, et. al.[38] or Schaub, et. al.[51]. Both used a Lyapunov type of approach. Tan applied the approach to the osculating orbital elements, while Schaub used the mean orbital elements.

3.6.3 Modification to Station Keeping Strategy due to the Earth's Planetary and Lunar Perturbations

To understand the effects of Earth's planetary, and Lunar perturbations, let's begin with a description of the software and its inputs. The Ada Simulation Development System (ASDS)[21] or, more commonly, BG14, has the following environment models available: Atmosphere, Gravity, Gravity Gradient Torque, Third Body Effects, Tidal Forces due to Sun and Moon, Solar Radiation Pressure and Solar System Models, including ephemeris and planet physical parameters. Two ephemeris modeling capabilities exist in ASDS. One uses an analytical approach to computing planetary ephemerides (Van Flandern), while the other one uses actual Jet Propulsion Laboratory (JPL) data for the planets and satellites. The Van Flandern model gives low-precision (1 degree) formulas for geocentric and heliocentric positions of the Sun, Moon, and planets, which are valid for any epoch within 300 years of the present. In the JPL version, an ephemeris of the Moon and nine planets has been numerically integrated from 1411 BC to 3002 AD. A long ephemeris has utility for comparison with both historical observations and analytical theories. The environment data set provides inputs as central body and the perturbing forces. It is seen that Central_ Body = Earth, Third_Body_Plantes= Sun and Moon, Gravity_Model=wgs_84 (forces the use of an Earth fixed system), Gravity(with various order and/or degree) and Solar_Radiation is set

to either 'on' or 'off'. Note that the solar system model(ephemeris) used is the JPL Ephemeris unless the date specified lies outside the valid ephemeris dates, in which case Van Flandern is used.

Higher harmonics of perturbations in three dimensions, can be seen from the more general form for the Earth's gravitational potential which can be written as

$$V(r,\varphi,\vartheta) = \frac{Gm}{r}\left[1 - \sum_{k=2}^{\infty} J_k \left(\frac{r_{eq}}{r}\right)^k P_k(\cos\varphi)\right]$$

$$+ \frac{Gm}{r} \sum_{k=2}^{\infty} \sum_{j=1}^{k} \left(\frac{r_{eq}}{r}\right)^k P_k^j(\cos\varphi)\left\{C_k^j \cos j\vartheta + S_k^j \sin j\vartheta\right\}$$

J_k is defined as $J_k = -C_k^0$. Values of the various coefficients are obtained from satellite observations. The k's correspond to degrees, whereby the j's depict the order. As the degree and order increase, the order of magnitude effect of each harmonic on satellite motion decreases.
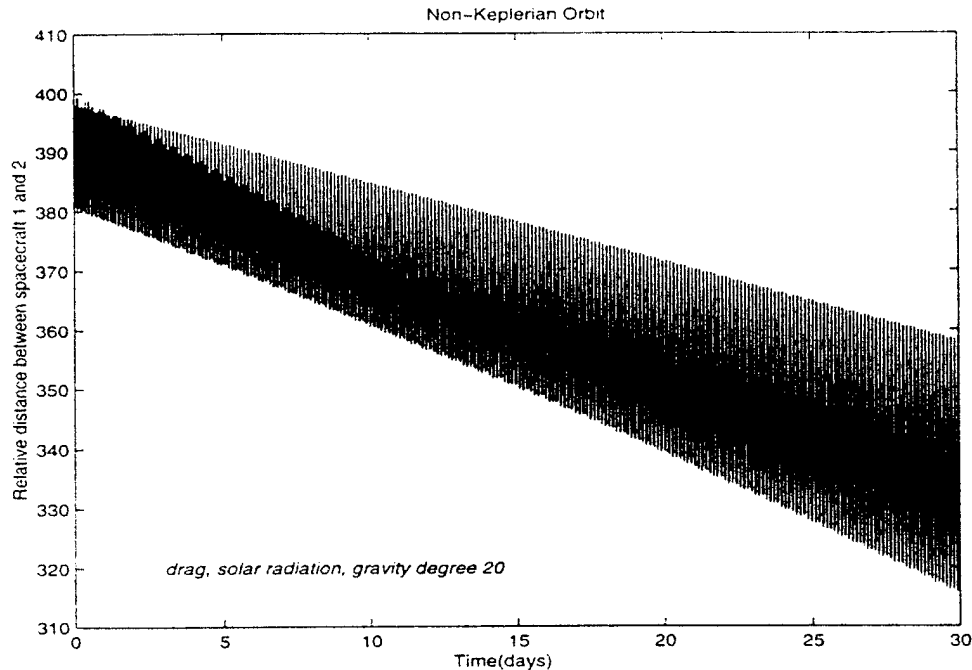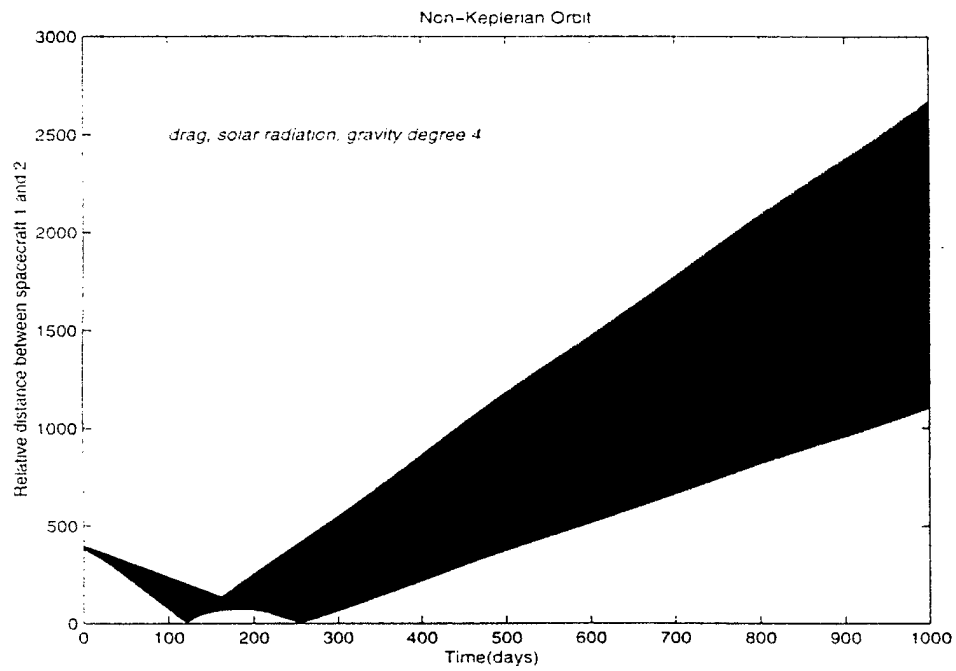
Figure 3.6.3.1(a)   30 Day Time History of Separation Distance
between Mother and Daughter Satellite Non-Keplerian Orbit

From Figure 3.6.3.1(a), the degree as well as order was set to equal 20. These higher

harmonics seemed to have negligible effect in comparison with Fig 3.4.1(b), for a satellite

with an initial separation of 400 km for a 30 day orbit.

On the other hand, higher harmonics do contribute, although slightly, for orbits in

excess of 100 days. Here the question of collision is answered; that is, if no other corrections

are given, "what happens?" The effects of including these higher harmonics (20 by 20)

delays the collision time by 25 days, otherwise collision time would have been reached at

approximately 125 days, instead of the now 150 days. See Figures 3.6.3.1 (b and c).

85

Figure 3.6.3.1(b) 1000 Day Time History of Separation Distance between Mother and Daughter Satellite Non-Keplerian Orbit
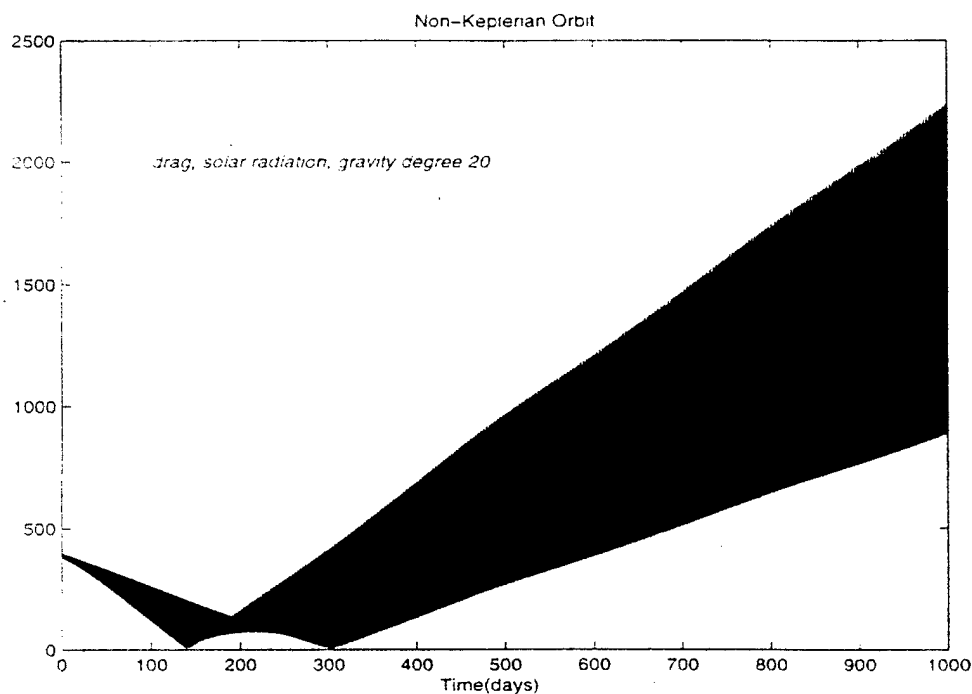
Figure 3.6.3.1(c)   1000 Day Time History of Separation Distance between Mother and Daughter Satellite Non-Keplerian Orbit

In summary, for relative short orbit periods (i.e. 30 days = 236+ orbits), the Earth's planetary and Lunar perturbation exhibited negligible effect. For higher harmonics, the Earth's planetary and Lunar perturbation became noticeable for orbits of 100 days or more. It is also shown that higher orders and degrees of perturbation increased the lifetime of the satellite by prolonging the time before zero separation is reached. The shifting of lines of apsides for this elliptical orbit, showed an order of magnitude improvement in reaching the time of collision, as compared to that of Badesha's circular orbit [32].

IV   THE IMPLEMENTATION OF MAINTAINING CONSTANT
DISTANCE BETWEEN SATELLITES IN ELLIPTIC ORBITS

4.1 INTRODUCTION

The scientific objectives of the Earth observation program are becoming more autonomous and more ambitious; this has created needs for innovative technical approaches to achieving and maintaining constellation and formation flights of spacecraft. The trend to develop small low-cost spacecraft has led many to recognize the advantage of flying multiple spacecraft in formation to achieve the correlated instrumentation formerly possible only by placing many instruments on a single platform.

A study was conducted of proposed NASA and ESA constellation configurations which would measure and study upper atmospheric phenomena. The Auroral Cluster (Multiscale) System, the Distance Measurement System, the Orbiting Interferometer System, as suggested by NASA for LEO missions together with the Solar Stereo System in heliocentric orbit were all considered as possible baseline or "strawman" configurations. In addition information was also obtained from the ESA web page on the proposed ESA Cluster mission with the objective of determining physical processes involved in the interaction between the solar wind and the magnetosphere by visiting key regions such as the polar cusps and magnetotail.

After reviewing the candidate configurations it was decided to select the Auroral Multiscale Mission (AMM) as a baseline or "strawman" model for this research: a brief description and sketch of this system is given in Fig.4.1 and Table 4.1. Initially for this study the "strawman" configuration would be based on four spacecraft in the same plane
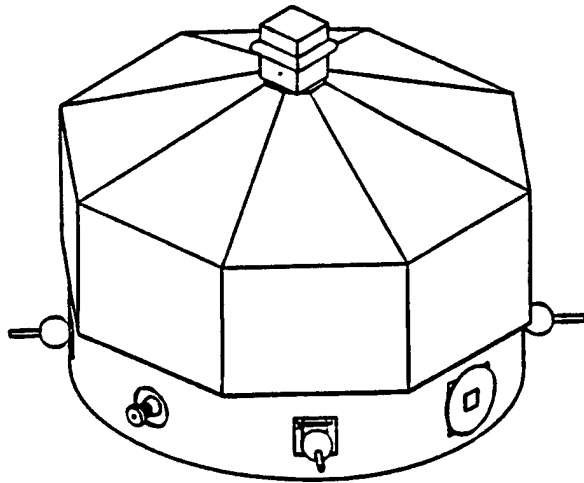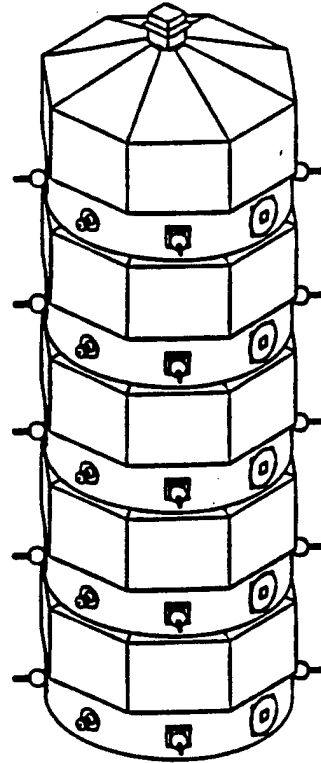
SingleAMM Spacecraft / Stowed Configuration   Launch Configuration

Fig. 4.1 Auroral Multiscale Mission System

Table 4.1. Strawman Configuration

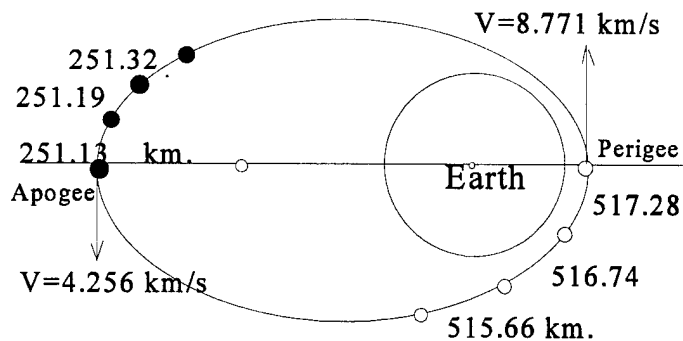|	
Mission	Multi-point 3-dimensional data collection of auroral phenomena
Orbit	600×8000 km, 83° inclination
Launch Vehicle	Taurus (2110 vehicle), Insertion Mass of 465.5 kg, argp=203.1°
Spacecraft Size	40 inch diameter (across flats)
Spacecraft Mass	90 kg each
Science Payload	Ion/Electron spectrometer, UV Auroral Imager, Magnetometer, Electric Fields (3-axis)
Position Knowledge	GPS, Knowledge to 100 meters (3 sigma)
Attitude Knowledge	0.01° Star Tracker (referenced to magnetometer), star-tracker implementation. Spinning sun-sensor / magnetometer provides coarse attitude.
Power	Solar array capability: 40 watts orbit average power Energy Storage: Dual IPACS Flywheel momentum bias system used for both power and attitude control

Fig.4.2 Variable Velocities & Phase Distances

principally along the orbit track. The perigee altitude is selected to be 600 km, the apogee altitude is selected to be 8000 km. and the nominal separation distance between two adjacent satellites is taken to be 500 km Without any perturbation or any control, the velocity at perigee and apogee as well as the separation distances are shown in Fig.4.2. From Fig.4.2 it is seen that the separation distances at perigee are more than twice the separation distances at apogee. To maintain constant separation distance in such an orbit, it would be necessary to correct the orbit continuously; the tremendous amount of energy required makes this strategy unfeasible.

A novel idea for implementation of constant separation distances for the AMM mission is developed[49]. The four satellites are launched by a single vehicle; the method to distribute the satellites into their positions using the least maneuver energy is given in this chapter.

Because of various perturbations (mainly caused by the J_2 effect) and/or initial errors, the separation can not be maintained without control. There are several mathematical models that can be
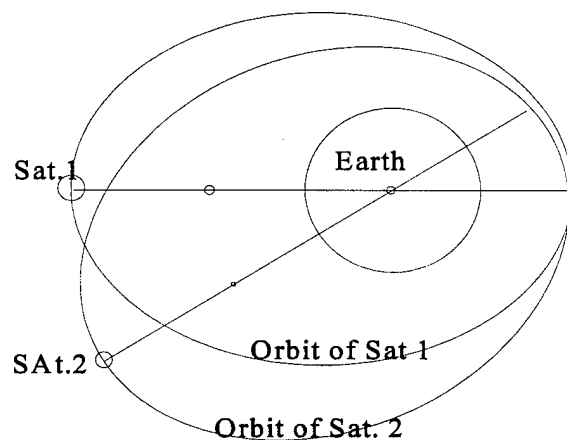

Fig.4.3 Angle Between Orbits of Two Satellites

90

used to design the controllers. The Clohessy-Wiltshire equations[22] (sometimes referred to as the Hill-Clohessy-Wiltshire equations[60]) assume circular orbits and a spherical Earth model, and the equations of motion of the orbiting spacecraft are linearized relative to the rotating frame of the reference spacecraft. Here, however, the orbit is elliptic.

In this chapter by controlling the osculating orbital elements the constant separation is successfully maintained. The advantage is taken of celestial mechanics insight to avoid the correction of orbital elements at ill-suited times. Since the model involving the osculating orbital elements is inherently nonlinear and time-variant, control logic based on a Lyapunov function is applied. The control is much simpler than the one of Schaub et al[51], therefore it is easier to implement in engineering practice. All simulations are performed by MATLAB and the BG14 orbital propagator [21].

4.2 REVIEW OF STRATEGY FOR MAINTAINING DISTANCE IN ELLIPTIC ORBITS

In order to maintain a constant distance between two satellites in elliptic orbits, the semi-major axis of the orbit of the second satellite should be shifted by a very small angle (something like 1.37°) with respect to the orbit of the mother satellite in order to achieve the constant separation distance. Both orbits are in the same plane (Fig.4.3). If there are two satellites flying in the orbits shown in Fig.4.3, both in the counter clockwise direction, at exactly the same time that they arrive at their perigees and apogees, respectively, the distance between the two satellites is defined as the geometric distance, roughly the distance caused by the shift of the semi-major axis of the orbit; if the satellites are flying in exactly the same orbit (shown in Fig.4.2), the distance between the adjacent satellites is defined as the phase distance, i.e . the distance accounted for during the time in which the first satellite will reach

the second satellite's current position. From Fig.4.3, it is seen that the geometric distance at the perigee is smaller than the one at the apogee. The strategy here is that if the phase distance is compensated by the geometric distance, then the resulting separation distance between the adjacent satellites is maintained to be essentially constant[49]. The details of the calculation are presented as follows:

From Fig.4.3, if the angle between the two semi-major axes is α, the distances between satellites 1 and 2 at perigee and apogee (the geometric distances) are

$$2\,(R_e + perigee\ \ altitude)\sin(\frac{\alpha}{2}) \quad and \quad 2\,(R_e + apogee\ \ altitude)\sin(\frac{\alpha}{2})$$

respectively, where R_e is the radius of the Earth. Let the phase distances at perigee and apogee be Pp and Pa, respectively (Fig.4.2), We try to make the resulting distance at apogee the same as the one at perigee, e.g. 512 km. i.e.

$$2\,(R_e + perigee\ \ altitude)\sin(\frac{\alpha}{2}) + Pp\ =\ 512 \qquad (1)$$

$$2\,(R_e + apogee\ \ altitude)\sin(\frac{\alpha}{2}) + Pa\ =\ 512 \qquad (2)$$

From Fig.4.2, it is noticed that

$$\frac{Pp}{Pa}\ =\ \frac{517.28}{251.13} \qquad (3)$$

The solution of equations (1)-(3) is α =1.37°, Pp=344.705 km, Pa=167.295 km. That means, satellite 1 arrives at its own perigee (or apogee) 39.5 seconds later than satellite 2 does.

An example of the constellation in an orbit described above, with nominal separation distance of 500 km., is given here. The simulation is done by MATLAB and BG14; the simulation results are identical, shown in Fig. 4.4, which shows the simulation results for 16
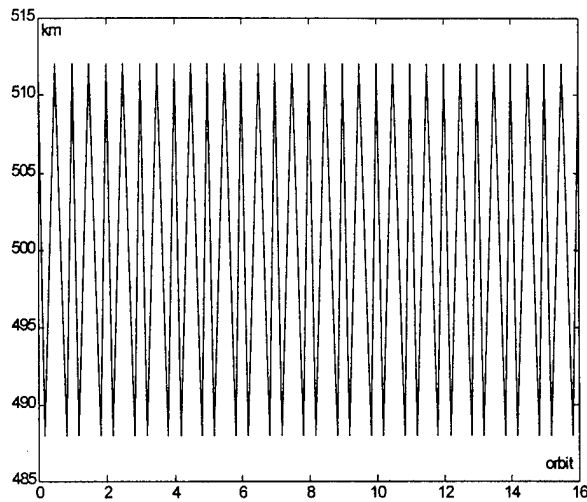
Fig.4.4. Separation Distance, Keplerian Orbit

Keplerian orbits. The maximum distance, 512 km, occurs at perigee and apogee; the minimum distance, 488 km, takes place between the perigee and apogee. Without perturbations and subsequent control this distance would be maintained forever; the drift from the nominal value, 500 km, is about ±2.4%.

4.3 INITIAL SEPARATION DEPLOYMENT

It is assumed that the four satellites are launched by a single vehicle, see Fig.4.1; therefore, it is important to study the method to separate the satellites using the least maneuver energy. After comparison of several maneuver methods, the following approach was selected, because all the work done by the thrusters is used to augment the energy which is required from the transient orbit to the final orbit.

There are two tasks for initial separation: one is to cause a shift in the angle (about 1.37°) between the semi-major-axes of the orbits of the adjacent satellites; the other is to create a phase difference, i.e. according to reference 1, the second satellite arrives at its perigee 39.5 seconds earlier than the first one does. It is well known that if a satellite travels in a circular orbit, its speed is the same at any point; and if the satellite is accelerated to a larger speed (V) along the track at some point, say A, then the satellite will go into an elliptical orbit, whose perigee is A, and the apogee depends on the speed V. Therefore, the

93

four satellites are launched by a single vehicle into a circular orbit 600 km from the Earth's surface with a required ascending node and inclination angle. From this orbit, if any satellite is accelerated to a larger speed along the track, its perigee must be 600 km.; and it is easy to cause a shift in the angle between the semi-major-axes of the orbits of the adjacent satellites.

① The four satellites are traveling in the circular orbit (orbit 5 in Fig.4.5), the speed of this orbit is 7.558 km/s. When they move to the position of the required argument of perigee of the mother satellite, the mother satellite will be released and accelerated along the track to 8.770 km/s, the perigee speed of the final orbit. Thus, the mother satellite will travel in an orbit whose perigee is at this point, 600 km from the Earth's surface, and the apogee is 8000 km from the Earth's surface (the orbit 1 in Fig.4.5). The other three daughter
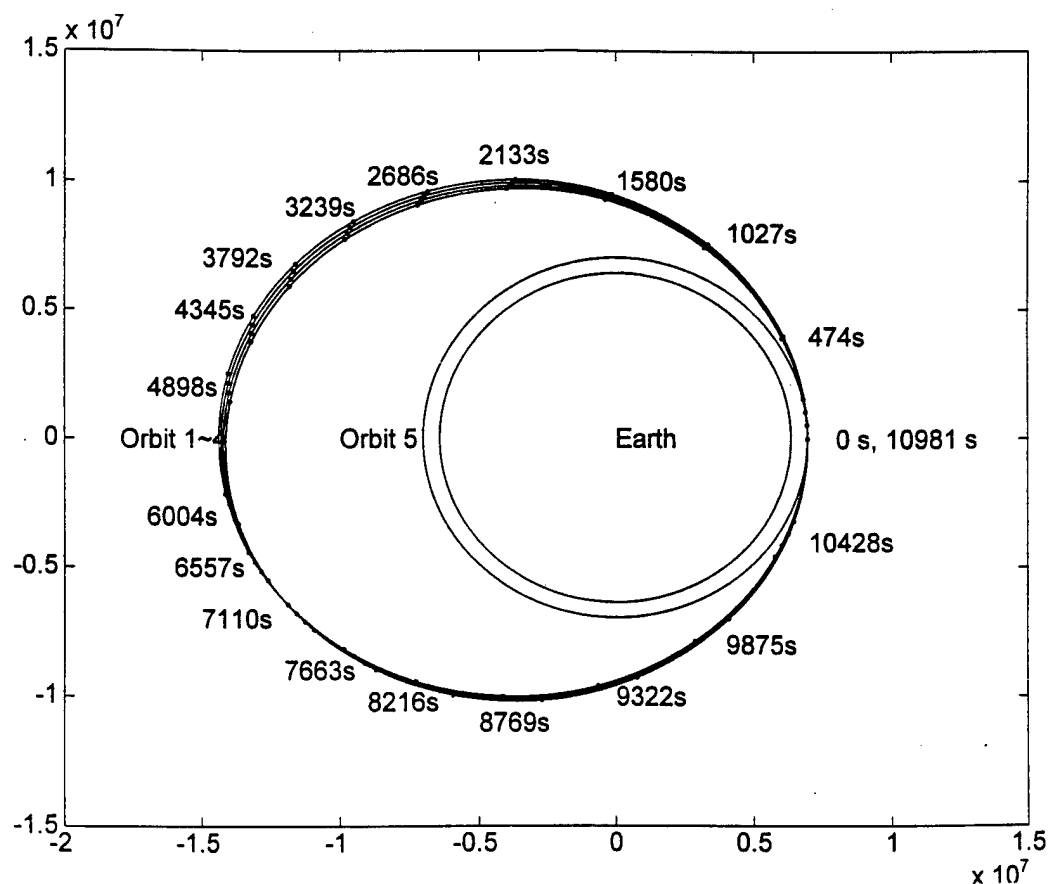

Fig.4.5 Deployment of the Four Satellites in Constellation

the unit for both coordinate axes is meter. s's inside the figure mean seconds, the position 10981 s is identical with the point 0. but at point 0. all four satellites are joined together. at 10981 s they are separated 500 km. apart.

94

satellites are still moving in orbit 5 at this moment.

② 22.56 seconds after the release of the mother satellite, the three daughter satellites have swept through 1.37° in the circular orbit. At this moment, if the first daughter satellite is released and accelerated along the track also to 8.770 km/s, the first daughter satellite will travel in an orbit whose perigee is at this point, 600 km from the Earth's surface, and the semi-major-axis is 1.37° apart from the one of the mother satellite. At this moment , however, the mother satellite already left its perigee 22.56 seconds earlier; that means the phase of the first daughter satellite is 22.56 seconds later than the one of mother satellite. But it is required that the phase of the first daughter satellite be 39.5 seconds *earlier* than the one of the mother satellite. Therefore we let the first daughter satellite travel in a transient orbit whose period is 22.56+39.5=62.06 seconds less than the period of the mother satellite's orbit. The period of the mother satellite's orbit is

$$T = 2\pi\sqrt{a^3/\gamma} = 10981.31 s$$

where a is semi-major-axis of the mother satellite's orbit; γ, the gravitational constant, =3.986005×10^{14}, so the period of the first daughter satellite's transient orbit T_1, its semi-major axis a_1 and the speed v_1 at its perigee are

$$T_1 = T - 62.06 = 10919.25 \ s \qquad a_1 = (\frac{T_1}{2\pi}\gamma^2)^{\frac{1}{2}\frac{2}{3}} = 10637.867 \ km$$

$$c_1 = a_1 - (perigee + R_e) = 10637.867 - 600 - 6378.137 = 3659.73 \ km.$$

$$e_1 = c_1/a_1 = 0.344028552 \qquad b_1^2 = a_1^2 - c_1^2, \qquad b_1 = 9988.523 \ km. \qquad (4)$$

$$p_1 = b_1^2/a_1 \qquad h_1 = \sqrt{p_1\gamma} \qquad v_1 = \frac{b_1 h_1}{a_1^2\sqrt{1 - e_1^2}(1 - e_1)} = 8.762 \ km/s$$

where R_e is the radius of the Earth. So the first daughter satellite is accelerated to 8.762 km/s

instead of 8.77 km/s. Thus it will travel in a smaller orbit (orbit 2 in Fig.4.5), whose semi-major-axis is 10637.867 km., and period is 10919.25 seconds. That means the first daughter satellite returns to its perigee in 62.06 seconds less than the mother satellite, but the first daughter satellite is released 22.56 seconds later than the mother satellite, so its phase is 39.50 seconds ahead of the mother satellite, i.e. the phase distance. Once the first daughter satellite returns to its perigee, it will be accelerated again until the speed reaches 8.770 km/s. So it will finally travel in an orbit with the same orbital elements as the mother satellite, i.e. the semi-major-axis, eccentricity, inclination, ascending node, except for the the argument of the perigee (the difference is 1.37°), and the mean anomaly (the difference is n×39.5).

③ Similarly, 22.56 seconds after the release of the first daughter satellite, the remaining two satellites have swept through another 1.37° in the circular orbit. At this moment the second daughter satellite is released by using the same method as in Eqs. (4), i.e., ❶ $T_2=T_1-62.06$, ❷ Calculating a_2 from T_2, ❸ Calculating c_2 from a_2, ❹ Calculating e_2 and b_2 from a_2 and c_2, then p_2 and h_2, ❺ Eventually $v_2 =8.754$ km/s. So the second daughter satellite is accelerated along the track to 8.754 km/s. In this way the second daughter satellite will travel in an orbit (orbit 3 in Fig.4.5) which is 1.37° away from the first daughter satellite and 39.50 seconds in phase ahead of the first daughter satellite. When the second daughter satellite returns to its perigee, it will also be accelerated to 8.770 km/s.

④ Similarly, 22.56 seconds after the release of the second daughter satellite, the last daughter satellite is released and accelerated along the track to 8.746 km/s so that the last daughter satellite will travel in orbit 4 in Fig.4.5. It will also be accelerated to 8.770 km/s when it returns to its perigee.

The simulation results are shown in Fig.4.5, where the unit for both coordinate axes

Table 4.2. Total Δv's Required for the Four Satellites and the Moments when They Should be Accelerated, Respectively.

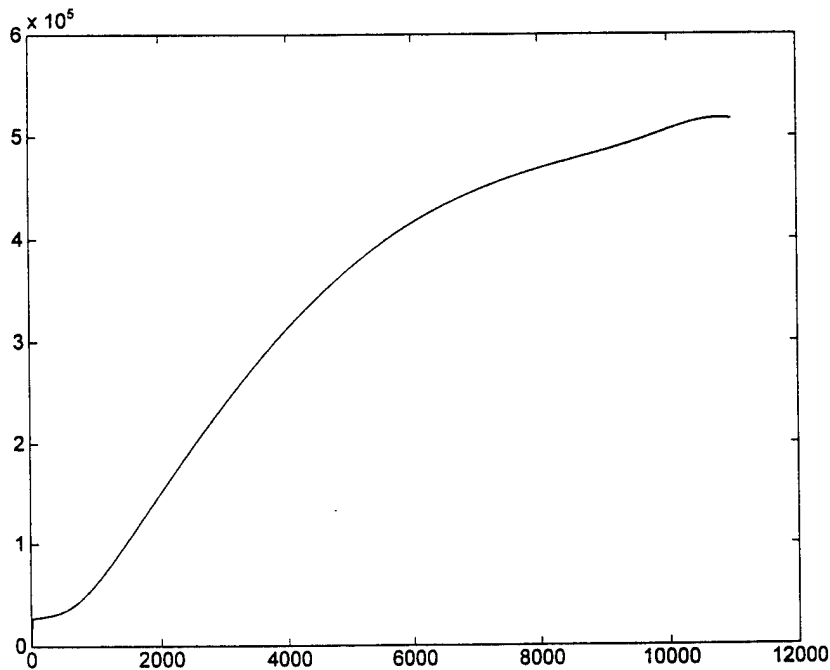|	THE FIRST MANEUVER		THE SECOND MANEUVER	
	Time, sec|	Δv required, m/s	Time, sec.	|Δv required, m/s
Mother Sat.	0	8770.1-7557.9=1212.2	10981.31	0
Daughter Sat.1	22.56	8762.0-7557.9=1204.1	10941.81	8770-8762=8.06
Daughter Sat.2	45.12	8753.9-7557.9=1196.0	10902.31	8770-8754=16.2
Daughter Sat.3	67.68	8745.6-7557.9=1187.8	10862.81	8770-8746=24.4

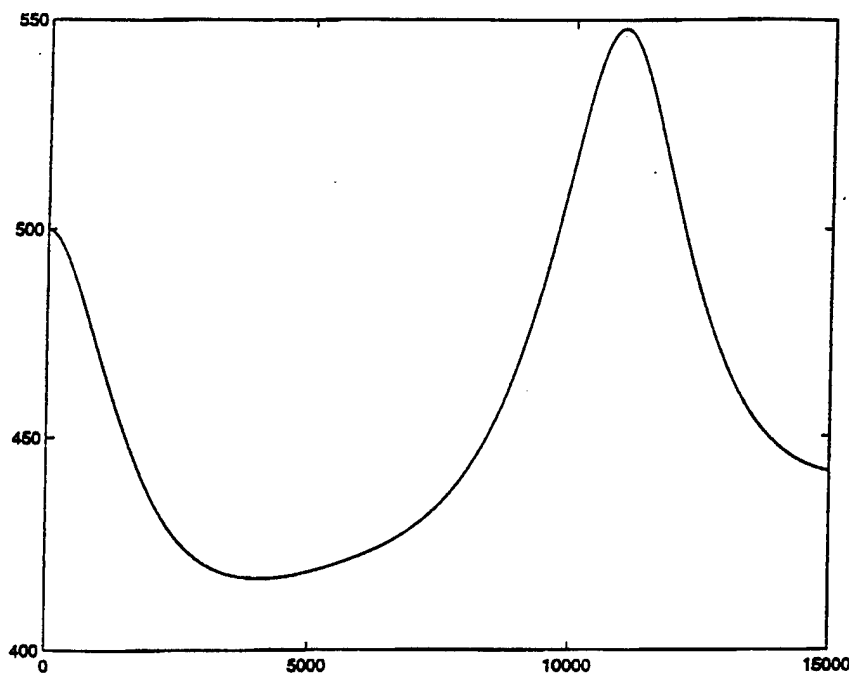Fig.4.6 Distance Between Mother and First Daughter Satellites

is meter, s's inside the figure mean seconds, i.e. the time for release of the mother satellite is 0 second, before that all four satellites are packed together in a single launch vehicle. The orbital period of the final orbits is 10981.31 seconds, so the position of 10981 s is identical with the point of 0 second, but the satellites are already separated 500 km apart. The history of the distance between the mother satellite and the first daughter satellite with respect to time is shown in Fig.4.6, and the total Δv required for the four satellites is shown in Table 4.2.

97

4.4 STATIONKEEPING MAINTENANCE

The analysis to this point is based on the Keplerian orbit theory[12], i.e. there is no perturbation. The orbital elements are very sensitive to the initial condition. Suppose at the time t=10981.31 sec. the mother satellite orbit's semi-major-axis is along the x axis, and its semilatus rectum is along the y axis, then for this problem, x should be 6978.137 km, y=0, dx/dt=0, dy/dt=8.77km/s; for the first daughter satellite, x=6962.313 km, y=0.49977km, dx/dt=-0.51917km/s, dy/dt=8.753km/s. If, somehow, possibly due to perturbations, the first daughter satellite has a small initial velocity error so that for the first daughter satellite dx/dt=-0.52842km/s, dy/dt=8.787 km/s then the distance between the mother satellite and the first daughter satellite vs. time is shown in Fig.4.7. It is obvious that the distance can not be maintained to be around 500 km., and the distance is diverging. Even though the first and second maneuvers are performed so perfectly that positions and velocities after the second maneuver are exactly as required, with perturbations (mainly J_2) the distance 500 ±12 km. can not maintained forever (as indicated in Fig.4.4).

Fig.4.7. The Distance (km) between Adjacent Satellites vs Time (sec.) with Small Initial Velocity Error.

98

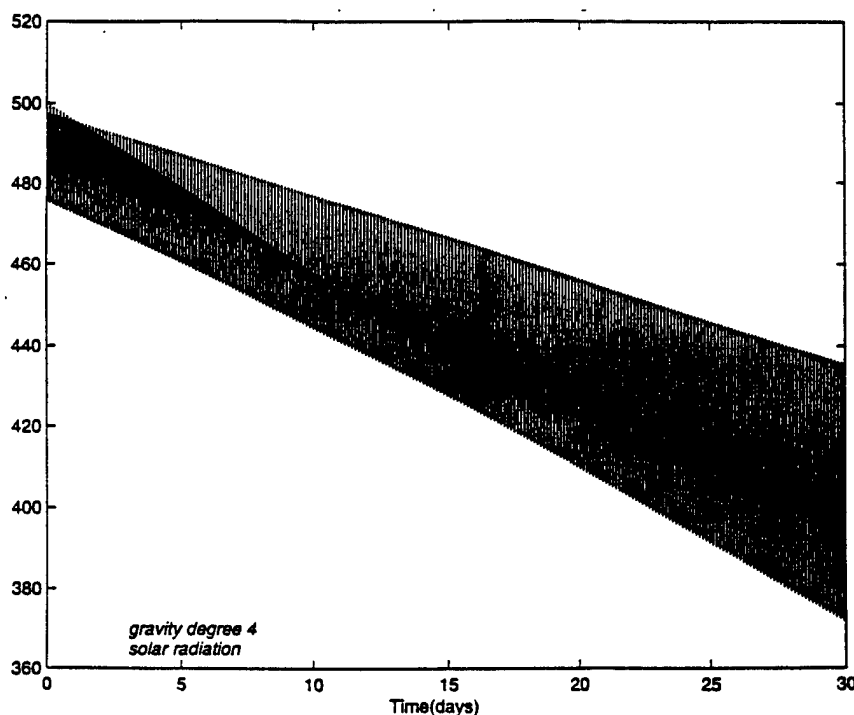Fig. 4.8. The Distance between Adjacent Satellites with Perturbations

Fig.4.8 is the 30 days simulation result of the distance between adjacent satellites using the BG14. From Fig.4.8, it is seen that with perturbations a secular drift appears in the transient response; by the thirtieth day the distance oscillates around 405±30 km. Therefore, some kind of control must be applied to the formation flight system. There are many papers dealing with formation control[51, 61, 37, 2]; most of them are approaches feeding back position and velocity vector errors. In this paper a feedback law in terms of osculating orbital elements is studied. By comparing the situations depicted in Fig.4.4 and Fig.4.8, we can develop a control strategy so that the control effect in the presence of perturbations (including J_2) is spent principally to remove the secular drift of the separation distance (Fig.4.8), and minimally to remove the amplitude of the small oscillations (Fig.4.4). This can be accomplished with the feedback of the variations in the osculating orbital elements of the daughter satellite from some nominal values. With this philosophy, control energy can be conserved as compared with the other traditional feedback strategies, e.g. feedback of position and velocity error components.

Gauss's variational equations of motion provide a convenient set of equations relating

the effect of a control acceleration vector **u** to the osculating orbital element time derivatives[52].

$$\dot{a} = (2a^2/h) \ (\ e \sin f \ u_r \ + \ (p/r) \ u_\theta \ ) \qquad (5a)$$
$$\dot{e} = [p \sin f \ u_r + ((p+r)\cos f + re) \ u_\theta]/h \qquad (5b)$$
$$\dot{i} = [(r \cos \theta) \ / \ h] \ u_h \qquad (5c)$$
$$\dot{\Omega} = [(r \sin \theta)/(h \sin \iota)] \ u_h \qquad (5d)$$
$$\dot{\omega} = \frac{1}{he}[-p\cos f u_r + (p+r)\sin f u_\theta] - \frac{r \sin \theta \cos \iota}{h \sin \iota} u_h \qquad (5e)$$
$$\dot{M} = n + [\eta/(he)][(p\cos f - 2re)u_r - (p+r)\sin f u_\theta] \qquad (5f)$$

where a is the semi-major axis; e is the eccentricity; ι is the inclination; Ω is the longitude of the ascending node; ω is the argument of the perigee, M is the mean anomaly. We define **x**=(a e ι Ω ω M)' as the state variable vector and **u**=(u_r u_θ u_h)' as the control acceleration vector, written in the Local-Vertical-Local-Horizontal frame, u_r points radially away from the Earth, u_h is aligned with the orbit angular momentum vector, u_θ is orthogonal to both u_r and u_h. f is the true anomaly, r is the scalar orbit radius, p is the semilatus rectum(see Eq.(4)), $\theta = \omega + f$, h, η and the mean angular velocity n are

$$h = \sqrt{p\gamma} \qquad \eta = \sqrt{1 - e^2} \qquad n = \sqrt{\gamma/a^3}$$

Incorporating the J_2 influence, Eq.(5) can be written as [52]

$$\dot{x} = B(x) \ u + D(x) \qquad (6)$$

where

$$D(x) = [0, \ 0, \ 0, \ -\frac{3}{2}J_2(\frac{R_e}{p})^2 n \cos \iota, \ \frac{3}{4}J_2(\frac{R_e}{p})^2 n(5\cos^2 \iota - 1), \ n + \frac{3}{4}J_2(\frac{R_e}{p})^2 \eta n(3\cos^2 \iota - 1)]^T \qquad (7)$$

100

and

$$
B(x) = \begin{bmatrix}
(2a^2 e \sin f)/h & (2a^2 p)/(hr) & 0 \\
(p \sin f)/h & [(p+r)\cos f + re]/h & 0 \\
0 & 0 & (r\cos\theta)/h \\
0 & 0 & (r\sin\theta)/(h\sin\iota) \\
-(p\cos f)/(he) & [(p+r)\sin f]/(he) & -(r\sin\theta\cos\iota)/(h\sin\iota) \\
\eta(p\cos f - 2re)/(he) & -[\eta(p+r)\sin f]/(he) & 0
\end{bmatrix}
\tag{8}
$$

Substituting the orbital parameters used in this paper into Eq.(7)

$$
D(x) = [0 \quad 0 \quad 0 \quad -5.218\times10^{-8} \quad -1.982\times10^{-7} \quad n+1.919\times10^{-7}]^T
\tag{9}
$$

The elements of D are very small, and if the formation flying system is under control the orbital parameters should not drift far away from the nominal values; thus D(x) should be very close to Eq.(9). Therefore, D(x) is treated as a minor disturbance instead of part of the plant matrix.

From Eq.(8), it is seen that the system is nonlinear and time variant, so a control law based on a Lyapunov function is applied. If the osculating orbital elements of the mother satellite are x_1, the required osculating orbital elements of the first daughter satellite are x_2, then

$$
\Delta x = x_2 - x_1 \qquad i.e. \qquad x_2 = x_1 + \Delta x
\tag{10}
$$

Assuming that the actual osculating orbital elements of the first daughter satellite are x_{2d}, then

$$
\delta x = x_{2d} - x_2 \qquad i.e. \qquad x_{2d} = x_2 + \delta x
\tag{11}
$$

101

We define a Lyapunov function as

$$V = \frac{1}{2}(a + be^{-\alpha t}) \cdot \delta x^T \delta x \qquad \text{where } a > 0,\ b > 0,\ \alpha > 0, \quad \therefore \ V > 0 \qquad (12)$$

then

$$\dot{V} = -\frac{1}{2} b\alpha e^{-\alpha t} \delta x^T \delta x + (a + be^{-\alpha t}) \delta x^T \delta \dot{x} \qquad (13)$$

where

$$\delta x = x_{2d} - x_2 = x_{2d} - x_1 - \Delta x \qquad \textit{see Eqs.(11) and (10)}$$
$$\therefore \quad \delta \dot{x} = \dot{x}_{2d} - \dot{x}_1 \qquad \textit{note that } \Delta x \textit{ does not vary with time.}$$

substituting Eqs.(6), (7) and (8) into the above equation, and noticing that there is no control for the mother satellite, we get

$$\delta \dot{x} = B(x)u + [D(x_{2d}) - D(x_1)] \qquad (14)$$

Since in Eq.(7), J_2 and R_e for mother and first daughter satellites are the same, p, n, ι, and η are almost the same, and D(x) itself is very small, therefore, $D(x_{2d})$-$D(x_1)$ in Eq.(14) can be ignored. If we select

$$u = -\beta(B^T B)^{-1} B^T \delta x \qquad (15)$$

where β is a scalar value used to adjust the feedback gain, and substituting Eq.(15) into Eq.(14), we get

$$\delta \dot{x} = -\beta B(B^T B)^{-1} B^T \delta x \qquad (16)$$

After substituting Eq.(16) into Eq.(13) there results,

$$\dot{V} = -\frac{1}{2}b\alpha e^{-\alpha t}\delta x^T\delta x - \beta(a+be^{-\alpha t})\delta x^T B(B^TB)^{-1}B^T\delta x \tag{17}$$

$\because \Phi = B(B^TB)^{-1}B^T$ is symmetric and semi-positive definite, and Rank(Φ) $\leq$ Rank(B), here B is 6×3, $\therefore$ the eigenvalues of Φ are $\lambda_1 \geq 0$, $\lambda_2 \geq 0$, $\lambda_3 \geq 0$, 0, 0, 0. There must be an orthogonal matrix so that

$$\Phi = T\Lambda T^T \quad where \ \Lambda = T^T\Phi T = \begin{bmatrix} \lambda_1 & 0 & 0 & 0 & 0 & 0 \\ 0 & \lambda_2 & 0 & 0 & 0 & 0 \\ 0 & 0 & \lambda_3 & 0 & 0 & 0 \\ 0 & 0 & 0 & 0 & 0 & 0 \\ 0 & 0 & 0 & 0 & 0 & 0 \\ 0 & 0 & 0 & 0 & 0 & 0 \end{bmatrix} \tag{18}$$

Eq.(17) can be written as

$$\begin{aligned} \dot{V} &= -\delta x^T\, 0.5b\alpha e^{-\alpha t}\, T\, I\, T^T\, \delta x - \delta x^T\, \beta(a+be^{\alpha t})T\Lambda T^T\delta x \\ &= -\delta x^T\, [T\, 0.5b\alpha e^{-\alpha t}I\, T^T + T\, \beta(a+be^{\alpha t})\Lambda T^T]\delta x \\ &= -\delta x^T T\, [0.5b\alpha e^{-\alpha t}I + \beta(a+be^{\alpha t})\Lambda]T^T\delta x \\ &= -\delta x^T\, T\, \Xi\, T^T\, \delta x \end{aligned} \tag{19}$$
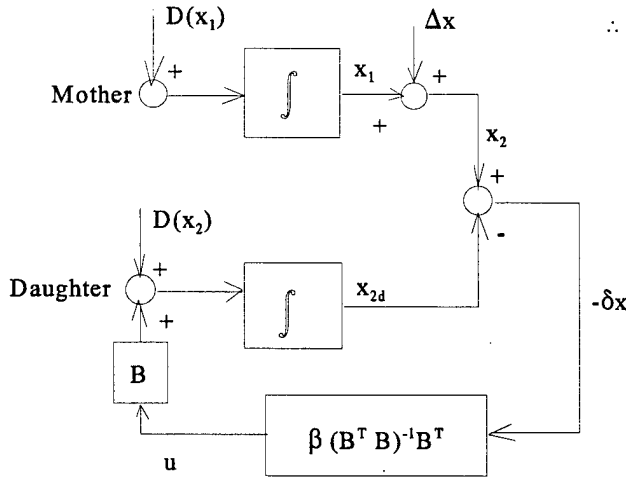
where

$$\Xi = [0.5b\alpha e^{-\alpha t}I + \beta(a+be^{\alpha t})\Lambda] \tag{20}$$

i.e.

$$\Xi = \begin{bmatrix} 0.5b\alpha e^{-\alpha t}+\beta(a+be^{-\alpha t})\lambda_1 & 0 & 0 & 0 & 0 & 0 \\ 0 & 0.5b\alpha e^{-\alpha t}+\beta(a+be^{-\alpha t})\lambda_2 & 0 & 0 & 0 & 0 \\ 0 & 0 & 0.5b\alpha e^{-\alpha t}+\beta(a+be^{-\alpha t})\lambda_3 & 0 & 0 & 0 \\ 0 & 0 & 0 & 0.5b\alpha e^{-\alpha t} & 0 & 0 \\ 0 & 0 & 0 & 0 & 0.5b\alpha e^{-\alpha t} & 0 \\ 0 & 0 & 0 & 0 & 0 & 0.5b\alpha e^{-\alpha t} \end{bmatrix}$$

Since $a>0$, $b>0$, $\alpha>0$, $\beta>0$, and $\lambda_1>0$, $\lambda_2>0$, $\lambda_3>0$, therefore Ξ is positive definite, and so is

$$T\Xi T^T. \text{ If } \delta x \neq 0, \text{ then } \delta x^T T\Xi T^T \delta x > 0,$$

Fig.4.9 Control System Diagram

$$\therefore \dot{V} = -\delta x^T T \Xi T^T \delta x < 0$$

That means the control law described by Eq.(15) can make the formation flight system asymptotically stable. It is obvious that the above analysis is also suitable for the control of the distance between the daughter satellites, e.g. for the control of the second daughter satellite to maintain the distance between it and the first daughter satellite, just replace x_1, the osculating orbital elements of the mother satellite, by x_2, the requiredosculating orbital elements of the first daughter satellite; replace x_2 by x_3, the required osculating orbital elements of the second daughter satellite, and replace x_{2d} by x_{3d}, the actual osculating orbital elements of the second daughter satellite, in Eqs.(10) and (11). The diagram of the control system is shown in Fig.4.9.

104

Table 4.3. Initial Conditions for Mother and First Daughter Satellites

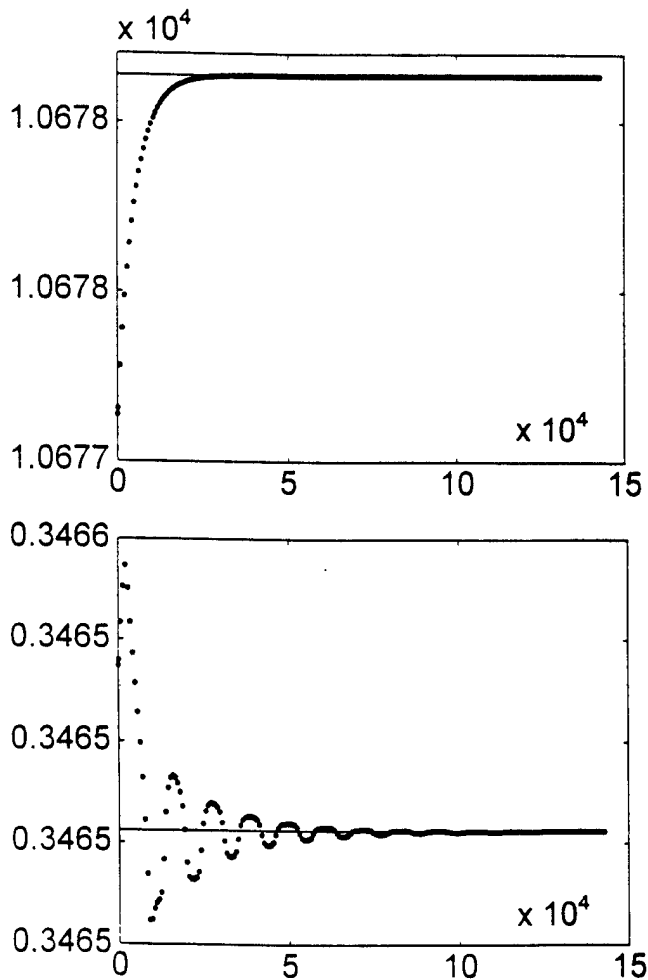| Initial Condition	Mother Satellite	Daughter Sat.1's Required Elements	Daughter Sat.1's Actual Elements	δx
a km	10678.137	10678.137	10677.137	-1
e	0.34650239	0.34650239	0.346534844	0.000032453
ι deg.	83	83	82.9985	-0.0015
Ω deg.	10	10	10	0
ω deg.	10	11.37	11.37	0
M deg.	0	0+39.5×n	39.5×n	0

Fig.4.10 Transient Responses of the Semi-major Axis and the Eccentricity

4.5 NUMERICAL SIMULATIONS

With various perturbations, including atmosphere drag, solar pressure, the Earth's magnetic field, perturbations from the Moon and other planets, and J_n's effect, where n=2 is the most important contribution, the osculating orbital elements do not remain constant. The values of α, the angle between the semi-major axes of the adjacent satellites, and the Pp, the phase distance (see Review section) at perigee should be modified when a or e is changed. The initial conditions for the mother and first daughter satellites are listed in Table 4.3. When $\beta=2\times10^{-4}$ (see Eq.(15)), the transient responses of the semi-

105

major axis and the eccentricity for ten orbits are shown in Fig.4.10; the difference of the

osculating orbital elements between the mother and the first daughter satellites as well as the

control efforts of the first daughter satellite are shown in Fig.4.11. From these figures it is

seen that the osculating orbital elements converge smoothly; the maximum control efforts

(see Fig.4.11, g~I) are less than 10^{-4} m/s^2, e.g. if the mass of the satellite is 100 kg., the

maximum control is less than 0.01 newton (it is quite small). For a long lifetime satellite

formation flight, this should be reasonable. The main purpose of this study is to maintain the

distance between adjacent satellites; the distance response with initial error and various
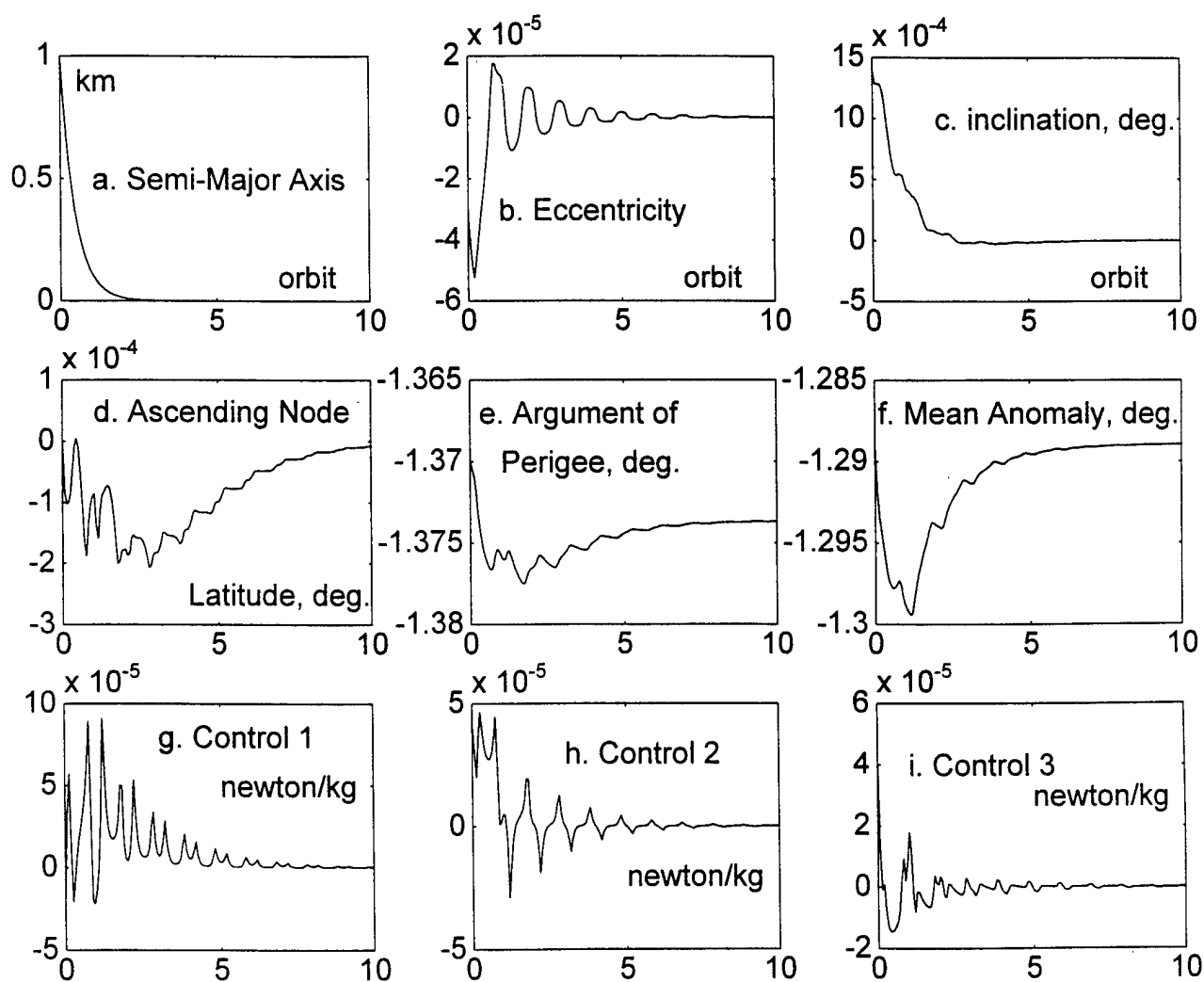
Fig.4.11. Difference of Orbital Elements Between Adjacent Satellites, and Control Efforts
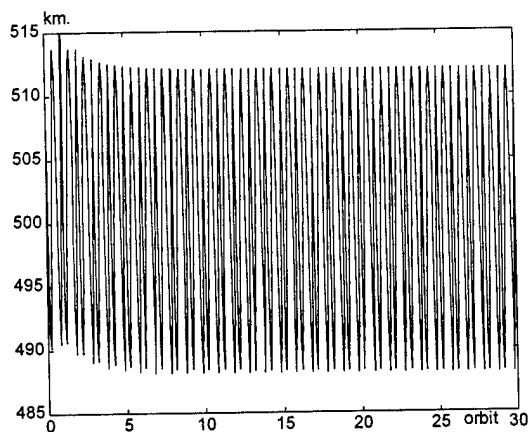
Fig.4.12 Distance Response for 30 Orbits

perturbations for 30 orbits is shown in Fig.4.12. By comparing the situations depicted in Fig.4.4 and Fig.4.12, we can see that in Fig.4.12, the initial error of the distance of the daughter satellite is gradually diminishing, after several orbits, the distance is oscillating around 500 ± 12 km., just like the situation in Fig.4.4, which is ideal stationkeeping, without initial error or perturbation. From Fig.4.12 it is also seen that although the control effort is small, it can perfectly compensate the perturbations (mainly J_2 effect). The distribution of the adjacent satellites at various times for the eleventh orbit is shown in Fig.4.13.

Fig.4.13 Distribution of Adjacent Sat.

4.6 CONCLUSIONS

A strategy for maintaining separation distance between satellites in a coplanar elliptical orbiting constellation is developed. This chapter studies the implementation of this strategy. This strategy would be implemented by two maneuvers that would cause a small angular shift in the directions of the semi-major axes with respect to the semi-major axis direction of a "mother" or reference satellite which is also included within the constellation, and a certain phase difference between adjacent satellites. With this approach for Keplerian
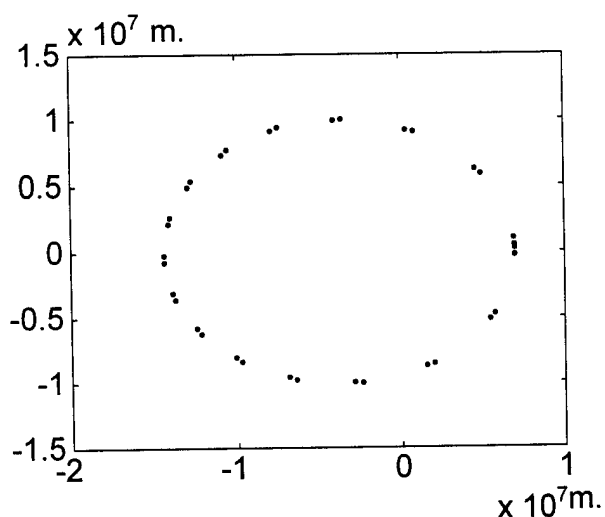
107

type orbits and nominal alignment of the satellites along the orbit track, the separation distance between adjacent satellites remains within a few percent of the nominal separation distance. The maneuvers are performed at the perigee point in the orbit; for a representative strawman configuration force-impulse requirements are within the limits for proposed pulse plasma thrusters[1]. It is clear that the over-all propulsion requirements would be far less than for the original situation in a Keplerian orbit without the semi-major axis angular shift maneuver. The initial separation strategy given in this paper results in the minimum maneuver energy, since the work done by the thrusters is all used to augment the orbital energy.

For stationkeeping, a control law based on the feedback of the tracking errors in the osculating orbital elements instead of feedback of the traditional Cartesian position and velocity errors is presented. One of the benefits of this feedback law is the removal of only the secular drift caused by the perturbations. Therefore, this kind of control can save energy; another benefit is that the orbital elements which do not have tracking errors are kept relatively close to the desired values during the maneuver.

Since the model is nonlinear and time-variant, the control law is based on a Lyapunov function. A unique Lyapunov function is given in this paper, based on which a control law is established, and the asymptotic stability of the formation flight system is strictly proven. The control law is quite simple, so it is easy to implement in engineering practice.

The preliminary analysis reported here could be extended to more complex geometrical configurations such as a triangular shaped constellation confined to the orbit plane, a double pyramid configuration with three spacecraft in the common bases of the pyramids nominally in the orbit plane and two spacecraft at the vertex points of the pyramids

out of the orbit plane of the base-plane spacecraft. Another configuration currently proposed would involve four in-plane spacecraft each at a vertex point of a trapezoid. For the more complex in-plane formations both along track and radial force (thrusters) would be required; for the out-of-plane double pyramid, normal forces would have to be applied to the spacecraft at the tips of the pyramids.

V. GENERAL CONCLUSIONS AND RECOMMENDATIONS

A strategy for maintaining separation distance between satellites in a coplanar elliptical orbiting constellation has been developed. This strategy can be implemented by force-impulse maneuvers that would cause a small angular shift in the direction of the semi-major axes with respect to the semi-major axis direction of a "mother" or reference satellite which is also included within the constellation. With this approach for Keplerian type orbits and nominal alignment of the satellites along the orbit track, the separation distance between adjacent satellites remains within a few percent of the nominal separation distance. If the maneuvers are performed at the perigee and/or apogee points in the orbit it is seen for a representative strawman configuration that force-impulse requirements are within the limits for proposed pulse plasma thrusters.

In the presence of perturbations mainly attributed to the first order effects of the Earth's oblateness for the highly elliptical strawman configuration orbit the results are critically dependent on the amplitude and the numerical accuracy in calculating the semi-major axis shift angle for a nominal along track separation distance. Without subsequent corrections a secular drift is observed in the time history of the separation distance and as the time increases collision or near collision situations can exist.

Additional feedback type of correctional control is recommended to prevent secular drifts above a certain level. Two types of stationkeeping feedback control techniques are considered here: (1) an application of linear quadratic regulator (LQR) theory based on errors in position and a piecewise adaptive application of the Tschauner-Hempel equations of motion as developed for elliptical orbits, and (2) also based on a Lyapunov function using osculating orbital elements. For the Lyapunov approach the asymptotic stability of the

closed-loop system model is strictly proven. In order to preserve stationkeeping fuel, the feedback type of control should be initiated only when the errors reach a certain threshold.

A preliminary deployment strategy is introduced based on near Hohmann-type of transfer orbits. Deployment of the strawman constellation configuration can be achieved in one orbit. This technique was selected because all the work done by the thrusters is used to augment the energy which is required from the transient orbit to the final orbit, resulting in near minimum maneuver energy.

The preliminary analysis reported here could be extended to more complex geometrical configurations such as a triangular or trapezoidal shaped constellation nominally located within the orbital plane, or a double pyramid configuration with the three spacecraft in the common bases of the pyramids nominally in the orbital plane and the two spacecraft at the vertex points of the pyramids out of the orbit plane of the base-plane spacecraft.

VI. IMPLICATIONS FOR FURTHER RESEARCH

1. Further Parametric Studies

The results of the first year will be reviewed and extensions implemented, in particular the completion of deployment maneuvers based on the solution to the nonlinear two point boundary value problem (TPBVP) following Pontryagin's principle. This work is in progress at the end of the first year, but final numerical results have not been reported in this volume. The parametric trade-off studies will be extended to study the effectiveness of both aerodynamic drag forces and solar radiation pressure forces for formation control and also, possibly, for attitude control. A key parameter in this study will be the ballistic coefficient of each satellite in the constellation, which could be deliberately altered by the deployment of extendible vanes from some or all of the satellites. With such systems the use of hybrid control strategies, including combinations of active (thrusting) control as well as the semi-passive control afforded by the orientation of the vanes, can be simulated and evaluated.

2. Implementation of Potential Methods to Maintain the Formation.

A study can then be initiated to compare full active propulsion techniques with active propulsion techniques assisted by aerodynamic / solar radiation pressure induced forces. Among full active propulsion candidates are: Pulse plasma thrusters (PPT's), vaporizing ammonia, resistojets - based on ammonia or hydrazine, and micro - propulsion systems. Aerodynamically / solar pressure assisted systems could consist of rotating (movable) drag panels for cross orbit track and along the track or a combination of PPT's for along the track and aerodynamic / solar pressure panels for cross orbit track.

112

3. Use of Aerodynamics / Solar Pressure with a Deployable Tether

The concept of using rotating aerodynamic drag / solar pressure panels pulling against the tether to maintain cross track positioning could be initiated. HU group has many years experience with the analysis of orbiting tethered systems (Phase A and B of Tethered Shuttle Sub-satellite System for NASA and Ball Research, followed by several years of studying the proposed orbiting tethered antenna / reflector system for AFOSR). A number of conference and journal publications have been prepared by HU. The introduction of the dynamics associated with a deploying or retrieving tether into the constellation system dynamics would involve additional modeling and simulation requirements which would need to be added to the existing software. Initial tether modeling could be based on a relatively short tether assumed to be massless with a concentrated end mass representing the panel. Later on modifications could account for the effects of distributed mass along the tether, a much more complex modeling problem.

4. Continuation of the Use of Aerodynamic Control with a Deployable Tether.

Task 3 could be continued to include more complex tether modeling as required. Different parametric studies would be conducted.

5. Analysis of Fixed Formation Flying Based on A Solid Boom.

The solid boom could represent an ultra violet hardened tether, a miniature Fairchild type boom, an ultra thin "scissors type" boom, or a thin "tape measure" type boom. The use of such a boom would also be accompanied by solar radiation induced forces and torques in the presence of associated thermal deflections, which may be important depending on the type

113

of boom, boom thickness, and material and cross sectional characteristics.

6. Analysis of Spinning Formation Flying Configurations.

The configuration could involve subsatellites as end bodies connected by a flexible boom or tether. In the 1970's rotating cable connected two-end mass configurations were studied with the aim of providing a certain level of gravity for long duration manned spaceflight applications. This concept can be revisited as a means of stabilizing a spinning cluster satellite configuration. In addition to the study of the complex system dynamics (especially if the dynamics of the end bodies are considered), a study of the effect of using different materials such as dental floss type material, Kevlar, or stainless steel should also be included.

References

1. Hartman, Kathy and Weidow, David, "Management of Guidance, Navigation and Control Technologies for Spacecraft Formations Under the NASA Cross-Enterprise Technology Development Program (CETDP)," Proceeding of Flight Mechanics Symposium, NASA Goddard Space Flight Center, May 18-20, 1999.

2. David Folta and David Quinn, "A Universal 3-D Method for Controlling the Relative Motion of Multiple Spacecraft in any Orbit," 1998 Astrodynamics Conference AIAA paper # 98 - 4193, Boston MA..

3. DeCou, A. B., "Orbital Station Keeping for Multiple Spacecraft Interferometry," Journal of the Astronautical Sciences, Vol. 39, No. 3, 1991, pp. 283-297.

4. Sedwick, Raymond, Miller, David, and Kong, Edmund, "Mitigation of Differential Perturbations in Clusters of Formation Flying Satellites," AAS/AIAA Space Flight Mechanics Meeting, Breckenridge, Colorado, February 7-10 1999, Paper No.99-124.

5. Sedwick, Raymond; Miller, David, and Kong, Edmund, "Exploiting Orbital Dynamics for Aperture Synthesis Using Distributed Satellite Systems: Application to a Visible Earth Imager System," AAS/AIAA Space Flight Mechanics Meeting, Breckenridge, Colorado, February 7-10 1999, Paper No.99-12 .

6. Walker, J. G., "Circular Orbit Patterns Providing Continuous Whole Earth Coverage" Royal Aircraft Establishment, Technical Report 70211 (UDC 629. 195: 521.6), Nov.1970.

7. Christopher, P., " Orbital Stability Considerations for Millimeter Wave

Communication", Proceeding of Flight Mechanics Symposium, NASA Goddard Space Flight Center, May 19-21, 1997, Publication 3345, pp.369-383.

8. Folta, David, Newman, Lauri Kraft, and Quinn, David, "Design and Implementation of Satellite Formations and Constellations", Spaceflight Dynamics 1998, Advances in the Astronautical Sciences, Vol.100, Part 1, Edited by Thomas H. Stengle, AAS paper 98- 304, pp.57-70.

9. Brochet, C., Garcia, J. M., Enjalbert, J.M., and Ceolin, T., "Models and Algorithms for Constellation Station Keeping Strategies and Satellite Replacement", Spaceflight Dynamics 1998, Advances in the Astronautical Sciences, Vol.100, Part 1, Edited by Thomas H. Stengle, AAS Paper 98-302, pp.31-45.

10. Geoffrion, A.M., "Generalized Benders Decomposition", Journal of Optimization, Theory and Applications, Vol. 10, No.4, 1972, p237.

11. Hooke, R., and Jeeves, T.A., "Direct Search Solution of Numerical and Statistical Problems", Journal ACM, Vol.8, 1961, pp.212-229.

12. Goldstein, Herbert, Classical Mechanics, Addison-Wesley Publishing Company, Inc., Second Edition, Cambridge, MA, 1980, Chapter 3.

13. Hughes, Steven P. and Hall, Christopher D., "Mission Performance Measures for Spacecraft Formation Flying," Proceeding of Flight Mechanics Symposium, NASA Goddard Space Flight Center, May 18-20, 1999, pp 309,318.

14. Ulybyshev, Y., "Long-Term Formation Keeping of Satellite Constellation Using Linear- Quadratic Controller," Journal of Guidance, Control, and Dynamics, Vol. 21, No. 1, 1998, pp. 109-115.

15. Carpenter, Russel J.,"Feasibility of Decentralized Linear-Quadratic-Gaussian Control of Autonomous Distributed Spacecraft," Proceeding of Flight Mechanics Symposium, NASA Goddard Space Flight Center, May 18-20, 1999, pp 345, 357.

16 Cao, Y., Modi, V. J., de Silva, C. W., and Misra, A. K., "On The Control of a Novel Manipulator with Slewing and Deployable Links,"50th International Astronautical Congress, Amsterdam, The Netherlands, 4 - 8 Oct 1999, IAF - 99 - A.5.06.

17. Chao, C. C., Pollard, J. E., and Janson, S. W., "Dynamics and Control of Cluster Orbits for Distributed Space Missions,"AAS/AIAA Space Flight Mechanics Meeting, Breckenridge, Colorado, February 7-10 1999, Paper No.99-126.

18. Battin, Richard H., Astronautical Guidance, McGraw-Hill Book Company, New York, San Francisco, Toronto, London, 1964.

19. Smith, James E., Proulx, Ronald J., Cefola, Paul J., and Draim, John E., "Optimal Station Keeping Strategies via Parallel Genetic Algorithms," AAS/AIAA Space Flight Mechanics Meeting, Breckenridge, Colorado, February 7-10 1999, Paper No.99-123.

20. Sabol, Chris, Burns, Richard, and McLaughlin, Craig A., "Satellite Formation Flying Design and Evolution," AAS/AIAA Space Flight Mechanics Meeting, Breckenridge, Colorado, February 7-10 1999, Paper No.99-121.

21. Ada Simulation Development System (ASDS), version 3, Volume I, McDonnell Douglas Aerospace - Houston, TX, Intermediate Revision: January 1994.

22. Clohessy, W. H. and Wiltshire, R. S., "Terminal Guidance System for Satellite Rendezvous," Journal of the Aerospace Sciences, Vol. 27, No. 9, 1960, pp. 653-

658,674.

23.   Tschauner, J., and Hempel, P., "Rendezvous zu einem in elliptischer Bahn umlaufenden Ziel," Astronautica Acta, Vol. 11, No. 2, 1965, pp. 104-109.

24.   Tschauner, J., "Neue Darstellung des Rendezvous bei elliptischer Ziel-bahn," Astronautica Acta, Vol. 11, No. 5, 1965, pp. 312-321.

25.   Tschauner, J., "Elliptic Orbit Rendezvous," AIAA Journal, Vol. 5, No. 6, 1967, pp. 1110-1113.

26.   Carter, T. E. and Humi, M., "Fuel-Optimal Rendezvous Near a Point in General Keplerian Orbit, Journal of Guidance, Control, and Dynamics, Vol. 10, 1987, pp. 567-573.

27.   Carter, T. E., "New Form for the Optimal Rendezvous Equations Near a Keplerian Orbit, Journal of Guidance, Control, and Dynamics, Vol. 10, 1990, pp. 183-186.

28.   Carter, T. E. and Brient, J. "Optimal Bounded-Thrust Space Trajectories Based on Linear Equations," Journal of Optimization Theory and Applications, Vol. 70, No. 2, 1991, pp. 299-317.

29.   Carter, T. E. and Brient, J., "Fuel-Optimal Rendezvous for Linearized Equations of Motion,"Journal of Guidance, Control, and Dynamics, Vol. 15, 1992, pp. 1411-1416

30.   Carter, T. E. and Brient, J. "Linearized Impulsive Rendezvous Problem," Journal of Optimization Theory and Applications, Vol. 86, No. 3, 1995, pp. 553-584.

31.   Van der Ha, J., and Mugellesi, R., "Analytical Models for Relative Motion Under Constant Thrust," Journal Guidance Control, and Dynamics, Vol. 13, No. 4, 1988, pp. 644-650.

32. Badesha, S., Heyler, G., Sharer, P., and Strikwerda, T., "Development of Formation Deployment and Initialization Concepts," Proceeding of Flight Mechanics Symposium, NASA Goddard Space Flight Center, May 18-20, 1999, pp 18-20.

33. George B. Dantzig, Linear Programming and Extensions, Princeton University Press, Princeton, New Jersey, 1963.

34. David G. Luenberger, Introduction To Linear and Nonlinear Programming, Addison - Wesley Publishing Company, Cambridge, Massachusetts, 1973.

35. Thomas E. Fortmann and Konrad L. Hitz, An Introduction To Linear Control Systems, Marcel Dekker, Inc. New York, New York, 1977.

36. Michael Athans and Peter L. Falb, Optimal Control - An Introduction to the Theory and Its Applications, McGraw - Hill Book Company, New York 1966.

37. Craig A. Kluver and Greg S. Tanck, "A Feedback Control Law Stationkeeping With On-Off Thrusters," Proceeding of AAS/AIAA Astrodynamics Specialist Conference, Sun Valley, Idaho, August 4 - 7, 1997, Astrodynamics 1997, Advances in the Astronautical Sciences, Vol. 97, AAS paper No. 97 - 624, pp. 387 - 399.

38. Zhaozhi Tan, Peter M. Bainum and Avaine Strong, "The Implementation of Maintaining Constant Distance Between Satellites in Elliptic Orbits," AAS/AIAA Spaceflight Mechanics Conference, Clearwater, Florida, 23-26 January, 2000, paper no. AAS 00 - 141.

39. Pontryagin, L. S., Boltyanskii, V. G., Gamkrelidze, R. V., and Mishchenko, E. F., The Mathematical Theory of Optimal Processes, A Pergamon Press Book, The Macmillan Company, New York, NY, 1964.

40. I. Flugge - Lotz and H. Marbach, "The Optimal Control of Some Attitude Control Systems for Different Performance Criteria," Journal Basic Engineering, Volume 85, 1963, pp 165 - 176.

41. F. Li, and P. M. Bainum, "_Numerical Approach for Solving Rigid Spacecraft Minimum Time Attitude Maneuvers," Journal of Guidance, Control and Dynamics, Vol. 13, No. 1, Jan - Feb 1990, pp. 38 - 45.

42. Feiyue Li, Peter M. Bainum, N. Glenn Creamer, Shalom Fisher, and Nimfa C. Teneza, "Three - Axis Near - Minimum - Time Maneuvers of RESHAPE; Numerical and Experimental Results," The Journal of the Astronautical Sciences, Vol. 43, No. 2, April - June 1995, pp. 161 - 178.

43. Bellman, R., "Functional equations in the theory of Dynamic Programming Positivity and Quasi-linearity," Proc. Natl Acad Sci U. S. 41, 743, 1959.

44. Kalaba, R., "On Nonlinear Differential Equations, The Maximum Operation, and Monotone Convergence," Journal of Mathematical Mechanics, Vol. 8, pp. 519, 1959.

45. Bellman, R. and Kalaba, R., Quasilinearization and Nonlinear Boundary Value Problems, American Elsevier, NY, NY, 1965.

46. Beckenbach, E. F. and Bellman, R., Inequalities, Springer, Berlin, 1961.

47. NASA Home Page: OSS Strategic Plan, Appendix 3, Mission Descriptions, 1997.

48. ESA Web Page, Cluster home page, ESA Cluster's Scientific Objectives and the Cluster Spacecraft Design, from Cluster home page, 13 May 1996.

49. Zhaozhi Tan, Peter M. Bainum and Avaine Strong, "A Strategy for Maintaining Distance Between Satellites in an Orbiting Constellation," 9th AAS/AIAA Spaceflight

Mechanics Conference, Breckenridge, CO, 7 - 10 February 1999, paper no. AAS 99 - 125.

50. Danby, J. M. A., <u>Fundamentals of Celestial Mechanics</u>, The MacMillan Company, New York, 1964, sect. 11.5, pp.238-242.

51. Schaub, Hanspeter, Vadali, Srinivas R., Junkins, John L., and Alfriend, Kyle T., "Spacecraft Formation Flying Control Using Mean Orbit Elements," AAS/AIAA Astrodynamics Specialist Conference, Girdwood, Alaska, 16-19 August 1999, paper no AAS 99 - 310.

52. Battin, Richard H., <u>An Introduction to the Mathematics and Methods of Astrodynamics</u>, American Institute of Aeronautics and Astronautics, Inc., Second Printing, New York, New York, 1987.

53. Neustadt, L. W., "Optimization, A Moment Problem, and Nonlinear Programming,"SIAM Journal on Control, Vol. 2, 1964, pp. 33-53.

54. Stern, R. G. and Potter, J. E., "Optimization of Mid-course Velocity Corrections,"Report RE-17, Experimental Astronomy Laboratory, MIT, Cambridge MA, 1965.

55. Bond, Victor and Allman, Mark C., <u>Modern Astrodynamics, Fundamentals and Perturbation Methods</u>, Princeton University Press, Princeton, New Jersey, 1996.

56. Kirk, D. E., <u>Optimal Control Theory, An Introduction</u>, Prentice Hall, New Jersey, 1970.

57. Lewis, Frank L., Syrmos, Vassilis L., <u>Optimal Control</u>, John Wiley and Sons, New York, 1995.

58.   Petkov, P. Hr., Christov, N. D., and Konstantinov, M. M., <u>Computational Methods for Linear Control Systems</u>, Prentice Hall, New York, New York, 1991.

59.   Moerder, D. D. and A. J. Calise, "Convergence of a Numerical Algorithm for Calculating Optimal Output Feedback Gains," IEEE Trans. Automatic Control, AC - 30, 900 - 903, 1985.

60.   Carter, T. E., "State Transition Matrix for Terminal Rendezvous Studies: Brief Survey and New Example", Journal of Guidance, Control and Dynamics, Vol. 21, No. 1, 1998, pp. 148 - 155.

61.   Collins, J. T., Wertz, J. R., "Autonomous Constellation Maintenance System", presented at the AIAA/Utah State University 10th Annual Small Satellite Conference, September 19, 1996.

BIBLIOGRAPHY OF PAPERS RESULTING FROM THIS RESEARCH

Tan, Zhaozhi, Bainum, Peter M., and Strong, Avaine, "The Implementation of Maintaining Constant Distance Between Satellites in Elliptic Orbits", AAS/AIAA Space Flight Mechanics Meeting, Clearwater, Florida, Jan.23-26, 2000, Paper No. AAS 00-141; to appear in Conference Proceedings, AAS Advances in the Astronautical Sciences, 2000.

This paper forms the basis of Chapter IV of this final report.